Mitochondrial-Nuclear Interactions Mediate Sex-Specific Transcriptional Profiles in Drosophila

Mitochondrial-Nuclear Interactions Mediate Sex-Specific Transcriptional Profiles in *Drosophila*

Jim A. Mossman,*,[1] Jennifer G. Tross,*,†,‡,§ Nan Li, Zhijin Wu,** and David M. Rand*,[1]**
*Department of Ecology and Evolutionary Biology, and **Department of Biostatistics, Brown University, Providence, Rhode Island 02912, †Department of Medical Oncology, and ‡Department of Biostatistics and Computational Biology, Dana–Farber Cancer Institute, Boston, Massachusetts 02215, §Harvard-MIT Division of Health Sciences and Technology, Harvard Medical School, Boston, Massachusetts 02115
ORCID ID: 0000-0001-6817-3459 (D.M.R.)

ABSTRACT The assembly and function of mitochondria require coordinated expression from two distinct genomes, the mitochondrial DNA (mtDNA) and nuclear DNA (nDNA). Mutations in either genome can be a source of phenotypic variation, yet their coexpression has been largely overlooked as a source of variation, particularly in the emerging paradigm of mitochondrial replacement therapy. Here we tested how the transcriptome responds to mtDNA and nDNA variation, along with mitonuclear interactions (mtDNA × nDNA) in *Drosophila melanogaster*. We used two mtDNA haplotypes that differ in a substantial number of single nucleotide polymorphisms, with >100 amino acid differences. We placed each haplotype on each of two *D. melanogaster* nuclear backgrounds and tested for transcription differences in both sexes. We found that large numbers of transcripts were differentially expressed between nuclear backgrounds, and that mtDNA type altered the expression of nDNA genes, suggesting a retrograde, *trans* effect of mitochondrial genotype. Females were generally more sensitive to genetic perturbation than males, and males demonstrated an asymmetrical effect of mtDNA in each nuclear background; mtDNA effects were nuclear-background specific. mtDNA-sensitive genes were not enriched in male- or female-limited expression space in either sex. Using a variety of differential expression analyses, we show the responses to mitonuclear covariation to be substantially different between the sexes, yet the mtDNA genes were consistently differentially expressed across nuclear backgrounds and sexes. Our results provide evidence that the main mtDNA effects can be consistent across nuclear backgrounds, but the interactions between mtDNA and nDNA can lead to sex-specific global transcript responses.

KEYWORDS mtDNA; epistasis; *Drosophila*; transcriptome; mitonuclear; retrograde signaling

THE ancient symbiosis that led to current day mitochondria and their eukaryotic host was a major milestone for intergenomic communication (Sagan 1967; Martin and Muller 1998). During the following ~2 billion years, the resulting eukaryotic cell consolidated the genetic information from two ancestral genomes to a reduced set of genes in the mitochondrial organelle [mitochondrial DNA (mtDNA)] and many nuclear-encoded genes that are required for mitochondrial function. At ~16.5 kb in size, the mtDNA encodes 13 oxidative phosphorylation (OXPHOS) proteins, 22 transfer RNAs (tRNAs), and 2 ribosomal RNAs (Taanman 1999). The remaining ~1200 proteins associated with mitochondria are encoded by the nucleus (Wallace 1999). Mitochondria therefore require coordinated expression of genes from both mitochondrial and nuclear genomes for efficient function (Rand 2001; Smeitink *et al.* 2001). Crucially, the effects of mtDNA variation, nuclear DNA (nDNA) variation, and their interactions on gene expression are poorly understood, yet they are expected to play a large role in an organism's response to environmental or cellular stress.

Mitochondria perform many functions in the cell other than ATP production, including maintaining homeostasis, regulating redox signaling, and apoptosis (Friedman and Nunnari 2014). Recent studies have shown that when mitochondrial function is perturbed, retrograde signaling to the nucleus occurs via the unfolded protein response (UPR) (Houtkooper *et al.* 2013; Quiros *et al.* 2016), however the role of underlying mitonuclear

doi: 10.1534/genetics.116.192328
Manuscript received June 5, 2016; accepted for publication August 17, 2016; published Early Online August 24, 2016.
Available freely online through the author-supported open access option.
Supplemental material is available online at www.genetics.org/lookup/suppl/doi:10.1534/genetics.116.192328/-/DC1.
[1]Corresponding authors: Department of Ecology and Evolutionary Biology, Box G, Brown University, Providence, RI 02912. E-mail: Jim_Mossman@brown.edu; and david_rand@brown.edu

genetic variation in retrograde signaling has not been studied in the context of gene expression. Aberrations in mitochondrial function are known to cause a wide spectrum of disorders in humans (DiMauro and Schon 2003; Lin and Beal 2006), and mitochondrial diseases with an mtDNA component can be difficult to characterize due to the complexity of dual genomic organization and large numbers of intergenomic interactions. The relatively high mutation rate, lack of protective histones, maternal inheritance, reduced effective population size, and no recombination all contribute to a higher frequency of deleterious mutations in mtDNA (Gemmell *et al.* 2004). These "natural" genetic variants segregate together in complete linkage disequilibrium in the form of mtDNA haplotypes. Importantly, both *de novo* (spontaneous) mutations and haplotype variation have been associated with disease phenotypes across a number of species (Roubertoux *et al.* 2003; Dimauro and Davidzon 2005).

While specific mtDNA mutations—associated with haplotype variation—increase the risks of some diseases, *e.g.*, neurodegenerative diseases and aging (Stewart and Chinnery 2015), they do not operate in isolation from the substantial nuclear-encoded contribution to mitochondrial phenotypes (Wallace 1999; Wong 2012). Deleterious mitochondrial mutations often demonstrate incomplete penetrance (Giordano *et al.* 2014), suggesting nuclear variants may dampen or amplify their effects. An unknown proportion of phenotypes demonstrating missing heritability are likely to involve the interactions (epistases) between mtDNA and nDNA (Mossman *et al.* 2016). Indeed, mitonuclear interactions have been largely overlooked as sources of phenotypic variation (Pesole *et al.* 2012), even though recent studies have shown mitonuclear interactions to be pervasive and context dependent in a suite of life history traits (Hoekstra *et al.* 2013; Mossman *et al.* 2016).

mtDNA variation is hypothesized to affect males more severely than females due to an imbalance in the strength of purifying selection between the sexes (Frank and Hurst 1996). Because mtDNAs are maternally inherited, males are at a genetical dead end for mtDNA evolution. Mutations that have negligible or zero effects in females, yet severe effects in males, can rise to high frequencies in populations by genetic drift (Frank and Hurst 1996). Under this hypothesis, it is predicted that mtDNA variation should promote larger phenotypic effects in males than females. Initial support for this hypothesis was suggested by mitochondrial disease cases that appeared more severe in males than females (Wallace 1992; Bernes *et al.* 1993; Casademont *et al.* 1994). More recent studies provide support for the Frank and Hurst hypothesis in *Drosophila* aging (Camus *et al.* 2012) and fertility (Yee *et al.* 2013; but see Friberg and Dowling 2008), yet there is a robust absence of support in development time and viability (egg-to-adult survival) (Mossman *et al.* 2016). In humans, there is also equivocal evidence for the role of mtDNA haplotypes in fertility-related traits in males (Ruiz-Pesini *et al.* 2000; Pereira *et al.* 2007; Mossman *et al.* 2012). There is some evidence in *Drosophila* that sex-specific mtDNA effects on gene expression exist (Innocenti *et al.* 2011), and that variation in male-limited gene expression is dominated by mtDNA variation. However, it is not known whether differential gene expression associated with mtDNA variation is a robust phenotype across nuclear genetic backgrounds.

Here, we use a *Drosophila* mitonuclear introgression model (Montooth *et al.* 2010; Meiklejohn *et al.* 2013; Villa-Cuesta *et al.* 2014; Holmbeck *et al.* 2015) to test the hypotheses that mtDNA variation, nDNA variation, and mtDNA × nDNA interactions impact gene expression in males and females. A main motivation of this experiment was to examine whether different mitonuclear genotypes have distinct gene expression profiles. Here, we focused on a 2 × 2 genotype table (*sensu* Roubertoux *et al.* 2003) to elucidate whether mtDNA variation *per se*, nuclear variation *per se*, and mitochondrial × nuclear variation influences gene expression in a sex-specific manner.

We have previously shown that across several *Drosophila* Genetic Reference Panel nuclear backgrounds, the *siI* and *OreR* mtDNA haplotypes diverge in phenotypic values (development time, egg-to-adult viability) (Mossman *et al.* 2016). We have also shown there are nucleotide substitutions between *siI* and *OreR* mtDNAs that have putative deleterious effect on protein function (Mossman *et al.* 2016), motivating an examination of gene expression variation that is associated with mtDNA and nuclear variation. We hypothesized that mtDNA variation preferentially modifies the expression of mitochondria-associated OXPHOS genes from both mitochondrial and nuclear genomes. Furthermore, we wanted to characterize the cellular processes and functional categories of genes that are modified by mtDNA, nuclear, and mitonuclear variation. We further hypothesized that mitochondrial protein translational machinery (Jacobs and Turnbull 2005) would be largely influenced due to its critical role in protein synthesis and the key participation of mitochondrial ribosomes. Finally, we investigated whether genes differentially expressed by mtDNA variation were enriched in male-limited genes (*e.g.*, those involved in testes and sperm-related proteins) to test the generality of the Frank and Hurst hypothesis in alternative nuclear backgrounds.

Materials and Methods

Mitonuclear panel

Experiments were performed on four genotypes whose nuclear genomes were introgressed with mtDNAs from two sources: (i) *OregonR* strain of *Drosophila melanogaster* and (ii) *siI* strain of *D. simulans*. The nuclear backgrounds were *Oregon R* (*OreR*) and *Austria W132* (*AutW132*), which are both *D. melanogaster* nuclear types. The four genotypes were (mito; nuclear): (i) *OreR*; *OreR*, (ii) *OreR*; *AutW132*, (iii) *siI*; *OreR*, and (iv) *siI*; *AutW132*. Specifically, the introgressions were performed by balancer chromosome replacement, followed by backcrossing to the original stock to homogenize the nuclear background and remove nuclear variation that may have been retained in the chromosome replacement process. The full double balancer replacement scheme is

described in Montooth *et al.* (2010). Alignments between mtDNA coding regions reveal substantial sequence divergence between *OreR* (NC_001709) and *siI* (AF00835) mtDNA haplotypes: a pairwise amino acid divergence (103 amino acids) and a pairwise synonymous divergence (418 SNPs) (Montooth *et al.* 2010).

All strains used in this study were cleared of *Wolbachia* using tetracycline, and *Wolbachia* negative status was confirmed by PCR (Montooth *et al.* 2010).

RNA sequencing sample preparation

Prior to RNA extraction, flies were reared on standard laboratory food at 25° on a 12 hr light:12 hr dark cycle, and density-controlled for one generation (five males and five females per vial). After density control, eclosed flies were allowed to mate for 3 days on standard food and were then separated by sex at a density of 50 males or 50 females per vial. After 2 days of recovery from CO_2 anesthesia, batches of flies were transferred into a 1.5-ml microcentrifuge tube and immediately flash frozen in liquid nitrogen.

RNA was extracted from 30, 5-day-old whole healthy flies in each genotype by sex treatment. We used whole flies to test whether sex-limited gene expression was associated with mtDNA and nDNA genetic effects, as found by Innocenti *et al.* (2011). In addition, a number of other studies of genetic variation for gene expression in *Drosophila* have used whole flies, allowing for more direct comparison with our results (Gibson *et al.* 2004; Ayroles *et al.* 2009; Huang 2012; Mackay *et al.* 2012; Huang *et al.* 2014). In males, there were three replicates per genotype and in females there were three replicates in all genotypes apart from the *siI*; *AutW132*, which had two replicates. We followed a modified RNA sequencing (RNA-seq) sample preparation protocol from the Gilad Laboratory (Chicago University; http://giladlab.uchicago.edu/data/RNASeq_v2%202.doc). Messenger RNA (mRNA) was first extracted, followed by RNA fragmentation, complementary DNA (cDNA) first strand synthesis, second strand synthesis, end repair, poly adenylation, adapter ligation, and PCR enrichment. Throughout, RNA and DNA were quantified using the Qubit Kits (RNA Broad Range, dsDNA Broad Range, and dsDNA High Sensitivity) with a Qubit 1.0 Fluorometer. All Qubit reagents were obtained from Molecular Probes (Eugene, OR). Following PCR enrichment, we size selected PCR products with size range of 334–500 bp using a Caliper LabChip XT (DNA 750 chip) (Caliper Life Sciences, Hopkington, MA).

Gene expression assays

Gene expression was assayed in both sexes in all four genotypes using Illumina RNA-seq (HiSeq; Illumina, San Diego) with a 50-bp, single-end protocol. Samples were processed at Brown University's Genomics Core Facility using an Illumina HiSeq2000 platform.

RNA-seq data preprocessing

RNA-seq read quality was first assessed using the FastQC v0.11.5 program (http://www.bioinformatics.babraham.ac.uk/projects/fastqc/). We then filtered the reads using a FASTQ quality filter (fastq_quality_filter) with –q 20 and –p 80 flags, as implemented in the FASTX-Toolkit (http://hannonlab.cshl.edu/fastx_toolkit/commandline.html#fastq_quality_filter_usage). These values correspond to removing reads with 80% bases having a quality score of <20. Adapters were clipped from the reads using the fastx_clipper tool in the FASTX-Toolkit (http://hannonlab.cshl.edu/fastx_toolkit/commandline.html#fastx_clipper_usage) and FastQC was repeated. We used TopHat v2.0.12 (https://ccb.jhu.edu/software/tophat/index.shtml) (Trapnell *et al.* 2012) with Bowtie2 v2.2.3 (http://bowtie-bio.sourceforge.net/index.shtml) to map the reads to the dm3 reference genome using the dm3flybase.gtf annotation file obtained from the University of California Santa Cruz Genome Browser (https://genome.ucsc.edu/). BAM files generated by TopHat were converted to SAM files using SAMtools (http://samtools.sourceforge.net/) (Li *et al.* 2009), and reads mapping to specific genome features (genes) were counted using htseq-count (http://www-huber.embl.de/users/anders/HTSeq/doc/count.html) (Anders *et al.* 2015). The read-count data table obtained via HTSeq was used for downstream analyses. All preprocessing was conducted using computational resources and services at the Center for Computation and Visualization, Brown University.

RNA-seq data analysis

Differential expression (DE) analyses were conducted using two methods: DESeq (Anders and Huber 2010) following the vignette workflow (http://bioconductor.org/packages/release/bioc/vignettes/DESeq/inst/doc/DESeq.pdf), and edgeR (Robinson *et al.* 2010). We also used a clustering algorithm to categorize genes based on their between-genotype expression profiles (see below). The measurement accuracy of RNA-seq was validated using a subset of genes and quantitative PCR (qPCR) as described in detail in Supplemental Material, File S1 (see also Table S1; Figure S13).

Gene filtering

In total we analyzed data generated from 23 RNA-seq libraries (11 female, 12 male). Throughout the data analyses, we used both complete data sets (including all genes), and filtered data (excluding the lowest 40th percentile of the data *sensu* the recommendations in the DESeq vignette). The purpose of the independent filtering was to remove genes from the total data set that have little or no chance of showing significant evidence of DE, while simultaneously increasing the detection power with a similar false discovery rate (FDR) (Bourgon *et al.* 2010). We specify in each *Results* section which data set (unfiltered or filtered) and which analysis program was used.

Gene clustering

We used four genotypes in total for this study and our primary aim was to detect genes that show expression profiles consistent with mtDNA effects, nDNA effects, and mtDNA × nucDNA (epistatic) effects. We rationalized that different

genetic effects would produce different norms of reaction shapes (profiles) across genotypes. We aimed to cluster genes based on their expression across different genotypes. For example, for all genotypes (independent variable), we asked which genes segregated with a similar pattern, and which of those patterns correspond with nuclear effects, mtDNA effects, and their mtDNA × nDNA interactions (see Figure S1 for theoretical gene expression outlines).

Model-based clustering of gene expression profiles was performed using MBClusterSeq (Si *et al.* 2014), with $k = 20$ clusters in both sexes. Negative binomial (NB) models were used to perform the hierarchical clustering and hybrid tree builds as implemented in the MBClusterSeq package. Clusters are described using interaction plots of individual genes in each cluster and the mean genotype values per cluster were calculated. The log-fold change is relative to the normalized gene expression across all treatments (genotypes) with each row of the log-fold change matrix having a zero sum. The clustering algorithm allocates genes to a group based on their gene expression profile (in this case, the shape of the gene expression–genotype relationship).

Gene ontology enrichment

Gene ontology (GO) enrichment analyses were performed on clustered genes using the Bioprofiling.de program (http://bioprofiling.de/) (Antonov 2011) and the GO Consortium database (http://geneontology.org/) with the default submission and "*Drosophila melanogaster*" organism selected. The outputs of the "ProfCom_GO" analyses (Antonov *et al.* 2008) were filtered for GO categories that evidenced a Bonferroni-corrected *P*-value of <0.05 and these GO categories were used in the heat map construction. In the sex-specific gene expression analysis, we used GOrilla GO enrichment (Eden *et al.* 2009) to investigate the GO processes that were enriched in the male- and female-biased gene sets.

Analyses of OXPHOS gene subset

In addition to the analyses of the global gene set, genes encoding OXPHOS-related proteins (complexes I, II, III, IV, and ATP synthase) were selected for closer examination because these are putative targets of mitochondrial variation. Both mtDNA and nuclear genes targeted to the mitochondrion were downloaded from the MitoDrome database (Sardiello *et al.* 2003; D'Elia *et al.* 2006). Arc diagrams were used to display the relationship between various genes in the OXPHOS pathway in *D. melanogaster* (Tripoli *et al.* 2005) and the effect of alternative mtDNA haplotype in each nuclear background and in each sex. DE was judged by DESeq in each nuclear background and sex separately. For clarity, only genes with a *P*-value of <0.1 are shown and a gene was only required to be included in one sex or nuclear background to be present in the arc diagram. A total of 78 nuclear genes and 13 mtDNA genes were included in the initial screen, of which 53 genes were included in the visualization (11 mtDNA genes and 42 nuclear genes; $P < 0.1$ in at least one genetic background).

Data availability

Drosophila strains used in this study are available upon request. FASTQ files from the 23 RNA-seq libraries are available at the Sequence Read Archive (SRA) under project accession SRP082430.

Results

Between-sex gene expression correlations

We first investigated whether there were signatures of sex-specific gene expression as a basis for understanding how mtDNAs may or may not modify gene expression in a sex-specific manner. Figure 1, A–D, shows biplots of the four mitonuclear genotypes using pseudocounts of the unfiltered data set. The pseudocount transformation is $\log_2$ (read count +1), and was calculated using the base mean in DESeq. There are clear gene subsets in the data distributions that show sex-biased expression, particularly for male-biased genes (Figure 1). The numbers of genes that are common across genotypic intersections are described for each sex (females, Figure 1E; males, Figure 1F). The female- and male-biased genes (red and blue data in Figure 1, A–D, respectively) were intersected separately and those elements that were common to all four genotypes were subjected to GO-enrichment analysis. GO-enrichment analyses (Eden *et al.* 2009) show male-biased genes are enriched for sperm-related processes (Figure 1F and Table 1). Genes with female-biased expression (shown as red in Figure 1) are associated with, among other processes, egg-related GO categories. Table 1 describes the male-specific enrichment of GO categories.

Genotype signatures of gene expression

There are large differences between the sexes in genotype signatures of gene expression. Figure 2 shows multidimensional scaling (MDS) plots (Ritchie *et al.* 2015) of each genotype in female and male data sets. The data are plotted in two dimensions and the distances between samples (libraries) approximately reflect the leading $\log_2$-fold change between the samples for the genes that distinguish those samples (Ritchie *et al.* 2015). Data were filtered as the top 10,000, top 1000, top 100, and top 10 genes. The top genes are those with the largest SD in expression between samples. In females, the progressive filtering increases the genotype-genotype distance, whereas in males, the progressive filtering increased the distance between mitochondrial genotypes only in the *Aut132* nuclear background (Figure 2).

mtDNA substitution effects

We next tested whether mtDNA substitution conferred DE of genes in each nuclear background and in both sexes, separately. We did this using DESeq (Anders and Huber 2010) on individual nuclear backgrounds for each sex (two tests per sex). The read-count data were modeled using NB distributions. The fold change and associated *P*-value were calculated for each gene and *P*-values were adjusted to account

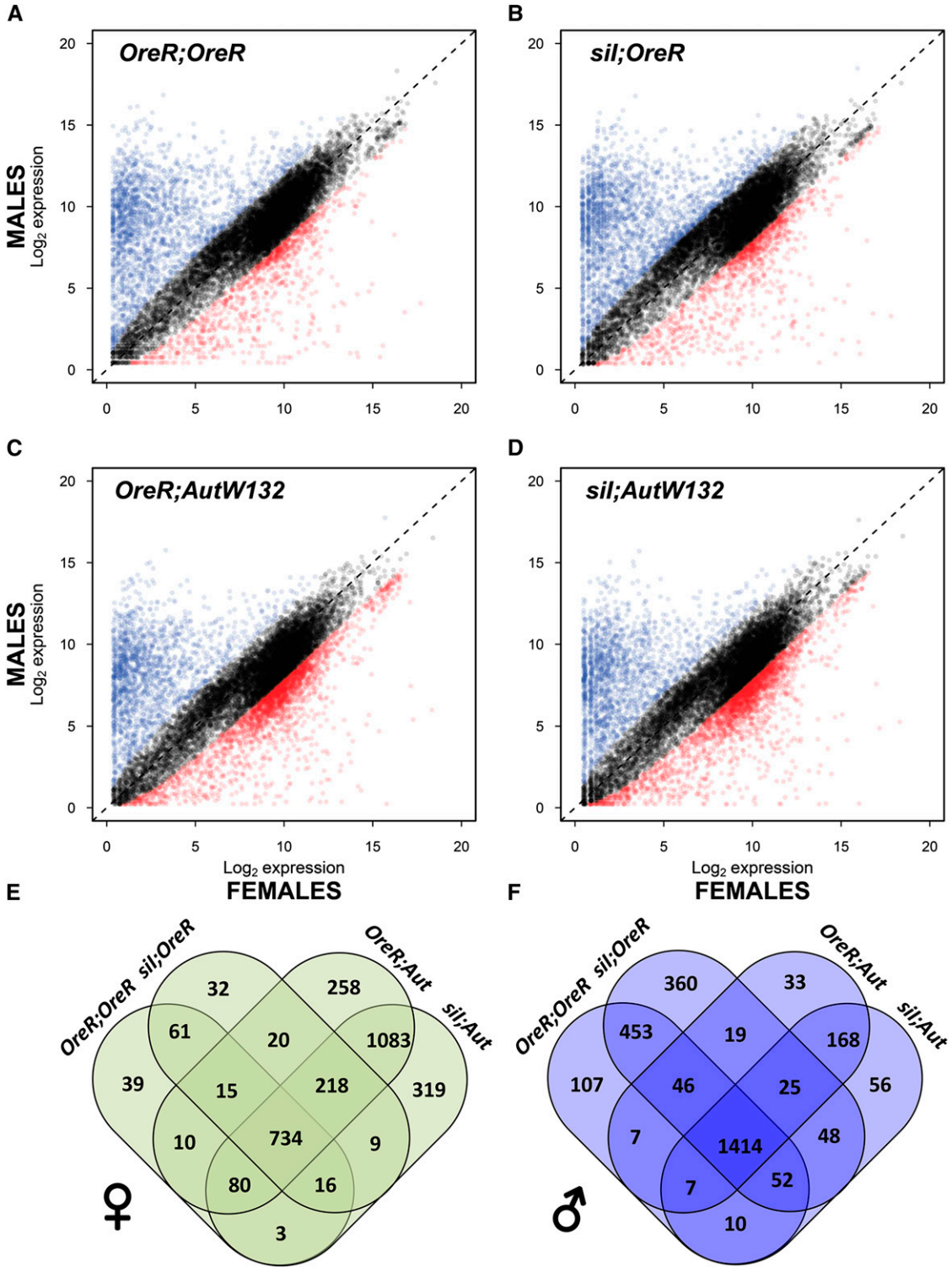

Figure 1 Sex-biased gene expression across four mitonuclear genotypes. Gene expression profiles of individual genes are shown for each genotype analyzed in this study: (A) *OreR;OreR*, (B) *sil;OreR*, (C) *OreR;AutW132*, and (D) *sil;AutW132*. Biplots show female gene expression on the abscissa with corresponding male gene expression values on the ordinal scale. Data highlighted in red and blue show female- and male-biased genes, respectively. Sex bias was determined as a $\log_2$-fold >2 difference between females and males. Data in black show no sex bias in expression. (E and F) Venn diagrams describe the number of genes that are intersected between genotypes for sex-biased expression (red and blue genes in A–D). (E) Female and (F) male intersections are shown. Generally, there were more intersected genes that demonstrated male-biased expression than female-biased expression. Genes at the four-genotype intersection were subject to GO analysis. Male-specific GO processes are described in Table 1.

Table 1 Male-biased gene expression

GO term	Description	No. genes	Enrichment	Adjusted *P*-value
GO:0032504	Multicellular organism reproduction	75	3.58	1.82e−20
GO:0000003	Reproduction	75	3.43	1.75e−19
GO:0046692	Sperm competition	17	6.34	5.37e−08
GO:0044706	Multi-multicellular organism process	17	6.12	9.30e−08
GO:0048232	Male gamete generation	33	2.89	1.45e−05
GO:0007283	Spermatogenesis	32	2.83	3.60e−05
GO:0003341	Cilium movement	12	6.04	4.64e−05
GO:0048515	Spermatid differentiation	10	5.6	1.47e−03

Significantly enriched GO categories are shown for the genes that are intersected between all four mitonuclear genotypes. *P*-values were adjusted using the Benjamini and Hochberg (1995) method.

for multiple testing using the Benjamini–Hochberg method (Benjamini and Hochberg 1995), providing FDRs. In all cases the *Oregon R* mtDNA was the reference mtDNA background and effects of the *siI* haplotype are reported in the analyses. For nDNA results, the *OregonR* nDNA was the reference and the reported fold changes are for *AutW132/OregonR*.

In both females and males, mtDNA substitution conferred DE of genes from both mtDNA and nuclear genomes (Figure 3). In general, the response to mtDNA substitution was greater in females than males. Both sexes and nuclear backgrounds responded with distinct patterns. Among the most consistently modified genes were those encoded by mtDNA, with *siI* haplotypes mainly conferring downregulation in gene expression relative to the *OregonR* baseline. The majority of mtDNA OXPHOS protein-coding genes were downregulated (comparison = *siI/OreR*) in both males and females and in both nuclear backgrounds, with exceptions for mtDNA *ND2*, which was consistently upregulated across sexes and nuclear backgrounds.

Volcano plots in Figure 3 describe the effects of mtDNA substitution. Shown are the results of DESeq analyses for the unfiltered data set. The results for the filtered data set (top 60% quantile) are shown in Figure S2. In the unfiltered- and filtered-gene analyses, estimation of size factors to normalize the counts to a common scale was performed on the unfiltered and filtered data, respectively.

We then intersected the genes that were significantly differentially expressed by mtDNA substitution in each nuclear background (×2) and in both sexes (×2). In this analysis, we did not require a specific direction of effect, *e.g.*, up- or down-regulated, just that the genes were present at a *P*-value threshold. A summary of the number of genes that are present, at various *P*-value thresholds, are shown in Figure S3. Those genes that are consistently differentially expressed (at $P < 0.05$) by mtDNA substitution across nuclear backgrounds and sexes are described in Table 2. Specifically, we report a conservative analysis in which all four nuclear background × sex treatments are intersected (A∩B∩C∩D)—where ∩ signifies intersection—and a more parsimonious analysis, in which a gene was only required to be included in a three-way intersection, *e.g.*, including A∩B∩C, A∩B∩D, A∩C∩D, and B∩C∩D (Table 2). In the strict four-genotype intersection, only five genes were significantly differentially expressed by mtDNA variation in (A) female *OregonR* background, (B) female *AutW132* background, (C) male *OregonR* background, and (D) male *AutW132* backgrounds. These were three mtDNA genes (*ND2*, *ATP6ase*, and *ND4L*), an unannotated computed gene (*CG11966*), and *Jonah 25Bi* (*Ser4*; a serine protease). High within-group variance that results from pooling across other experimental factors (*e.g.*, nuclear backgrounds) is likely to reduce the sensitivity to detect first-order effects of mtDNA, so the five core genes influenced by mtDNA variation is likely a conservative estimate of the true number.

Mitochondrial OXPHOS genes and mtDNA variation

mtDNA variation conferred different effects on global gene expression between the sexes and nuclear backgrounds (Figure 3). We next focused on the nuclear and mtDNA genes of the OXPHOS pathway, since these are jointly encoded by mtDNA and nuclear genes and hypothesized to be more sensitive to mtDNA and nuclear covariation. We filtered our global DE data sets for the OXPHOS genes and graphed those genes that were differentially expressed (Figure 4). We divided the genes into their respective OXPHOS complexes.

In males, there was a high degree of symmetry in the effects of mtDNA variation across the nuclear backgrounds (Figure 4). The differentially expressed genes (with $P < 0.05$) were exclusively targeted to mtDNA-encoded proteins within the various complexes (red gene identifiers in Figure 4) across both *OregonR* and *AutW132* nuclear backgrounds. In the *AutW132* nuclear background, fewer mtDNA OXPHOS genes achieved significance, particularly those in complex IV. In addition, several genes were consistently differentially expressed across nuclear backgrounds, including *CG34092* (*ND1*), *CG34063* (*ND2*), *CG34076* (*ND3*), *CG34086* (*ND4L*), *CG34090* (*CytB*), and *CG34073* (*ATPase6*).

In females the patterns were different and a much larger suite of OXPHOS-associated genes were differentially expressed from both mtDNA and nuclear-encoded genes. This effect was mainly isolated to the *AutW132* nuclear background, which demonstrated a high degree of DE driven by alternative mtDNAs. In *AutW132*, genes that were differentially expressed in males were more significantly differentially expressed in females. The opposite effect is evident in the *OregonR* nuclear background, in which only a small number of OXPHOS-associated genes were differentially expressed in females.

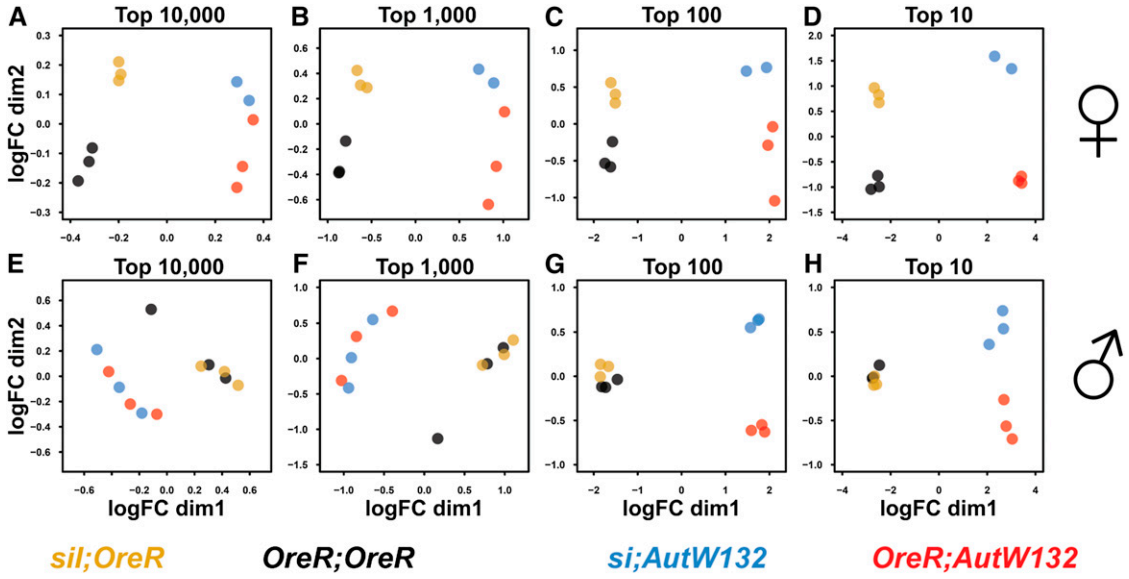

Figure 2 Genotype signatures of transcript variation. MDS plots show progressive filtering of genes based on their expression differences. The distance between points in a plot approximately reflects the relatedness between libraries based on their transcript measures. (A–D) Female and (E–H) male profiles are shown. The top 10,000 (A, E), top 1000 (B, F), top 100 (C, G), and top 10 (D, H) most deviant genes are shown. Separate genotypes are color coded: *sil;OreR*, yellow; *OreR;OreR*, black; *sil;AutW132*, blue; *OreR;AutW132*, red. Mitonuclear genotypes were clearly distinguishable across all filtering levels in females. Only the most differentially expressed genes were able to distinguish mtDNA haplotypes in males.

Global gene expression and mtDNA substitution

The different patterns we observed between males and females in the OXPHOS gene subset suggest the relationships between gene expression and mtDNA substitution differs between the sexes. To investigate whether this effect is evident at a global gene-expression level, we plotted the $\log_2$-fold change in gene expression between *siI* and *OregonR* mtDNAs for each nuclear background within each sex (Figure 5). We found there were dramatic differences between the sexes in the patterns of $\log_2$-fold change; the majority of genes were significantly positively correlated in females (global gene correlation $r = +0.14$, $t = 16.42$, d.f. $=12{,}623$, $P < 2.2e{-}16$), but negatively correlated in males ($r = -0.12$, $t = -13.99$, d.f. $= 13{,}165$, $P < 2.2e{-}16$). Notably, the mtDNA genes (highlighted in Figure 5) were consistently positively correlated between nuclear backgrounds in both sexes (females: $r = +0.97$, $t = 12.56$, d.f. $= 11$, $P = 7.279e{-}08$; males: $r = +0.86$, $t = 5.51$, d.f. $= 11$, $P = 0.0002$). Figure 5 shows the results for the unfiltered data set. The plots of the filtered data are shown in Figure S4. In both sexes, the genes from OXPHOS complex IV and ATP synthase are generally clustered together and this may reflect their stoichiometric dependence and strict regulation. Complex I genes, by contrast, demonstrate wide variation in $\log_2$-fold change as a result of mtDNA substitution. The CG34063 (*ND2*) gene is the only gene that is consistently upregulated in both nuclear backgrounds and in both sexes as a result of mtDNA substitution. For the mtDNA OXPHOS genes, the *ND2* gene was consistently ranked as the highest upregulated $\log_2$-fold change and *ND3* was consistently the lowest ranked (highest negative $\log_2$-fold change).

Clustering genes by between-genotype expression profiles

Using a clustering approach, we identified subsets of genes from the global distribution that demonstrated distinct expression patterns across the four genotypes. Theoretical profiles corresponding with mtDNA, nDNA, and mtDNA × nDNA interactions are described in Figure S1. In total, we produced $k = 20$ clusters for each sex and the filtered data set was used, since a large number of genes in the unfiltered data have zero read counts. Hybrid tree topologies and clusters are shown for females and males in Figure S5 and Figure S6, respectively. We identified a number of clusters that were consistent with first-order nuclear effects in both females and males (Figure 6 and Figure S7, respectively). Clear mtDNA effects were only apparent in the female data set and males showed very little evidence of mtDNA effects (see above).

Males showed an overwhelming enrichment of mitonuclear interactions across gene clusters (Figure S7). The effects of mtDNA substitution are largely in opposite directions in the alternative nuclear backgrounds, an effect that confirms the patterns of global gene expression we observed in Figure 5 using an independent analysis tool. In contrast, the female data set showed only a few examples of clusters consistent with mitonuclear interactions (black squares in Figure 6).

Cluster GO-enrichment analysis

To better understand which GO processes are associated with mitonuclear interactions, we performed a GO-enrichment analysis on each cluster in each sex. In females, 16/20 clusters contained GO terms that were significant ($P < 0.05$) after

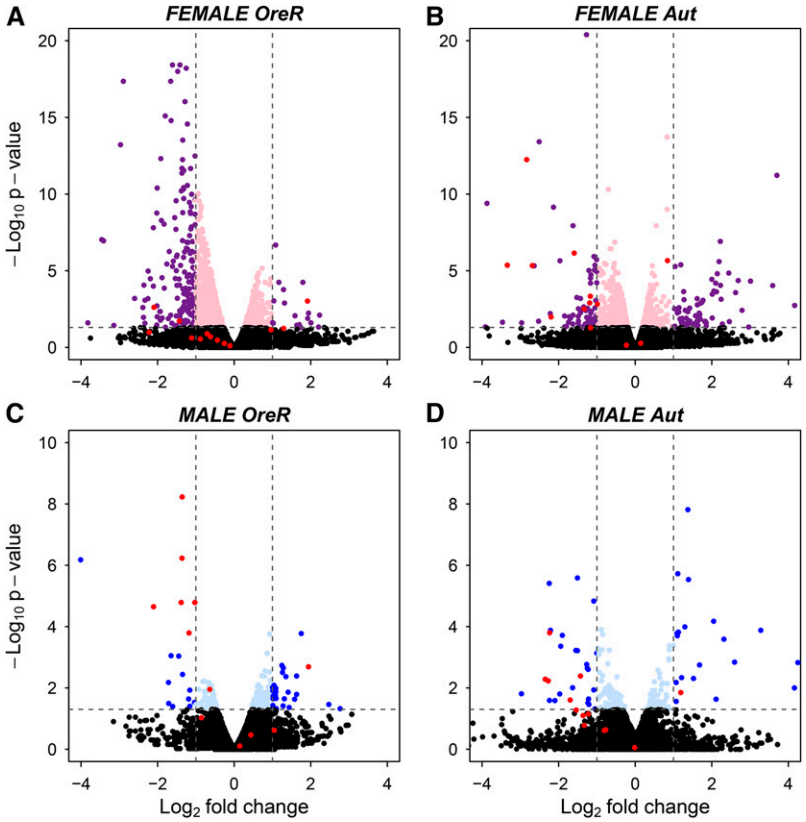

Figure 3 Effects of mtDNA substitution on gene expression across nuclear backgrounds and sexes. Volcano plots describe the $\log_2$-fold change in expression of genes and their corresponding $-\log_{10}$ *P*-value, as determined by DESeq. Female genotypes are shown on the top panel: (A) *Oregon R* nDNA, and (B) *AutW132* nDNA. Males are shown on the bottom panel: (C) *Oregon R* nDNA, and (D) *AutW132* nDNA. Data in red are the mtDNA genes. There are nuclear background effects on mtDNA substitution and females generally showed more effects of mtDNA haplotype on nuclear gene expression. Horizontal dashed lines show *P*-value cut offs at equivalent $P = 0.05$. Vertical dashed lines show $\pm 2 \times$ fold up- or downregulation of a gene due to alternative mtDNAs with values shown for *sil* mtDNA, relative to the *OregonR* mtDNA. Outliers are not shown and females have a different magnitude of variation on the ordinal scale than males. Note the consistent red datum in the top right section of each plot (*ND2* gene).

Bonferroni correction (Antonov *et al.* 2008), whereas only 13/20 clusters contained enriched terms in males. The full lists and significance of the GO terms are shown in Figure S8 (females) and Figure S9 (males).

Clusters with clear mitonuclear effects in females were clusters 17 and 18 (Figure 6). The most significantly enriched GO terms in these clusters were generally related to mitochondrial-ribosomal and protein translational processes (see clusters 17 and 18 in Figure S8).

edgeR statistical analyses

The clustering approach provided qualitative support for an excess of mitonuclear interactions in males, and a larger proportion of mtDNA effects in females. To formally test the effects of mtDNA, nuclear, and mitonuclear variation, we conducted a DE analysis using *edgeR* (Robinson *et al.* 2010) in each sex separately. We conducted separate tests in males and females because the RNA-seq libraries have inherent differences in dispersion (biological coefficients of variation) between sexes. Stratifying the analyses by sex ensured that we made comparisons of genetic effects using appropriate dispersion estimates without conflating the DE estimates.

Figure 7, A and B, describes the distributions of significantly differentially expressed genes ($P < 0.05$) in a sex-biased expression context. The plotted data are the mean expression values across all RNA-seq libraries in each sex. Significantly, DE genes corresponding to the three forms of genetic variation (mtDNA, nuclear, and mitonuclear) are highlighted as black, purple, and green data, respectively. In females (Figure 7A), there was a large overlap between DE genes from all three sources of genetic manipulation but these significant genes were not enriched in female- or male-biased genes. Likewise in males, the majority of genes significantly differentially expressed by nuclear type were found in both non-sex-biased regions of the distribution, along with male-limited regions that correspond with testes and sperm-related biological processes (Figure 1, Table 1). While we found a few genes in the male-limited region of the distribution that were DE by mtDNA variation, DE genes associated with mtDNA haplotype variation were not enriched in this region (Figure 7B).

Across sexes, there were magnitudinal differences in the numbers of genes differentially expressed by mtDNA, nuclear, and mtDNA $\times$ nuclear variation (Figure 7C); females showed larger responses to mtDNA and mitonuclear interactions, whereas males demonstrated marginally greater numbers of nuclear DE genes. For mtDNA variation (*siI/OregonR*), females demonstrated upregulation of 70 genes, and 39 genes were upregulated in males. There were 621 downregulated genes in females and 26 in males. By far the largest source of DE was for nuclear genetic variation (*AutW132/OregonR*) in both females (1737 up, 1952 down) and males (1836 up, 2246 down). Far fewer genes were associated with mitonuclear interactions (contrast *siI*; *AutW132 vs. OregonR*; *OregonR*) and these included 1462 in females and 556 in males. Interestingly, males showed larger numbers of DE genes in the mitonuclear category than in the first-order

Table 2 Genes intersected in both males and females and in both nuclear backgrounds in response to mtDNA substitution

Gene name	Flybase ID	Location	Symbol	CG number
A∩B∩C∩D intersection				
CG11966	FBgn0037645	3R: 8,950,246..8,963,037 (−)	CG11966	CG11966
Mitochondrial NADH-ubiquinone oxidoreductase chain 2	**FBgn0013680**	**mitochondrion_genome:240..1,265 (+)**	**mt:ND2**	**CG34063**
Mitochondrial ATPase subunit 6	**FBgn0013672**	**mitochondrion_genome:4,062..4,736 (+)**	**mt:ATPase6**	**CG34073**
Mitochondrial NADH-ubiquinone oxidoreductase chain 4L	**FBgn0013683**	**mitochondrion_genome:9,545..9,835 (−)**	**mt:ND4L**	**CG34086**
Jonah 25Bi	FBgn0020906	2L: 4,954,279..4,955,144 (−)	Jon25Bi	CG8867
A∩B∩C intersection				
Cyp28d1	FBgn0031689	2L: 5,210,460..5,212,445 (+)	Cyp28d1	CG10833
—	FBgn0035300	3L: 1,971,638..1,974,285 (+)	CG1139	CG1139
—	FBgn0038068	3R: 12,636,540..12,637,976 (+)	CG11600	CG11600
—	FBgn0033774	2R: 12,762,113..12,763,825 (+)	CG12374	CG12374
Chemosensory protein B 38c	FBgn0032888	2L: 20,820,089..20,820,867 (−)	CheB38c	CG14405
Integrin βν subunit	FBgn0010395	2L: 21,053,033..21,058,044 (+)	Itgbn	CG1762
εTrypsin	FBgn0010425	2R: 11,345,237..11,346,066 (−)	εTry	CG18681
Bent	FBgn0005666	4: 724,400..776,474 (+)	Bt	CG32019
—	FBgn0032494	2L: 13,239,989..13,241,773 (+)	CG5945	CG5945
—	FBgn0046999	2R: 16,873,015..16,873,755 (+)	CG6429	CG6429
Esterase 6	FBgn0000592	3L: 12,188,818..12,190,705 (+)	Est-6	CG6917
Hemolectin	FBgn0029167	3L: 13,846,054..13,860,001 (+)	Hml	CG7002
Henna	FBgn0001208	3L: 7,760,453..7,763,166 (+)	Hn	CG7399
Immune-regulated catalase	FBgn0038465	3R: 17,002,875..17,007,208 (+)	Irc	CG8913
A∩B∩D intersection				
Phosphoenolpyruvate carboxykinase	FBgn0003067	2R: 18,536,767..18,539,416 (+)	Pepck	CG17725
Ugt36Bc	FBgn0040260	2L: 16,799,025..16,801,584 (+)	Ugt36Bc	CG17932
Cyp6d5	FBgn0038194	3R: 14,029,228..14,031,483 (+)	Cyp6d5	CG3050
	FBgn0052023	3L: 8,803,602..8,804,182 (−)	CG32023	CG32023
Ankyrin 2	FBgn0261788	3L: 7,655,389..7,718,395 (−)	Ank2	CG42734[a]
	FBgn0053346	3R: 28,669,233..28,670,452 (+)	CG33346	CG33346
lectin-37Db	FBgn0053533	2L: 19,419,075..19,419,767 (+)	lectin-37Db	CG33533
	FBgn0053965	3L: 1,232,882..1,234,015 (+)	CG33965	CG33965
	FBgn0085256	2R: 11,248,126..11,248,610 (+)	CG34227	CG34227
	FBgn0038820	3R: 20,676,224..20,677,351 (−)	CG4000	CG4000
	FBgn0039474	3R: 27,020,238..27,021,378 (−)	CG6283	CG6283
	FBgn0037936	3R: 11,688,381..11,690,051 (−)	CG6908	CG6908
	FBgn0039670	3R: 29,587,237..29,588,104 (−)	CG7567	CG7567
	FBgn0039687	3R: 29,724,159..29,724,950 (−)	CG7593	CG7593
B∩C∩D intersection				
PGRP-SC2	FBgn0043575	2R: 8,716,950..8,717,695 (+)	PGRP-SC2	CG14745
PGRP-SC1a	FBgn0043576	2R: 8,709,733..8,710,320 (+)	PGRP-SC1a	CG14746
Mitochondrial NADH-ubiquinone oxidoreductase chain 3	**FBgn0013681**	**mitochondrion_genome: 5,608..5,961 (+)**	**mt:ND3**	**CG34076**
Mitochondrial cytochrome b	**FBgn0013678**	**mitochondrion_genome: 10,499..11,635 (+)**	**mt:Cyt-b**	**CG34090**
Mitochondrial NADH-ubiquinone oxidoreductase chain 1	**FBgn0013679**	**mitochondrion_genome: 11,721..12,659 (−)**	**mt:ND1**	**CG34092**

The genes required an unadjusted *P*-value ≤0.05 to be included in the analysis. The four-genotype intersection along with three three-way intersections are shown: (A) female *OregonR* background, (B) female *AutW132* background, (C) male *OregonR* background, and (D) male *AutW132* backgrounds. There were no genes present in the A∩C∩D intersection. Genes in boldface font are mtDNA protein coding genes.

[a] CG42734 overlaps with two additional computed genes (CGs): CG44195 and CG32373.

mtDNA category, consistent with the patterns we observed in the clustering analysis (see above).

To determine if genes behaved consistently across the sexes in response to genetic manipulation, we intersected those genes that were significantly differentially expressed ($P < 0.05$) by mtDNA, nuclear, and mitonuclear variation from females and males. The between-sex intersections are shown in Figure 8. There were 26 genes that were consistently differentially expressed by mtDNA variation, 1426 genes differentially expressed by nDNA variation, and 124 that were consistently differentially expressed by mitonuclear variation (Figure 8; gene identifications of the intersected genes can be found in Figure S10, Figure S11, and Figure S12). mtDNA genes are enriched in the intersected genes for mtDNA and nuclear variation, and *ATPase6*, *ND5*, and *ND6* demonstrate a consistent mitonuclear effect across the sexes. We found a large overlap between the consistently differentially expressed genes identified by DESeq (Table 2) and those identified by edgeR (Figure S10) as a consequence of mtDNA variation.

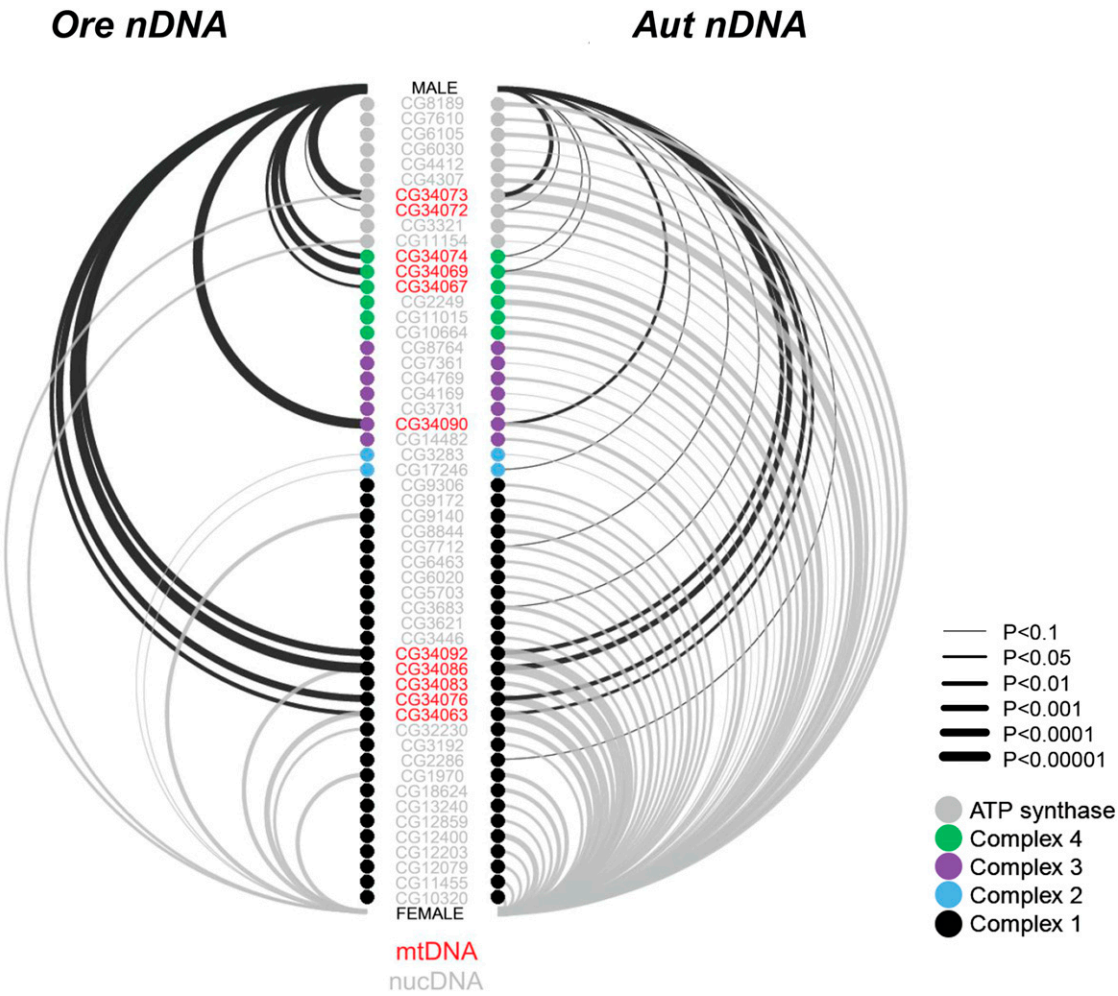

Figure 4 OXPHOS-related genes are differentially expressed by mtDNA substitution. Arcdiagrams (Sanchez 2014) show the identities of OXPHOS genes whose expression levels are affected by mtDNA variation. Line thicknesses correspond with the significance level. Gene identifiers in red are those encoded by mtDNA. Male effects (black lines) and female effects (gray lines) are shown. Different OXPHOS complexes are differentiated by circle color: complex I, black; complex II, blue; complex III, purple; complex IV, green; ATP synthase (complex V), gray. The effects in the *OregonR* nuclear background are shown in the left plot; *AutW132*, on the right. The data shown are from the filtered data set. nucDNA, nDNA.

Validating RNA-seq using qPCR

We used six nuclear genes that showed DE by nuclear variation and one internal control gene (*rp49*) to test whether the fold changes we measured using RNA-seq were correlated with qPCR. The methods and results can be found in File S1. The $\log_2$-fold change between *AutW132* and *Oregon R* in each mtDNA background was calculated for each gene in both sexes using the comparative threshold cycle (C_T) method ($2^{-\Delta\Delta CT}$) (Schmittgen and Livak 2008). We found a significant positive correlation between the $\log_2$-fold changes measured with RNA-seq and qPCR ($r = +0.69$, $t = 4.52$, d.f. $= 22$, $P = 0.00016$; Figure S13).

Discussion

We tested for the effects of mtDNA, nuclear, and mitonuclear variation on gene expression variation and found both genotype- and sex-specific responses to all three forms of genetic variation. Females showed overall stronger effects of genetic variation than males, and males showed little evidence of sex-limited expression of DE genes associated with mtDNA variation. mtDNA variation was most significantly associated with variation in mitochondrial OXPHOS gene expression and particularly those genes that are encoded by the mtDNA. In this panel of genotypes we found an overall opposing direction of mtDNA variation on global gene expression between the sexes, yet a conserved effect of mtDNA-encoded genes. Our findings are important to the *Drosophila* community, in which our reference strain, *OregonR*, has been widely adopted as a commonly used wild-type laboratory stock. Ongoing work in our laboratory aims to understand whether these effects are universal across multiple nuclear backgrounds, and not restricted to this particular nuclear *OregonR-AutW132* pair. We discuss our results in the context of OXPHOS protein organization, mtDNA–nDNA covariation, and the evolutionary significance of sex and genotype interactions.

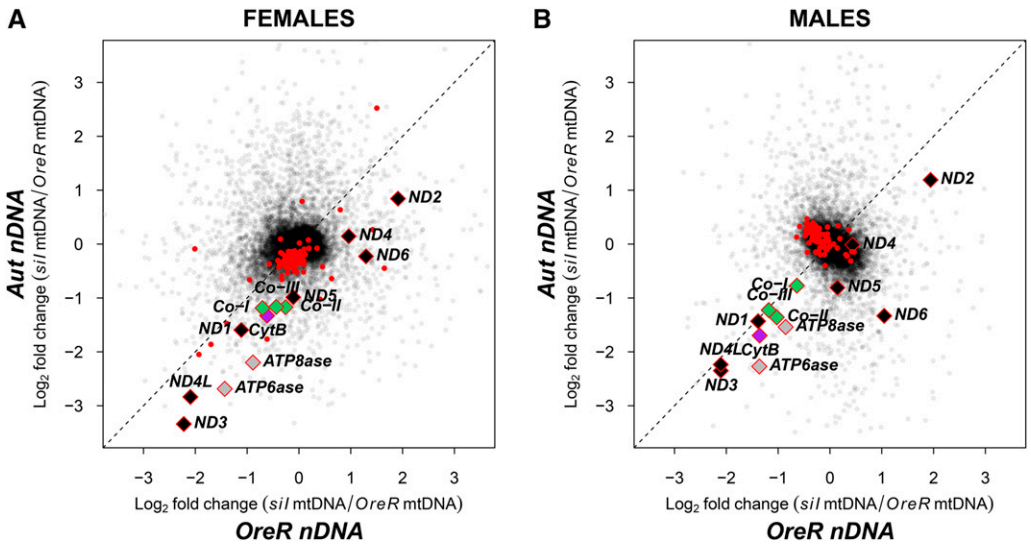

Figure 5 Mitonuclear effects on gene expression differ between the sexes. Biplots of mtDNA effects on gene expression are shown for (A) females and (B) males. The effects of mtDNA substitution are reported as $\log_2$-fold changes in the *OregonR* and *AutW132* background on the abscissa and ordinal, respectively. mtDNA genes are labeled with their gene identifiers and show positive correlations between nuclear backgrounds in both sexes. Nuclear OXPHOS genes (n = 73) are shown as red points. ND2 and ND3 genes were consistently ranked as the highest and lowest mtDNA genes, respectively. mtDNA genes are color coded by complex: complex I, black; complex III, purple; complex IV, green; ATP synthase, gray. Global gene correlations are reported in the main text.

Mitochondrial gene expression and fitness

Gene expression variation in mtDNA and nuclear-encoded mitochondrial genes has been associated with a large number of human diseases, including cancer (Penta *et al.* 2001), neurodegenerative diseases (Schapira 1998; Swerdlow and Khan 2009), aging (Toń ska *et al.* 2009), and type 2 diabetes mellitus (Mootha *et al.* 2003); however the exact mechanisms of action are poorly understood (Borowski *et al.* 2010). Early studies suggested the expression of OXPHOS genes in early development conditions the rate of electron transport enzyme activity throughout life in *Caenorhabditis elegans* (Dillin *et al.* 2002). More recently, knockdown of mitochondrial ribosomal proteins causes mitonuclear protein imbalance, reduced respiration, and activation of the mitochondrial UPR (Houtkooper *et al.* 2013). Paradoxically, this imbalance confers an overall positive, hormesis-like effect on life span and appears to be conserved between *C. elegans* and mammalian (mouse hepatocyte) cell lines. The regulation of mitochondrial genes is therefore important for organismal health, and transcript (or protein) imbalance between mitochondrial proteins may provide one arena for a cell to sense aberrant gene or protein function.

mtDNA substitution affects mtDNA expression

We found expression levels of mtDNA genes to be among the most differentially expressed between mtDNA haplotypes. Importantly, these differences were not unidirectional across all genes. In all nuclear background × sex combinations, the *siI* haplotype conferred upregulation of expression in some genes (*e.g.*, *ND2* gene), whereas genes from the same complex (complex I, *e.g.*, *ND3*) were among the most downregulated genes as a consequence of mtDNA substitution. This suggests that the relative abundance of transcripts is lower in *siI* haplotypes, however, there are exceptions to this rule (*e.g.*, *ND2*). For mtDNA genes, we found a strong positive correlation between $\log_2$-fold changes in each nuclear background, suggesting that mtDNA genes behave similarly in different nuclear backgrounds and sexes. Importantly, there was a consistent rank order for the genes that were most up- and downregulated as a consequence of mtDNA substitution.

Mitochondrial haplotype variation has previously been shown to modify mtDNA copy number variation and mtDNA protein coding gene expression on a common nuclear background in *Drosophila* (Camus *et al.* 2015). In that study, the *ND5* gene showed expression values consistent with phenotypic divergence, suggesting the mtDNA polymorphisms may behave as expression quantitative trait loci. The *ND2* gene was not assayed in Camus *et al.*'s study due to its high A+T content, so comparisons between the present study and that study cannot be made. We show that mtDNA substitution can have a large impact on relative gene expression when large numbers of nucleotide polymorphisms are present in the contrasting genotypes (*e.g.*, ∼103 amino acid substitutions and 418 synonymous SNPs between *Oregon R* and *siI* haplotypes). The results from the current study show that the impact of mtDNA haplotypes on mtDNA gene expression may be an additive effect of the point mutations that differ between the compared haplotypes.

Protein sequences or regulatory sequences?

Using the mitonuclear introgression model we specifically substituted alleles in the mtDNA coding region. We do not know the extent of mutations in the regulatory control region of the mtDNAs (D-loop), which is where transcription is initiated in *D. melanogaster* (Goddard and Wolstenholme

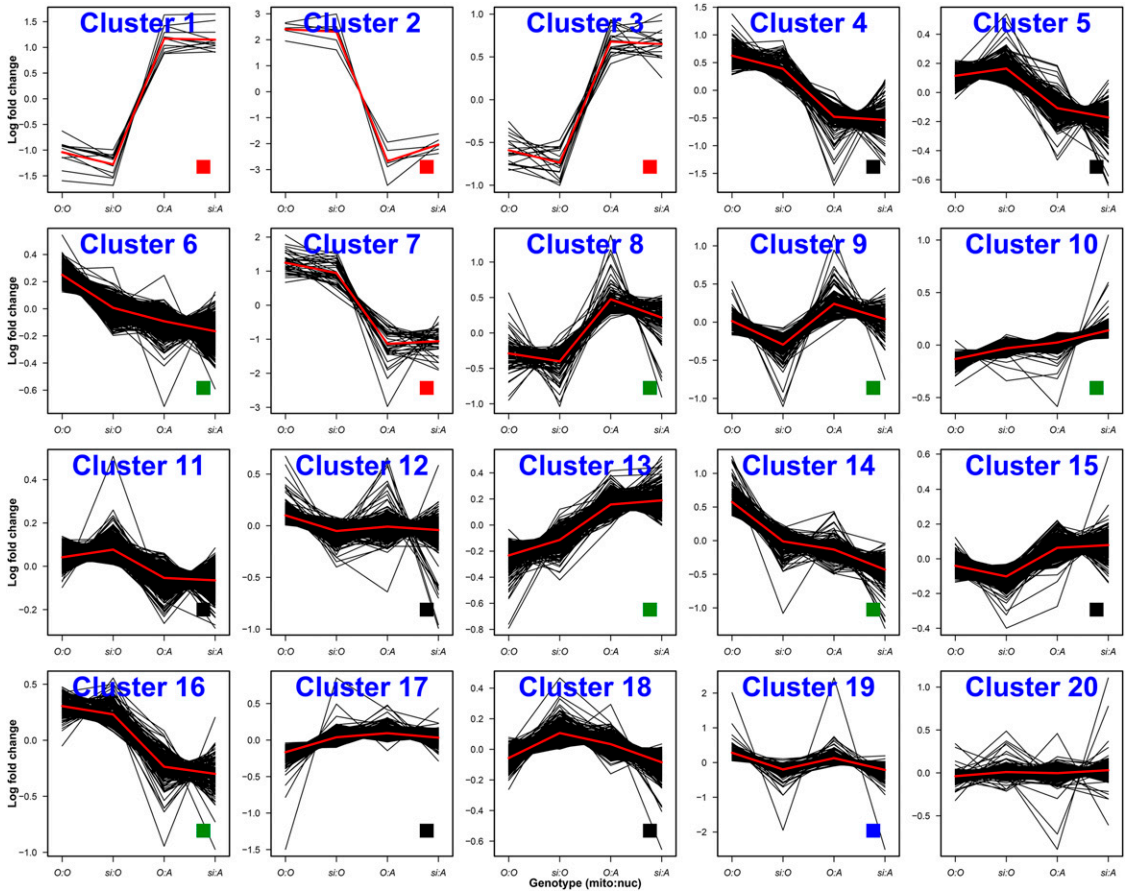

Figure 6 Gene clusters demonstrating a spectrum of genetic effects in females. The abscissa shows the (mito; nuclear) genotype. The log-fold change is shown on the ordinal as determined by MBClusterSeq. The black lines outline individual zero-centered gene profiles across genotypes. The red line is the per-genotype mean value across all genes in the cluster. The cluster figure for males is shown in Figure S7. Colored squares show the main genetic effect captured by the cluster, as cartooned in Figure S1: red, nuclear effect; blue, mtDNA effect; green, nuclear + mtDNA effect; black, mtDNA × nDNA interaction. *A*, *AutW132*; *O*, *OregonR*.

1978) and *D. simulans* (Goddard and Wolstenholme 1980). In both species, at least one (Clayton 1982) origin of replication occurs roughly in the center of the A+T-rich region (Goddard and Wolstenholme 1978; Wolstenholme 1992; Lewis *et al.* 1994; Torres *et al.* 2009). Our findings suggest that protein products of genes that assemble in a single complex (complex I) can have drastically different transcript abundance, and the mutations that segregate between *siI* and *OregonR* haplotypes alter expression in a gene-by-gene basis.

Complex I is one of the largest and most complicated enzymes in the eukaryotic cell (Vinothkumar *et al.* 2014), and its crystal structure has been resolved across a wide range of species, *e.g.*, *Escherichia coli* (Efremov and Sazanov 2011), *Thermus thermophilus* (Efremov *et al.* 2010), and *Bos taurus* (Vinothkumar *et al.* 2014). Among the consistent characteristics are the protein identifiers and their spatial organization within the membrane domain (Vinothkumar *et al.* 2014). One of the earliest genome-wide coexpression analyses provided good evidence in *Saccharomyces cerevisiae* that genes that physically interact or are present in the same metabolic pathway have similar expression levels (DeRisi *et al.* 1997). Our results show that a "healthy" fly can exhibit wide variation in mtDNA transcripts from some complexes (*e.g.*, complex I), yet consistent coexpression patterns across other complexes (*e.g.*, complex IV and ATP synthase). Taken together, these results suggest some transcripts are more sensitive to genetic polymorphism than others, and that transcript *variation* within a protein complex may provide a useful trait to characterize the effects of mutations, and whether these effects are associated with deleterious phenotypes. Finally, the phenotypic effects on separate mitochondrial respiratory functions could help pinpoint whether complexes with tightly regulated transcripts perform better than those that have wide variation. If wide variation is deleterious, we would predict that complex I function, for example, would show more wide-ranging phenotypes between *siI* and *OregonR* haplotypes, than complex IV.

Why would *ND2* be massively upregulated and *ND3* massively downregulated as a result of *siI* mutations? In spite of their physical proximity in the mitochondrial inner membrane domain, we found those OXPHOS genes that were most sensitive to mtDNA variation are adjacent proteins (Vinothkumar *et al.* 2014). For example, Figure 5 shows that gene transcripts *ND3* and *ND4L* are closely grouped in the

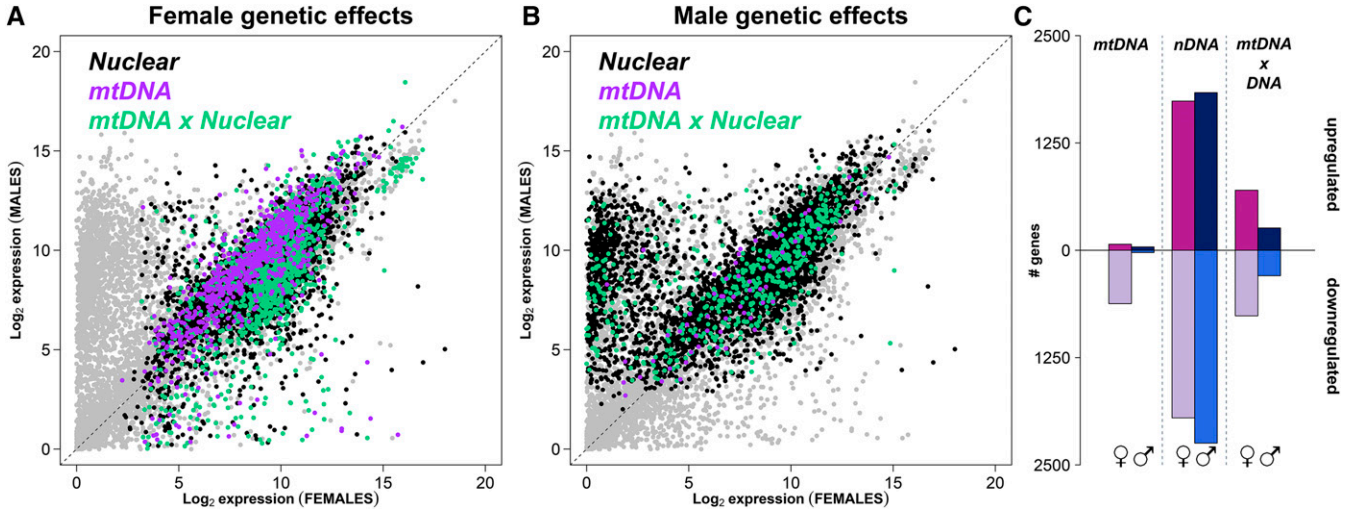

Figure 7 The distribution of significant mtDNA, nDNA, and mitonuclear genotypes in expression space. Results of edgeR analyses on the complete data set are shown. Female expression is plotted on the abscissa, males on the ordinal. The position of differentially expressed genes by nuclear (black), mtDNA (purple), and mtDNA × nDNA (green) variation are shown for (A) females and (B) males. The absolute numbers of significant genes in each category are described in bar plots in (C). Results for each category are divided into up- and downregulated genes. For each category females are shown leftmost, males rightmost.

plot. Likewise, *ND2* and *ND4* are consistently upregulated in both nuclear backgrounds and in both sexes. The patterns of expression are coextensive with the position of protein products; *ND3* and *ND4L*, and *ND2* and *ND4* are adjacent proteins in the membrane. Given that there are only seven mtDNA-encoded proteins in the membrane domain it is possible that this observation would be expected by chance, however it does suggest that conversion rates of transcript to protein may depend on the position of a protein in the membrane.

We have previously identified a number of SNPs that are different between the coding regions of *siI* and *OregonR* haplotypes and which have putative deleterious effects on protein function (Mossman *et al.* 2016). One of the private mutations to the *siI-OregonR* pair resides in the *ND2* gene and is two amino acids downstream of a putative deleterious amino acid polymorphism. Future work will aim to characterize whether this putative mutation is involved in the upregulation of the gene, possibly as a response to deleterious protein function; resulting in overall genetic robustness. Previous studies have shown that gene transcription responds to genetic mutation and may rescue phenotypes via a compensatory network (Kafri *et al.* 2005; Rossi *et al.* 2015). Moreover, during mammalian mtDNA transcription, polypeptides are theoretically transcribed in a 1:1 ratio because the polycistronic transcripts are fully transcribed from both mtDNA duplex strands (Gagliardi *et al.* 2004). In *Drosophila* mtDNA there are five different transcription initiation sites and transcript cleavage is signaled by the presence of cloverleaf structures of tRNAs (Ojala *et al.* 1981). There is considerable heterogeneity in mRNA expression between mtDNA genes within OXPHOS complexes, and these differences are largest in complex I (NADH dehydrogenase) (Torres *et al.* 2009). We also found NADH dehydrogenase to have the widest variation in $\log_2$-fold change when comparisons were conducted within a gene (as a consequence of mtDNA variation). That is, mtDNA genetic variation was associated with differences in $\log_2$-fold change. Taken together, these results suggest complex I gene expression shows wide variation (i) across genes within a complex and (ii) within genes as a consequence of mtDNA variation.

Following cleavage via endonucleases, polypeptide mRNAs are processed with a theoretical uniform abundance, which we did not observe. Given our haplotypes were from separate species, and those species have different control regions, with variable length and possibly SNP polymorphisms, it is possible that these regions alone are associated with the expression differences, with SNP variation having negligible effect. However, we favor the hypothesis that SNP variation does impact transcript levels, simply because a main effect of the regulatory (D-loop) region would presumably affect transcript levels in a more universal way, with little evidence of gene-specific expression patterns. Heterogeneity in transcript abundance across genes in *Drosophila* has been suggested to result from various post-transcriptional mechanisms including differential transcript stability and differences in the processing of mature transcripts (Torres *et al.* 2009). Our results suggest mtDNA variation can modify mtDNA gene transcriptional regulation and that complex I is particularly sensitive to mtDNA variation in this mtDNA haplotype pair (*OregonR vs. siI*).

Gene-by-gene interactions for transcription

mtDNA-encoded protein genes showed the most consistent patterns of DE identified using multiple analysis tools. Three mtDNA genes (ND5, ND6, and ATPase6; Figure S12) demonstrated a significant mitochondrial × nuclear effect in both

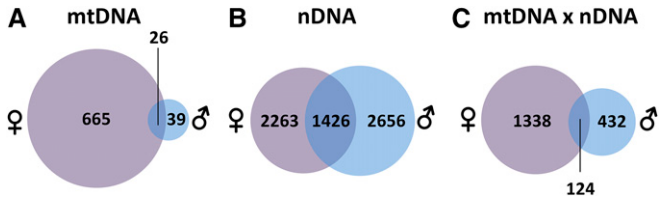

Figure 8 Robust differentially expressed genes across (A) mtDNA, (B) nDNA, and (C) mtDNA × nDNA categories. Venn diagrams describe the intersection of gene identifiers by sex in each category, as determined by DE analysis in edgeR on the complete data set. The area of the circles is relative to the number of genes within a category. Females are shown on the left, and males on the right of each diagram. Genes within the intersection between females and males are listed in Figure S10, Figure S11, and Figure S12 for each category, respectively.

sexes. That is, the effect of mtDNA substitution in one nuclear background was different from the effect in the other. As expected, nDNA variation was associated with DE in many genes in both males and females, however, we found females were generally more sensitive to mtDNA variation, particularly for OXPHOS complex genes. While males showed gene clusters consistent with mitonuclear effects, these were generally low magnitude differences and were not detected using DE analyses. We also found a larger effect in the *AutW132* nuclear background than in the *OregonR* nuclear background in females. Our gene lists (in Figure S10, Figure S11, and Figure S12) documenting the genes that were consistently differentially expressed across sexes are likely conservative estimates. On the other hand, they represent core sets of genes that are robustly differentially expressed across genetic backgrounds and sexes. Our clustering analyses showed clear evidence that many transcripts have gene-by-gene interaction patterns in males, yet mainly mtDNA effects in females; a pattern that was consistent across analysis tools. Interestingly, the nuclear genes involved in OXPHOS showed mitonuclear patterns in males, but no mitonuclear effects in females (red dots in Figure 5). Using an agnostic clustering approach, we identified sets of genes that showed similar expression patterns across genotypes and which were enriched for GO categories associated with mitochondrial function. It is now well established that genes in the same pathway share similar levels of expression (Stuart *et al.* 2003; Kafri *et al.* 2005) and we detected a strong signal that mitonuclear interaction gene clusters were enriched for processes involving translation and mitochondrial metabolism in both sexes. Moreover, the mtDNA OXPHOS genes tended to cluster in complex-specific clusters and this effect was more noticeable in females than in males. Similar results have been observed in humans where genes from distinct OXPHOS complexes tend to cluster together (van Waveren and Moraes 2008).

The female transcriptome is more sensitive to genetic variation

Considering the global gene set, we found that females exhibit clear genotype-specific transcript profiles regardless of the gene set analyzed. In contrast, the MDS plots revealed males are distinguishable by nuclear backgrounds across all genes, but the effects of mtDNA are only present in the most differentially expressed gene sets and mainly restricted to the *AutW132* nuclear background. This first suggests that mtDNA genes are among the most differentially expressed in males, and second, that mtDNA × nDNA interactions are present in males, and these operate on a large subset of the complete gene set. These were generally smaller in magnitude than in females. This phenomenon may help explain why a greater number of mitonuclear interactions were observed in males via gene clustering and these made detection of first-order effects of mtDNA and nuclear variation more difficult as fewer genes achieved statistical significance with DE-analysis tools. Using a combination of DE analyses provides clearer evidence that male and female transcriptomes respond differently to mitonuclear variation, and suggests a much larger number of genes are sensitive to mitonuclear variation in males, even though these are not "significantly" differentially expressed.

Retrograde signaling is more prevalent in females

We found mtDNA substitution in females conferred large effects on nuclear genes, suggesting pervasive retrograde signaling (mtDNA-to-nDNA feedback) between the genomes, and a clear separation of genotypes based on transcript expression. The effects of mtDNA variation were less obvious in males and a significantly smaller number of nuclear genes responded to mtDNA variation. While we acknowledge that there could be inherent differences between the male and female RNA-seq libraries due to a block effect, we conducted the majority of analyses within a sex to minimize a block effect on analyses interpretation. The magnitude and direction of $\log_2$-fold change in mtDNA genes were similar across sexes, suggesting we were able to capture real biological signal for the most differentially expressed genes. Importantly, when correlations (Figure 5) were compared across sexes, our mitonuclear results demonstrate a clear sexual dimorphism, even though the within-sex effects were calculated with sex-specific dispersion parameters. Under a null hypothesis of no sex-specific mitonuclear effect, we would not expect the sexes to differ in the direction of effect for the global pattern of expression. Given that the majority of male transcripts did not respond significantly to first-order mtDNA variation, the global transcript negative correlation we observed between nuclear backgrounds may be a product of reduced signal of mtDNA effects. However, mtDNA genes did respond and the mtDNA effect, while small for the majority of the transcriptome, was in the opposite direction in females. Our results show that the sensitivity to detect first-order effects of mtDNA variation are hindered by mitonuclear interactions, and a clustering approach is more likely to capture interaction effects. One interesting question arises: is this evidence of sexual antagonism (Rice 1984) for gene expression?

Genes from both mtDNA and nDNA genomes can respond to selection in females. The female environment likely provides the only opportunity for mitonuclear expression to be

exposed to selection, even though genes spend, on average, half their lifetime in each sex. Under this scenario, it has been suggested that nuclear genes that interact with mtDNAs would benefit from being on the *X* chromosome because there is greater opportunity for cotransmission and therefore coadaptation with mtDNA (Rand *et al.* 2001; Wade and Goodnight 2006). In *Drosophila*, the *X* chromosome has been implicated in mitonuclear epistatic interactions (Rand *et al.* 2001; Montooth *et al.* 2010), providing an opportunity to reduce intraindividual genetic conflict (*sensu* Werren 2011). However, mitonuclear genes are underrepresented on the *X* chromosome in *Drosophila* (Rogell *et al.* 2014), a pattern that is consistent also across various mammals (Drown *et al.* 2012) and *C. elegans* (Dean *et al.* 2014). Further, nuclear-mitochondrial gene duplications, which could help mitigate sexual conflict, are rarely relocated to the *X* chromosome in *Drosophila* (Gallach *et al.* 2010). In contrast, birds do not show under- or overrepresentation of mitonuclear genes on the *Z* chromosome (in birds, males are the homogametic sex and genes on the *Z* chromosome were tested; Drown *et al.* 2012).

Alternative sexual conflict-based hypotheses have been proposed to explain these observations (Drown *et al.* 2012; Dean *et al.* 2014; Rogell *et al.* 2014). Our results suggest pervasive retrograde signaling occurs between mtDNA and nuclear genes, motivating that future investigations on mitonuclear coevolution should focus on key regions of the nuclear genome that harbor mitonuclear interacting genes, and not just canonical OXPHOS or mitochondrial genes encoded by nDNA. For example, do these nuclear loci demonstrate evidence of unique patterns of selection compared to closely linked loci? We identified two nuclear genes, *CG11966* and *Jonah 25Bi*, that show consistent evidence of retrograde signaling in all genotypes and in both sexes. These genes are sensitive to mtDNA polymorphism, yet are not OXPHOS genes. We have also described a gene list of mitonuclear genes that are attractive targets of such a study (Figure S12).

mtDNA effects are not limited to males or male-limited genes

The Frank and Hurst hypothesis (Frank and Hurst 1996)—that males are more sensitive to mtDNA substitution—has limited support in this study. We found the mtDNA protein coding genes to be enriched in the gene list that was differentially expressed by mtDNA variation, and this effect was consistent across nuclear backgrounds. We also found a similar effect in females. While these findings suggest males are not suffering *more* than females as a result of mtDNA substitution, the enrichment of mtDNA genes *per se* is some evidence that males are sensitive to exclusively OXPHOS genes (Figure 4). It is possible that the nucleotide substitutions between *siI* and *OregonR* do not manifest with sufficiently large effect sizes on globally expressed genes to be detected in males, as has been observed in other mtDNA-variation studies on gene expression (Innocenti *et al.* 2011). Moreover in Innocenti *et al.*'s study, the effects of mtDNA substitution in a *w1118 D. melanogaster* background were enriched in male-limited genes. Their finding evidenced a sex-specific selective sieve, whereby mtDNA mutations that were not under selection in males (due to maternal inheritance) could principally manifest in male-limited tissue as males are at a genetic dead end for mtDNA evolution. To independently test for mtDNA-associated expression differences in sex-limited genes, we also conducted our investigation on whole flies, including all reproductive tissue. We acknowledge that whole fly analyses cannot resolve sex-biased expression that may be due to differences in tissue contributions. However, we wanted to make our analyses comparable to other whole organism gene expression studies in *Drosophila*. We found no differences in fecundity between the strains used in this study (see File S1, Figure S14, Table S2, Table S3), suggesting the rate of turnover of gametes, and hence reproductive tissue mass, was not significantly different between strains and was unlikely to bias gene expression values between genotypes. Pathological mtDNA mutations principally manifest in tissues with high ATP demand (reviewed in Stewart and Chinnery 2015). The tissue-specific pathological effects of mtDNA variants in humans is a good motivation for future work to specifically test gene expression differences in tissues with high ATP demand in fruit flies, such as neuronal tissue, or flight muscle.

We did not recapitulate the sex-specific selective sieve effect in our study, in spite of (i) significant numbers of genes that demonstrated sex-specific gene expression (Figure 1), and (ii) large amounts of nucleotide variation between our haplotypes (>100 amino acid substitutions, and >400 synonymous mtDNA polymorphisms). Instead, we found no enrichment for mtDNA effects in male-biased genes [in regions of the gene expression space associated with male-limited traits (*e.g.*, spermatogenesis and testes)]. We only considered a pairwise comparison of mtDNA variation, in contrast to Innocenti *et al.*'s five haplotypes, and hence do not have the same polymorphisms present in our experiment. However, it is possible that the *w1118* nuclear background used in Innocenti *et al.* (2011) is more sensitive to mtDNA variation than other nuclear backgrounds and these differences may manifest disproportionately in males. In the present study we found greater mtDNA sensitivity in the *AutW132* background, providing good evidence that nuclear background *per se* can alter the sensitivity of the transcriptome to mtDNA variation. A main take home message in the present study is that there are differences between nuclear backgrounds and these can modify the effects of mtDNA variation. Extensive evidence of mtDNA × nDNA interactions on phenotypes (Mossman *et al.* 2016), including comparisons with the *w1118* background (Zhu *et al.* 2014), suggests mtDNA haplotype-associated phenotypes are not always general results across nuclear backgrounds. We are now assessing the effects of environment on mitonuclear interactions to test whether mitonuclear effects are influenced by environment (gene-by-gene-by-environment interactions), or whether genotypes are robust to environmental perturbation. Previous studies suggest environment can have a large and sometimes

unpredictable effect on mitonuclear interactions (Mossman *et al.* 2016), however, there are no studies quantifying this in *Drosophila* gene expression.

In summary, we found considerable variation in transcript expression as a result of mtDNA, nDNA, and mitonuclear substitution. Contrary to the Frank and Hurst hypothesis, we did not find enrichment of mtDNA effects targeting male-limited gene expression in males. However, we did find large sex differences in the effects of genetic manipulation. In general, females showed larger genetic effects on transcript abundance and female genotypes were distinguishable based on their global gene-expression patterns, inconsistent with the lower sensitivity in males. In males, the majority of transcripts demonstrated mitonuclear effects in clustering analyses. Although mtDNA genes were preferentially differentially expressed, we interpret this as evidence that both mtDNA and nDNA covariation are important for transcript expression in this genotype panel. Future work will identify: (i) if these effects are general over a larger suite of genotypes, and (ii) by what mechanisms of action do mtDNA haplotypes affect gene expression. For example, are the polymorphisms in genic regions of the mtDNA responsible, or is variation in the mtDNA regulatory region key to the observed expression patterns? Are these effects tissue specific? Our general findings suggest that mtDNA effects can vary between nuclear genetic backgrounds depending on the sex tested, and therefore therapeutic methods to overcome mitochondrial diseases in humans should consider mitonuclear covariation as potential sources of phenotypic variation and therapy outcomes.

Acknowledgments

We thank Christoph Schorl for assistance in the processing of RNA sequencing libraries, and Mark Howison for demultiplexing the samples. Jason Wood provided scripting help and Leann Biancani provided assistance with fly husbandry. A.-M. Hernandez gave critical comments on the manuscript. This work was conducted using computational resources and services at the Center for Computation and Visualization, Brown University. This project was funded by National Institutes of Health grants R01 GM-067862 and AG-027849 to D.M.R.

Author contributions: J.G.T. prepared flies for the experiment. J.A.M. and J.G.T. extracted RNA and conducted RNA sequencing. J.A.M. conducted the quantitative PCR analyses, analyzed the data with input from N.L. and W.Z., and wrote the manuscript with comments from D.M.R.

Literature Cited

Anders, S., and W. Huber, 2010 Differential expression analysis for sequence count data. Genome Biol. 11: 1–12.

Anders, S., P. T. Pyl, and W. Huber, 2015 HTSeq—a Python framework to work with high-throughput sequencing data. Bioinformatics 31: 166–169.

Antonov, A. V., 2011 BioProfiling.de: analytical web portal for high-throughput cell biology. Nucleic Acids Res. 39: 323–327.

Antonov, A. V., T. Schmidt, Y. Wang, and H. W. Mewes, 2008 ProfCom: a web tool for profiling the complex functionality of gene groups identified from high-throughput data. Nucleic Acids Res. 36: 347–351.

Ayroles, J. F., M. A. Carbone, E. A. Stone, K. W. Jordan, R. F. Lyman *et al.*, 2009 Systems genetics of complex traits in Drosophila melanogaster. Nat. Genet. 41: 299–307.

Benjamini, Y., and Y. Hochberg, 1995 Controlling the false discovery rate: a practical and powerful approach to multiple testing. J. R. Stat. Soc. B 57: 289–300.

Bernes, S. M., C. Bacino, T. R. Prezant, M. A. Pearson, T. S. Wood *et al.*, 1993 Identical mitochondrial DNA deletion in mother with progressive external ophthalmoplegia and son with Pearson marrow-pancreas syndrome. J. Pediatr. 123: 598–602.

Borowski, L. S., R. J. Szczesny, L. K. Brzezniak, and P. P. Stepien, 2010 RNA turnover in human mitochondria: more questions than answers? Biochim Biophys Acta 1797: 1066–1070.

Bourgon, R., R. Gentleman, and W. Huber, 2010 Independent filtering increases detection power for high-throughput experiments. Proc. Natl. Acad. Sci. USA 107: 9546–9551.

Camus, M. F., D. J. Clancy, and D. K. Dowling, 2012 Mitochondria, maternal inheritance, and male aging. Curr. Biol. 22: 1717–1721.

Camus, M. F., J. B. Wolf, E. H. Morrow, and D. K. Dowling, 2015 Single nucleotides in the mtDNA sequence modify mitochondrial molecular function and are associated with sex-specific effects on fertility and aging. Curr. Biol. 25: 2717–2722.

Casademont, J., A. Barrientos, F. Cardellach, A. Rotig, J. M. Grau *et al.*, 1994 Multiple deletions of mtDNA in 2 brothers with sideroblastic anemia and mitochondrial myopathy and in their asymptomatic mother. Hum. Mol. Genet. 3: 1945–1949.

Clayton, D. A., 1982 Replication of animal mitochondrial DNA. Cell 28: 693–705.

D'Elia, D., D. Catalano, F. Licciulli, A. Turi, G. Tripoli *et al.*, 2006 The MitoDrome database annotates and compares the OXPHOS nuclear genes of Drosophila melanogaster, Drosophila pseudoobscura and Anopheles gambiae. Mitochondrion 6: 252–257.

Dean, R., F. Zimmer, and J. E. Mank, 2014 The potential role of sexual conflict and sexual selection in shaping the genomic distribution of mito-nuclear genes. Genome Biol. Evol. 6: 1096–1104.

DeRisi, J. L., V. R. Iyer, and P. O. Brown, 1997 Exploring the metabolic and genetic control of gene expression on a genomic scale. Science 278: 680–686.

Dillin, A., A.-L. Hsu, N. Arantes-Oliveira, J. Lehrer-Graiwer, H. Hsin *et al.*, 2002 Rates of behavior and aging specified by mitochondrial function during development. Science 298: 2398–2401.

Dimauro, S., and G. Davidzon, 2005 Mitochondrial DNA and disease. Ann. Med. 37: 222–232.

DiMauro, S., and E. A. Schon, 2003 Mechanisms of disease: mitochondrial respiratory-chain diseases. N. Engl. J. Med. 348: 2656–2668.

Drown, D. M., K. M. Preuss, and M. J. Wade, 2012 Evidence of a paucity of genes that interact with the mitochondrion on the X in mammals. Genome Biol. Evol. 4: 875–880.

Eden, E., R. Navon, I. Steinfeld, D. Lipson, and Z. Yakhini, 2009 GOrilla: a tool for discovery and visualization of enriched GO terms in ranked gene lists. BMC Bioinformatics 10: 1–7.

Efremov, R. G., and L. A. Sazanov, 2011 Structure of the membrane domain of respiratory complex I. Nature 476: 414–420.

Efremov, R. G., R. Baradaran, and L. A. Sazanov, 2010 The architecture of respiratory complex I. Nature 465: 441–445.

Frank, S. A., and L. D. Hurst, 1996 Mitochondria and male disease. Nature 383: 224.

Friberg, U., and D. K. Dowling, 2008 No evidence of mitochondrial genetic variation for sperm competition within a population of Drosophila melanogaster. J. Evol. Biol. 21: 1798–1807.

Friedman, J. R., and J. Nunnari, 2014 Mitochondrial form and function. Nature 505: 335–343.
Gagliardi, D., P. P. Stepien, R. J. Temperley, R. N. Lightowlers, and Z. M. A. Chrzanowska-Lightowlers, 2004 Messenger RNA stability in mitochondria: different means to an end. Trends Genet. 20: 260–267.
Gallach, M., C. Chandrasekaran, and E. Betrán, 2010 Analyses of nuclearly encoded mitochondrial genes suggest gene duplication as a mechanism for resolving intralocus sexually antagonistic conflict in Drosophila. Genome Biol. Evol. 2: 835–850.
Gemmell, N. J., V. J. Metcalf, and F. W. Allendorf, 2004 Mother's curse: the effect of mtDNA on individual fitness and population viability. Trends Ecol. Evol. 19: 238–244.
Gibson, G., R. Riley-Berger, L. Harshman, A. Kopp, S. Vacha *et al.*, 2004 Extensive sex-specific nonadditivity of gene expression in Drosophila melanogaster. Genetics 167: 1791–1799.
Giordano, C., L. Iommarini, L. Giordano, A. Maresca, A. Pisano *et al.*, 2014 Efficient mitochondrial biogenesis drives incomplete penetrance in Leber's hereditary optic neuropathy. Brain 137: 335–353.
Goddard, J. M., and D. R. Wolstenholme, 1978 Origin and direction of replication in mitochondrial DNA molecules from Drosophila melanogaster. Proc. Natl. Acad. Sci. USA 75: 3886–3890.
Goddard, J. M., and D. R. Wolstenholme, 1980 Origin and direction of replication in mitochondrial DNA molecules from the genus Drosophila. Nucleic Acids Res. 8: 741–757.
Hoekstra, L. A., M. A. Siddiq, and K. L. Montooth, 2013 Pleiotropic effects of a mitochondrial-nuclear incompatibility depend upon the accelerating effect of temperature in Drosophila. Genetics 195: 1129–1139.
Holmbeck, M. A., J. R. Donner, E. Villa-Cuesta, and D. M. Rand, 2015 A Drosophila model for mito-nuclear diseases generated by an incompatible interaction between tRNA and tRNA synthetase. Dis. Model. Mech. 8: 843–854.
Houtkooper, R. H., L. Mouchiroud, D. Ryu, N. Moullan, E. Katsyuba *et al.*, 2013 Mitonuclear protein imbalance as a conserved longevity mechanism. Nature 497: 451–457.
Huang, W., 2012 Epistasis dominates the genetic architecture of Drosophila quantitative traits. Proc. Natl. Acad. Sci. USA 109: 15553–15559.
Huang, W., A. Massouras, Y. Inoue, J. Peiffer, M. Ramia *et al.*, 2014 Natural variation in genome architecture among 205 Drosophila melanogaster Genetic Reference Panel lines. Genome Res. 24: 1193–1208.
Innocenti, P., E. H. Morrow, and D. K. Dowling, 2011 Experimental evidence supports a sex-specific selective sieve in mitochondrial genome evolution. Science 332: 845–848.
Jacobs, H. T., and D. M. Turnbull, 2005 Nuclear genes and mitochondrial translation: a new class of genetic disease. Trends Genet. 21: 312–314.
Kafri, R., A. Bar-Even, and Y. Pilpel, 2005 Transcription control reprogramming in genetic backup circuits. Nat. Genet. 37: 295–299.
Lewis, D. L., C. L. Farr, A. L. Farquhar, and L. S. Kaguni, 1994 Sequence, organization, and evolution of the A+T region of Drosophila melanogaster mitochondrial DNA. Mol. Biol. Evol. 11: 523–538.
Li, H., B. Handsaker, A. Wysoker, T. Fennell, J. Ruan *et al.*, 2009 The sequence alignment/map format and SAMtools. Bioinformatics 25: 2078–2079.
Lin, M. T., and M. F. Beal, 2006 Mitochondrial dysfunction and oxidative stress in neurodegenerative diseases. Nature 443: 787–795.
Mackay, T. F. C., S. Richards, E. A. Stone, A. Barbadilla, J. F. Ayroles *et al.*, 2012 The Drosophila melanogaster genetic reference panel. Nature 482: 173–178.
Martin, W., and M. Muller, 1998 The hydrogen hypothesis for the first eukaryote. Nature 392: 37–41.
Meiklejohn, C. D., M. A. Holmbeck, M. A. Siddiq, D. N. Abt, D. M. Rand *et al.*, 2013 An incompatibility between a mitochondrial tRNA and its nuclear-encoded tRNA synthetase compromises development and fitness in Drosophila. PLoS Genet. 9: e1003238.
Montooth, K. L., C. D. Meiklejohn, D. N. Abt, and D. M. Rand, 2010 Mitochondrial-nuclear epistasis affects fitness within species but does not contribute to fixed incompatibilities between species of Drosophila. Evolution 64: 3364–3379.
Mootha, V. K., C. M. Lindgren, K.-F. Eriksson, A. Subramanian, S. Sihag *et al.*, 2003 PGC-1[alpha]-responsive genes involved in oxidative phosphorylation are coordinately downregulated in human diabetes. Nat. Genet. 34: 267–273.
Mossman, J. A., J. Slate, T. R. Birkhead, H. D. Moore, and A. A. Pacey, 2012 Mitochondrial haplotype does not influence sperm motility in a UK population of men. Hum. Reprod. 27: 641–651.
Mossman, J. A., L. M. Biancani, C.-T. Zhu, and D. M. Rand, 2016 Mitonuclear epistasis for development time and its modification by diet in Drosophila. Genetics 203: 463–484.
Ojala, D., J. Montoya, and G. Attardi, 1981 tRNA punctuation model of RNA processing in human mitochondria. Nature 290: 470–474.
Penta, J. S., F. M. Johnson, J. T. Wachsman, and W. C. Copeland, 2001 Mitochondrial DNA in human malignancy. Mutat. Res. Rev. Mutat. Res. 488: 119–133.
Pereira, L., J. Goncalves, R. Franco-Duarte, J. Silva, T. Rocha *et al.*, 2007 No evidence for an mtDNA role in sperm motility: data from complete sequencing of asthenozoospermic males. Mol. Biol. Evol. 24: 868–874.
Pesole, G., J. F. Allen, N. Lane, W. Martin, D. M. Rand *et al.*, 2012 The neglected genome. EMBO Rep. 13: 473–474.
Quiros, P. M., A. Mottis, and J. Auwerx, 2016 Mitonuclear communication in homeostasis and stress. Nat. Rev. Mol. Cell Biol. 17: 213–226.
Rand, D. M., 2001 The units of selection on mitochondrial DNA. Annu. Rev. Ecol. Syst. 32: 415–448.
Rand, D. M., A. G. Clark, and L. M. Kann, 2001 Sexually antagonistic cytonuclear fitness interactions in Drosophila melanogaster. Genetics 159: 173–187.
Rice, W. R., 1984 Sex chromosomes and the evolution of sexual dimorphism. Evolution 38:735–742.
Ritchie, M. E., B. Phipson, D. Wu, Y. Hu, C. W. Law *et al.*, 2015 limma powers differential expression analyses for RNA-sequencing and microarray studies. Nucleic Acids Res. 43: e47.
Robinson, M. D., D. J. McCarthy, and G. K. Smyth, 2010 edgeR: a Bioconductor package for differential expression analysis of digital gene expression data. Bioinformatics 26: 139–140.
Rogell, B., R. Dean, B. Lemos, and D. K. Dowling, 2014 Mitonuclear interactions as drivers of gene movement on and off the X-chromosome. BMC Genomics 15: 330.
Rossi, A., Z. Kontarakis, C. Gerri, H. Nolte, S. Holper *et al.*, 2015 Genetic compensation induced by deleterious mutations but not gene knockdowns. Nature 524: 230–233.
Roubertoux, P. L., F. Sluyter, M. Carlier, B. Marcet, F. Maarouf-Veray *et al.*, 2003 Mitochondrial DNA modifies cognition in interaction with the nuclear genome and age in mice. Nat. Genet. 35: 65–69.
Ruiz-Pesini, E., A. C. Lapena, C. Diez-Sanchez, A. Perez-Martos, J. Montoya *et al.*, 2000 Human mtDNA haplogroups associated with high or reduced spermatozoa motility. Am. J. Hum. Genet. 67: 682–696.
Sagan, L., 1967 On the origin of mitosing cells. J. Theor. Biol. 14: 225–274.

Sanchez, G., 2014 Introduction to the R package arcdiagram. Available at: http://gastonsanchez.com/software/arcdiagram_introduction.pdf. Accessed September 8, 2016.
Sardiello, M., F. Licciulli, D. Catalano, M. Attimonelli, and C. Caggese, 2003 MitoDrome: a database of Drosophila melanogaster nuclear genes encoding proteins targeted to the mitochondrion. Nucleic Acids Res. 31: 322–324.
Schapira, A. H. V., 1998 Human complex I defects in neurodegenerative diseases. Biochim Biophys Acta. 1364: 261–270.
Schmittgen, T. D., and K. J. Livak, 2008 Analyzing real-time PCR data by the comparative CT method. Nat. Protoc. 3: 1101–1108.
Si, Y., P. Liu, P. Li, and T. P. Brutnell, 2014 Model-based clustering for RNA-seq data. Bioinformatics 30: 197–205.
Smeitink, J., L. van den Heuvel, and S. DiMauro, 2001 The genetics and pathology of oxidative phosphorylation. Nat. Rev. Genet. 2: 342–352.
Stewart, J. B., and P. F. Chinnery, 2015 The dynamics of mitochondrial DNA heteroplasmy: implications for human health and disease. Nat. Rev. Genet. 16: 530–542.
Stuart, J. M., E. Segal, D. Koller, and S. K. Kim, 2003 A gene-coexpression network for global discovery of conserved genetic modules. Science 302: 249–255.
Swerdlow, R. H., and S. M. Khan, 2009 The Alzheimer's disease mitochondrial cascade hypothesis: an update. Exp. Neurol. 218: 308–315.
Taanman, J.-W., 1999 The mitochondrial genome: structure, transcription, translation and replication. Biochim Biophys Acta. 1410: 103–123.
Tońska, K., A. Sołyga, and E. Bartnik, 2009 Mitochondria and aging: innocent bystanders or guilty parties? J. Appl. Genet. 50: 55–62.
Torres, T. T., M. Dolezal, C. Schlötterer, and B. Ottenwälder, 2009 Expression profiling of Drosophila mitochondrial genes via deep mRNA sequencing. Nucleic Acids Res. 37: 7509–7518.
Trapnell, C., A. Roberts, L. Goff, G. Pertea, D. Kim *et al.*, 2012 Differential gene and transcript expression analysis of RNA-seq experiments with TopHat and Cufflinks. Nat. Protoc. 7: 562–578.
Tripoli, G., D. D'Elia, P. Barsanti, and C. Caggese, 2005 Comparison of the oxidative phosphorylation (OXPHOS) nuclear genes in the genomes of Drosophila melanogaster, Drosophila pseudoobscura and Anopheles gambiae. Genome Biol. 6: 1–17.
van Waveren, C., and C. T. Moraes, 2008 Transcriptional co-expression and co-regulation of genes coding for components of the oxidative phosphorylation system. BMC Genomics 9: 1–15.
Villa-Cuesta, E., M. A. Holmbeck, and D. M. Rand, 2014 Rapamycin increases mitochondrial efficiency by mtDNA-dependent reprogramming of mitochondrial metabolism in Drosophila. J. Cell Sci. 127: 2282–2290.
Vinothkumar, K. R., J. Zhu, and J. Hirst, 2014 Architecture of mammalian respiratory complex I. Nature 515: 80–84.
Wade, M. J., and C. J. Goodnight, 2006 Cyto-nuclear epistasis: two-locus random genetic drift in hermaphroditic and dioecious species. Evolution 60: 643–659.
Wallace, D. C., 1992 Diseases of the mitochondrial DNA. Annu. Rev. Biochem. 61: 1175–1212.
Wallace, D. C., 1999 Mitochondrial diseases in man and mouse. Science 283: 1482–1488.
Werren, J. H., 2011 Selfish genetic elements, genetic conflict, and evolutionary innovation. Proc. Natl. Acad. Sci. USA 108: 10863–10870.
Wolstenholme, D. R., 1992 Animal mitochondrial DNA: structure and evolution, pp. 173–216 in *International Review of Cytology*, edited by R. W. David, and W. J. Kwang. Academic Press, San Diego.
Wong, L. J. C., 2012 *Mitochondrial Disorders Caused by Nuclear Genes*. Springer, New York.
Yee, W. K. W., K. L. Sutton, and D. K. Dowling, 2013 In vivo male fertility is affected by naturally occurring mitochondrial haplotypes. Curr. Biol. 23: 55–56.
Zhu, C.-T., P. Ingelmo, and D. M. Rand, 2014 GxGxE for lifespan in Drosophila: mitochondrial, nuclear, and dietary interactions that modify longevity. PLoS Genet. 10: e1004354.

Communicating editor: J. A. Birchler

Nuclear effect, no mito effect

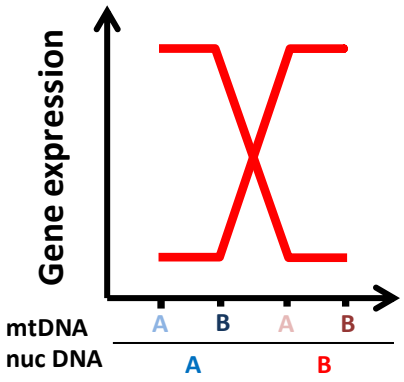

Mito effect, no nuclear effect

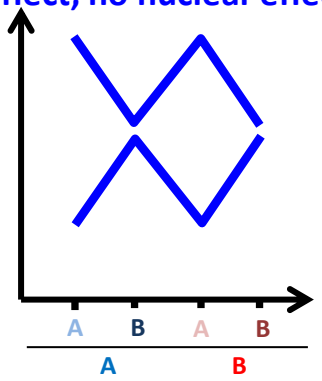

Nuclear + mito effect

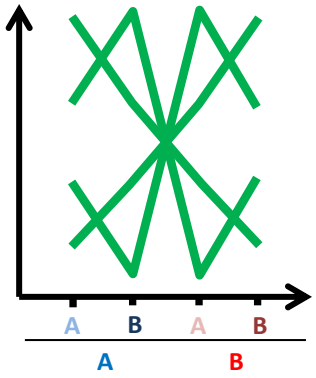

Nuclear x mito interaction

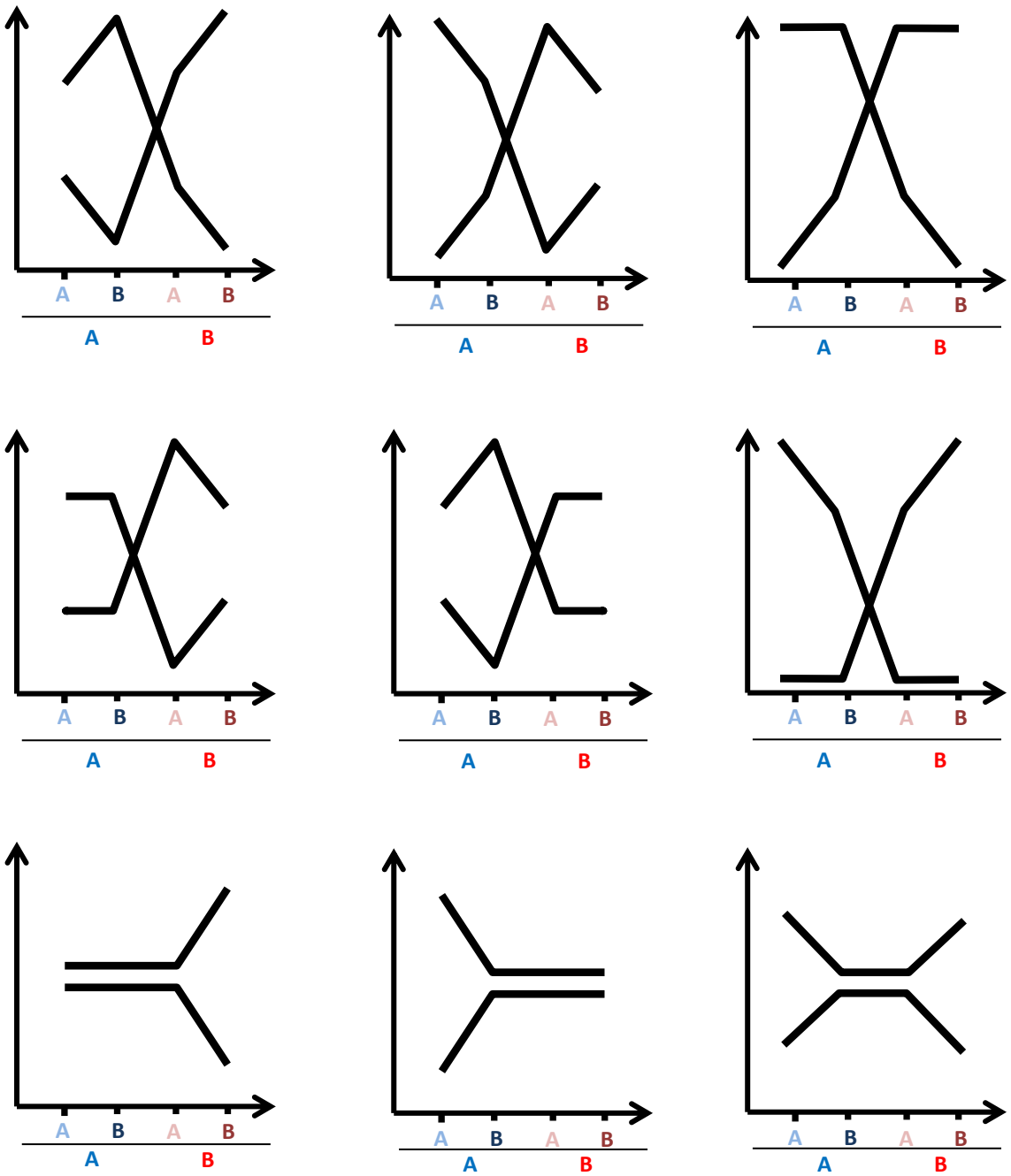

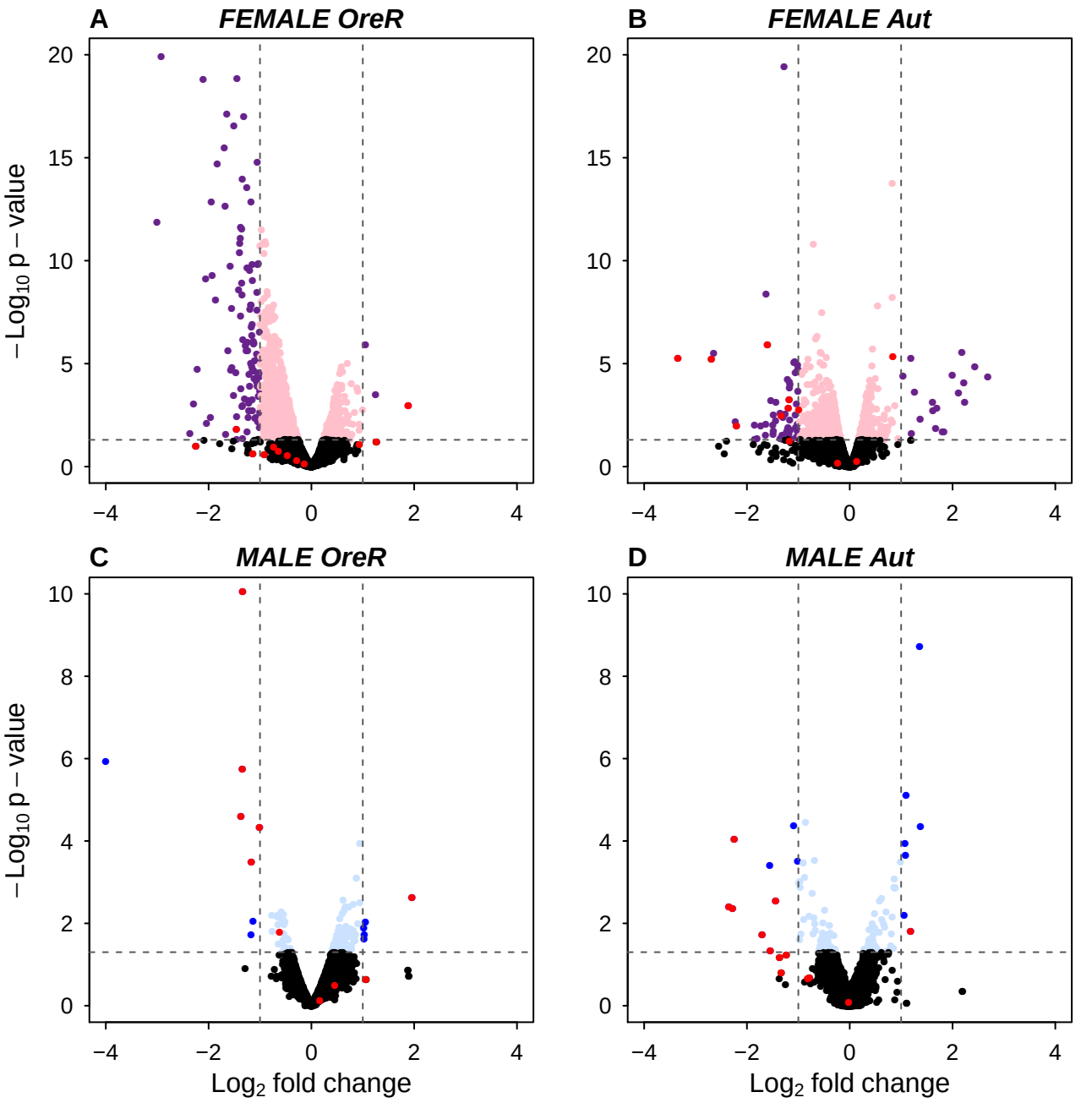
A
FEMALE OreR
B
FEMALE Aut
C
MALE OreR
D
MALE Aut
−Log10 p−value
Log2 fold change
20
15
10
5
0
8
6
4
2
−4
−2
0
2
4

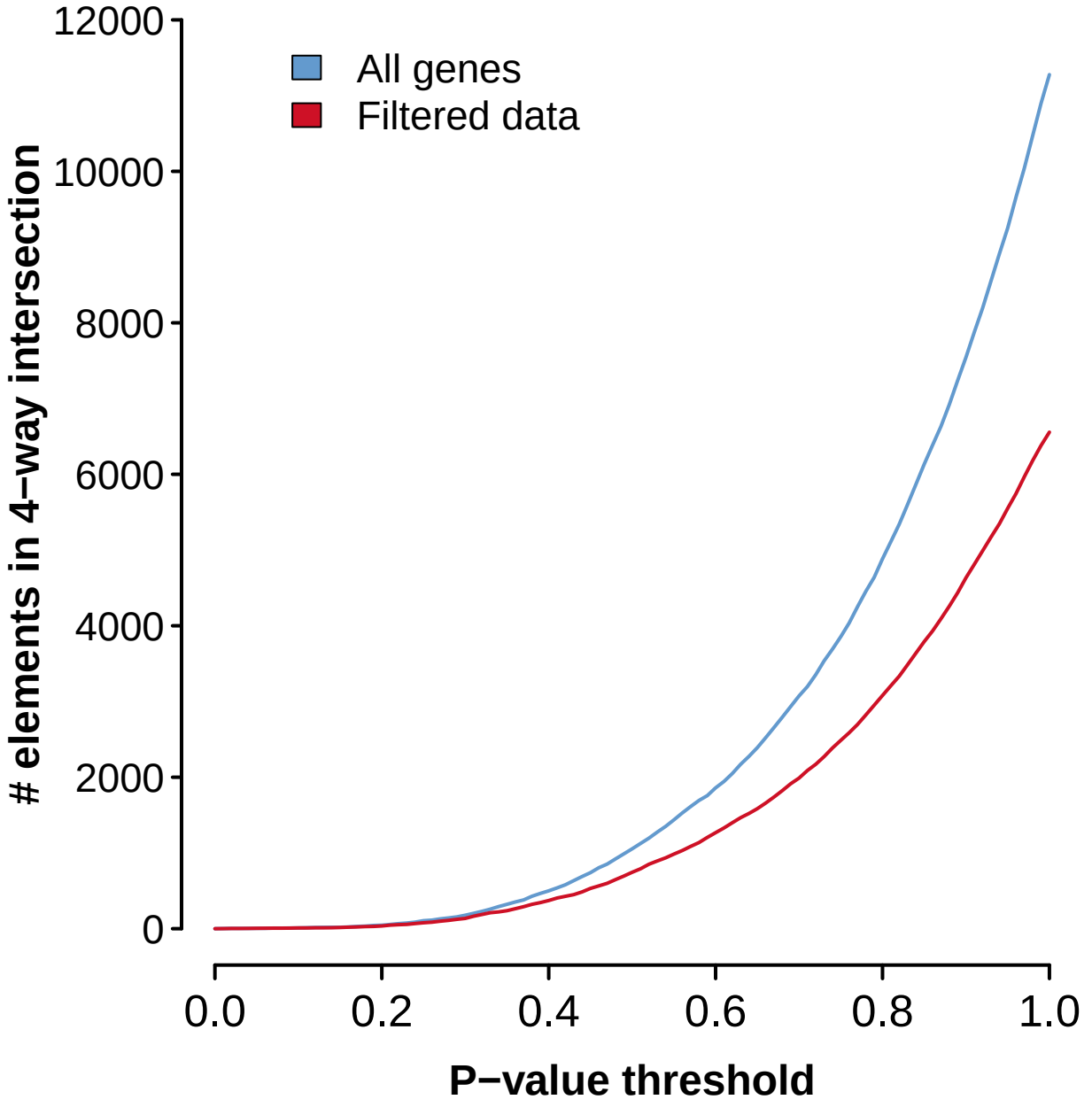
All genes
Filtered data
elements in 4−way intersection
12000
10000
8000
6000
4000
2000
0
0.0
0.2
0.4
0.6
0.8
1.0
P−value threshold

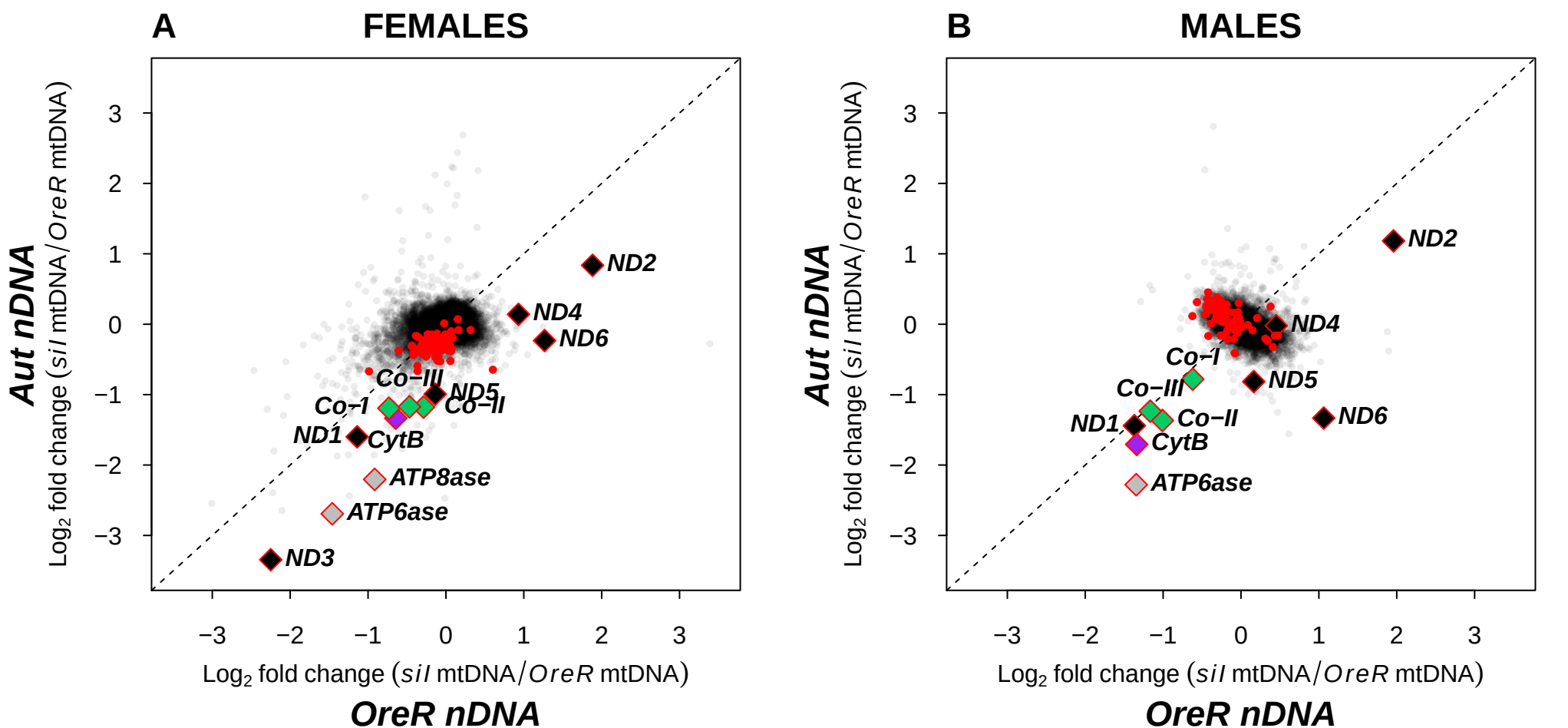
A
FEMALES
B
MALES
Aut nDNA
Log2 fold change (sil mtDNA/OreR mtDNA)
OreR nDNA
Log2 fold change (sil mtDNA/OreR mtDNA)
ND2
ND4
ND6
Co−III
ND5
Co−I
Co−II
ND1
CytB
ATP8ase
ATP6ase
ND3
−3
−2
−1
0
1
2
3

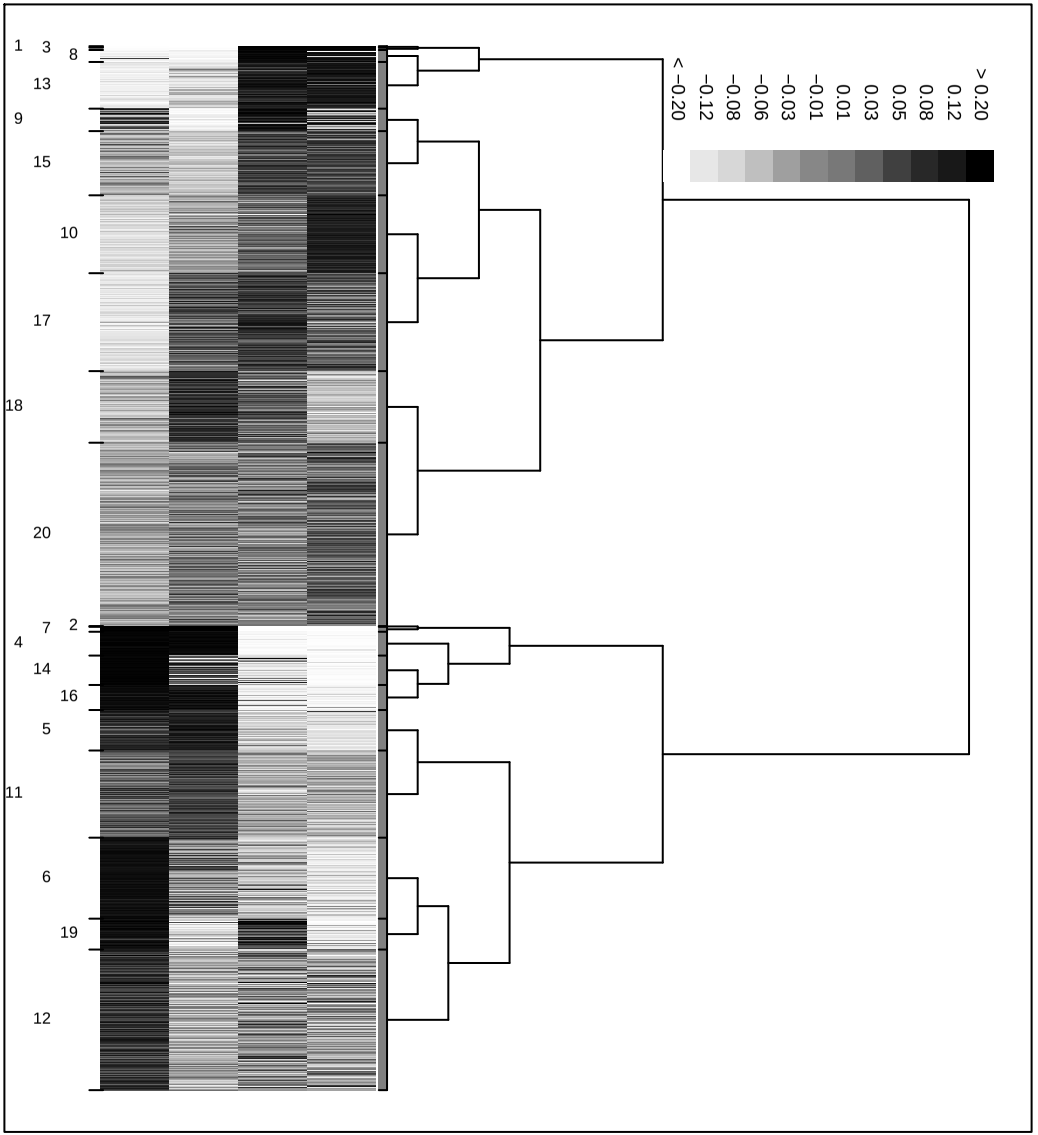
1
3
8
13
9
15
10
17
18
20
7
2
4
14
16
5
11
6
19
12
< −0.20
−0.12
−0.08
−0.06
−0.03
−0.01
0.01
0.03
0.05
0.08
0.12
> 0.20

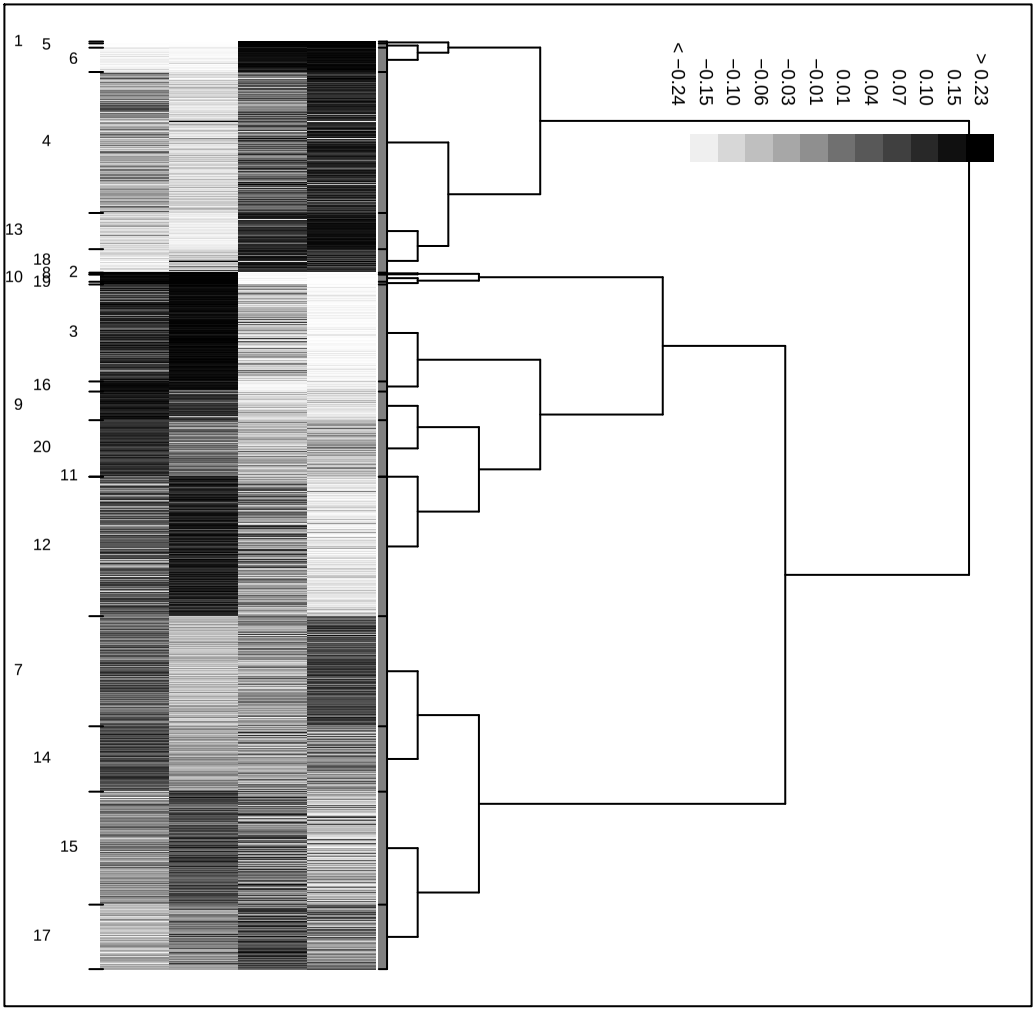
1
5
6
4
13
18
10
19
2
3
16
9
20
11
12
7
14
15
17
< −0.24
−0.15
−0.10
−0.06
−0.03
−0.01
0.01
0.04
0.07
0.10
0.15
> 0.23

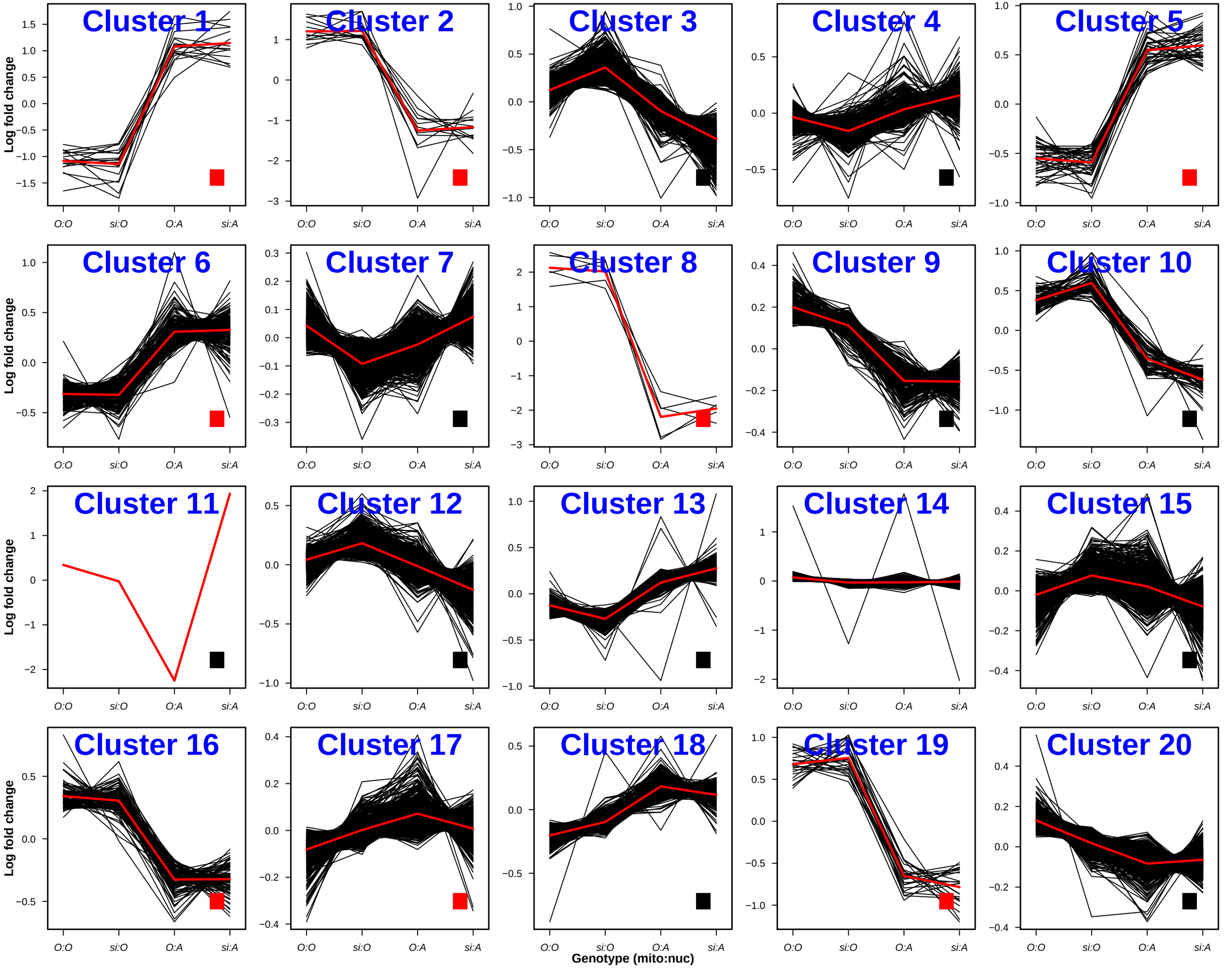
Cluster 1
Cluster 2
Cluster 3
Cluster 4
Cluster 5
Cluster 6
Cluster 7
Cluster 8
Cluster 9
Cluster 10
Cluster 11
Cluster 12
Cluster 13
Cluster 14
Cluster 15
Cluster 16
Cluster 17
Cluster 18
Cluster 19
Cluster 20
Log fold change
O:O
si:O
O:A
si:A
Genotype (mito:nuc)

GO enrichment FEMALES

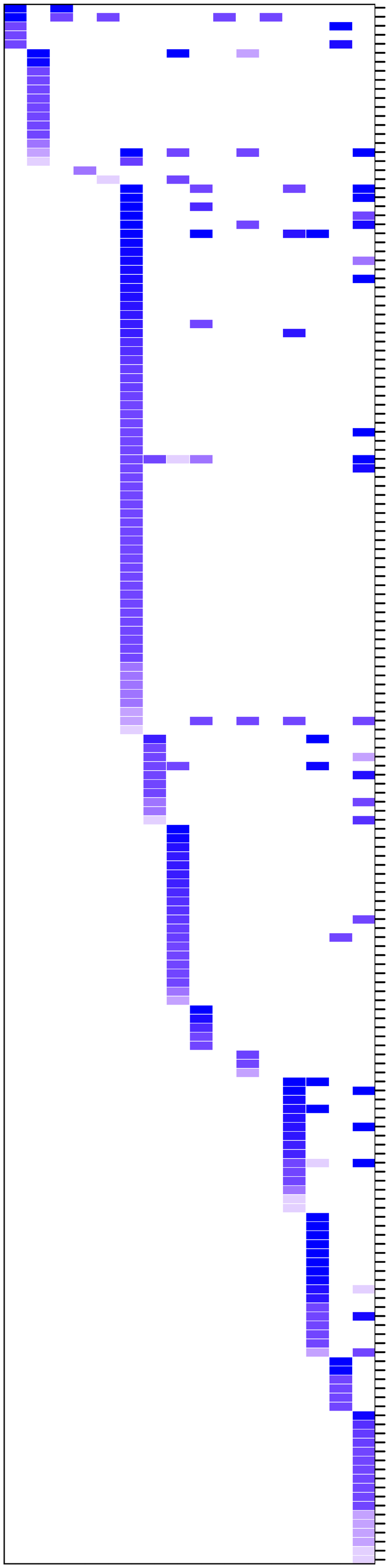

GO:0004252 SERINE−TYPE ENDOPEPTIDASE ACTIVITY
GO:0006508 PROTEOLYSIS
GO:0004497 MONOOXYGENASE ACTIVITY
GO:0005576 EXTRACELLULAR REGION
GO:0005792 MICROSOME
GO:0005886 PLASMA MEMBRANE
GO:0007427 EPITHELIAL CELL MIGRATION, OPEN TRACHEAL SYSTEM
GO:0005887 INTEGRAL TO PLASMA MEMBRANE
GO:0007432 SALIVARY GLAND BOUNDARY SPECIFICATION
GO:0007498 MESODERM DEVELOPMENT
GO:0007602 PHOTOTRANSDUCTION
GO:0016028 RHABDOMERE
GO:0016059 DEACTIVATION OF RHODOPSIN MEDIATED SIGNALING
GO:0016199 AXON MIDLINE CHOICE POINT RECOGNITION
GO:0016477 CELL MIGRATION
GO:0006123 MITOCHONDRIAL ELECTRON TRANSPORT, CYTOCHROME C TO OXYGEN
GO:0005515 PROTEIN BINDING
GO:0007411 AXON GUIDANCE
GO:0008152 METABOLIC PROCESS
GO:0023034 INTRACELLULAR SIGNALING PATHWAY
GO:0005634 NUCLEUS
GO:0008270 ZINC ION BINDING
GO:0003677 DNA BINDING
GO:0005700 POLYTENE CHROMOSOME
GO:0005737 CYTOPLASM
GO:0007052 MITOTIC SPINDLE ORGANIZATION
GO:0007143 FEMALE MEIOSIS
GO:0030178 NEGATIVE REGULATION OF WNT RECEPTOR SIGNALING PATHWAY
GO:0048477 OOGENESIS
GO:0016251 GENERAL RNA POLYMERASE II TRANSCRIPTION FACTOR ACTIVITY
GO:0003676 NUCLEIC ACID BINDING
GO:0042023 DNA ENDOREDUPLICATION
GO:0009987 CELLULAR PROCESS
GO:0017148 NEGATIVE REGULATION OF TRANSLATION
GO:0004386 HELICASE ACTIVITY
GO:0003887 DNA−DIRECTED DNA POLYMERASE ACTIVITY
GO:0000776 KINETOCHORE
GO:0048666 NEURON DEVELOPMENT
GO:0005819 SPINDLE
GO:0005813 CENTROSOME
GO:0000278 MITOTIC CELL CYCLE
GO:0000932 CYTOPLASMIC MRNA PROCESSING BODY
GO:0007062 SISTER CHROMATID COHESION
GO:0007476 IMAGINAL DISC−DERIVED WING MORPHOGENESIS
GO:0000082 G1/S TRANSITION OF MITOTIC CELL CYCLE
GO:0000910 CYTOKINESIS
GO:0003714 TRANSCRIPTION COREPRESSOR ACTIVITY
GO:0003729 MRNA BINDING
GO:0003730 MRNA 3'−UTR BINDING
GO:0004003 ATP−DEPENDENT DNA HELICASE ACTIVITY
GO:0005524 ATP BINDING
GO:0005622 INTRACELLULAR
GO:0005828 KINETOCHORE MICROTUBULE
GO:0005838 PROTEASOME REGULATORY PARTICLE
GO:0005871 KINESIN COMPLEX
GO:0006338 CHROMATIN REMODELING
GO:0006511 UBIQUITIN−DEPENDENT PROTEIN CATABOLIC PROCESS
GO:0006911 PHAGOCYTOSIS, ENGULFMENT
GO:0007049 CELL CYCLE
GO:0007067 MITOSIS
GO:0007094 MITOTIC CELL CYCLE SPINDLE ASSEMBLY CHECKPOINT
GO:0007265 RAS PROTEIN SIGNAL TRANSDUCTION
GO:0007307 EGGSHELL CHORION GENE AMPLIFICATION
GO:0007465 R7 CELL FATE COMMITMENT
GO:0008017 MICROTUBULE BINDING
GO:0008586 IMAGINAL DISC−DERIVED WING VEIN MORPHOGENESIS
GO:0016055 WNT RECEPTOR SIGNALING PATHWAY
GO:0016563 TRANSCRIPTION ACTIVATOR ACTIVITY
GO:0035019 SOMATIC STEM CELL MAINTENANCE
GO:0035060 BRAHMA COMPLEX
GO:0045879 NEGATIVE REGULATION OF SMOOTHENED SIGNALING PATHWAY
GO:0045893 POSITIVE REGULATION OF TRANSCRIPTION, DNA−DEPENDENT
GO:0048813 DENDRITE MORPHOGENESIS
GO:0004221 UBIQUITIN THIOLESTERASE ACTIVITY
GO:0004842 UBIQUITIN−PROTEIN LIGASE ACTIVITY
GO:0005912 ADHERENS JUNCTION
GO:0006261 DNA−DEPENDENT DNA REPLICATION
GO:0006367 TRANSCRIPTION INITIATION FROM RNA POLYMERASE II PROMOTER
GO:0003682 CHROMATIN BINDING
GO:0005875 MICROTUBULE ASSOCIATED COMPLEX
GO:0042127 REGULATION OF CELL PROLIFERATION
GO:0022625 CYTOSOLIC LARGE RIBOSOMAL SUBUNIT
GO:0000165 MAPK CASCADE
GO:0005525 GTP BINDING
GO:0005811 LIPID PARTICLE
GO:0006886 INTRACELLULAR PROTEIN TRANSPORT
GO:0006914 AUTOPHAGY
GO:0016192 VESICLE−MEDIATED TRANSPORT
GO:0000381 REGULATION OF ALTERNATIVE MRNA SPLICING, VIA SPLICEOSOME
GO:0005778 PEROXISOMAL MEMBRANE
GO:0004004 ATP−DEPENDENT RNA HELICASE ACTIVITY
GO:0005925 FOCAL ADHESION
GO:0003954 NADH DEHYDROGENASE ACTIVITY
GO:0005747 MITOCHONDRIAL RESPIRATORY CHAIN COMPLEX I
GO:0008137 NADH DEHYDROGENASE (UBIQUINONE) ACTIVITY
GO:0007016 CYTOSKELETAL ANCHORING AT PLASMA MEMBRANE
GO:0045202 SYNAPSE
GO:0045197 ESTABLISHMENT OR MAINTENANCE OF EPITHELIAL CELL APICAL/BASAL POLARITY
GO:0005856 CYTOSKELETON
GO:0003779 ACTIN BINDING
GO:0045169 FUSOME
GO:0008360 REGULATION OF CELL SHAPE
GO:0005938 CELL CORTEX
GO:0055085 TRANSMEMBRANE TRANSPORT
GO:0006120 MITOCHONDRIAL ELECTRON TRANSPORT, NADH TO UBIQUINONE
GO:0006754 ATP BIOSYNTHETIC PROCESS
GO:0007155 CELL ADHESION
GO:0007268 SYNAPTIC TRANSMISSION
GO:0007391 DORSAL CLOSURE
GO:0016323 BASOLATERAL PLASMA MEMBRANE
GO:0016021 INTEGRAL TO MEMBRANE
GO:0006260 DNA REPLICATION
GO:0006270 DNA REPLICATION INITIATION
GO:0016321 FEMALE MEIOSIS CHROMOSOME SEGREGATION
GO:0006281 DNA REPAIR
GO:0007088 REGULATION OF MITOSIS
GO:0031625 UBIQUITIN PROTEIN LIGASE BINDING
GO:0051276 CHROMOSOME ORGANIZATION
GO:0000922 SPINDLE POLE
GO:0005762 MITOCHONDRIAL LARGE RIBOSOMAL SUBUNIT
GO:0071011 PRECATALYTIC SPLICEOSOME
GO:0006974 RESPONSE TO DNA DAMAGE STIMULUS
GO:0003735 STRUCTURAL CONSTITUENT OF RIBOSOME
GO:0004298 THREONINE−TYPE ENDOPEPTIDASE ACTIVITY
GO:0071013 CATALYTIC STEP 2 SPLICEOSOME
GO:0005839 PROTEASOME CORE COMPLEX
GO:0000502 PROTEASOME COMPLEX
GO:0004175 ENDOPEPTIDASE ACTIVITY
GO:0000398 MRNA SPLICING, VIA SPLICEOSOME
GO:0007080 MITOTIC METAPHASE PLATE CONGRESSION
GO:0031262 NDC80 COMPLEX
GO:0019773 PROTEASOME CORE COMPLEX, ALPHA−SUBUNIT COMPLEX
GO:0007305 VITELLINE MEMBRANE FORMATION INVOLVED IN CHORION−CONTAINING EGGSHELL FORMATION
GO:0051603 PROTEOLYSIS INVOLVED IN CELLULAR PROTEIN CATABOLIC PROCESS
GO:0006412 TRANSLATION
GO:0022627 CYTOSOLIC SMALL RIBOSOMAL SUBUNIT
GO:0000022 MITOTIC SPINDLE ELONGATION
GO:0005840 RIBOSOME
GO:0005763 MITOCHONDRIAL SMALL RIBOSOMAL SUBUNIT
GO:0000175 3'−5'−EXORIBONUCLEASE ACTIVITY
GO:0000176 NUCLEAR EXOSOME (RNASE COMPLEX)
GO:0000177 CYTOPLASMIC EXOSOME (RNASE COMPLEX)
GO:0003723 RNA BINDING
GO:0006396 RNA PROCESSING
GO:0003899 DNA−DIRECTED RNA POLYMERASE ACTIVITY
GO:0005681 SPLICEOSOMAL COMPLEX
GO:0006413 TRANSLATIONAL INITIATION
GO:0030532 SMALL NUCLEAR RIBONUCLEOPROTEIN COMPLEX
GO:0042254 RIBOSOME BIOGENESIS
GO:0003743 TRANSLATION INITIATION FACTOR ACTIVITY
GO:0020037 HEME BINDING
GO:0009055 ELECTRON CARRIER ACTIVITY
GO:0005215 TRANSPORTER ACTIVITY
GO:0005975 CARBOHYDRATE METABOLIC PROCESS
GO:0043169 CATION BINDING
GO:0055114 OXIDATION−REDUCTION PROCESS
GO:0000166 NUCLEOTIDE BINDING
GO:0043234 PROTEIN COMPLEX
GO:0003724 RNA HELICASE ACTIVITY
GO:0030036 ACTIN CYTOSKELETON ORGANIZATION
GO:0003924 GTPASE ACTIVITY
GO:0004674 PROTEIN SERINE/THREONINE KINASE ACTIVITY
GO:0006468 PROTEIN PHOSPHORYLATION
GO:0007015 ACTIN FILAMENT ORGANIZATION
GO:0016197 ENDOSOMAL TRANSPORT
GO:0042054 HISTONE METHYLTRANSFERASE ACTIVITY
GO:0046974 HISTONE METHYLTRANSFERASE ACTIVITY (H3−K9 SPECIFIC)
GO:0004672 PROTEIN KINASE ACTIVITY
GO:0010883 REGULATION OF LIPID STORAGE
GO:0016571 HISTONE METHYLATION
GO:0046667 COMPOUND EYE RETINAL CELL PROGRAMMED CELL DEATH
GO:0005705 POLYTENE CHROMOSOME INTERBAND
GO:0008356 ASYMMETRIC CELL DIVISION

GO enrichment MALES

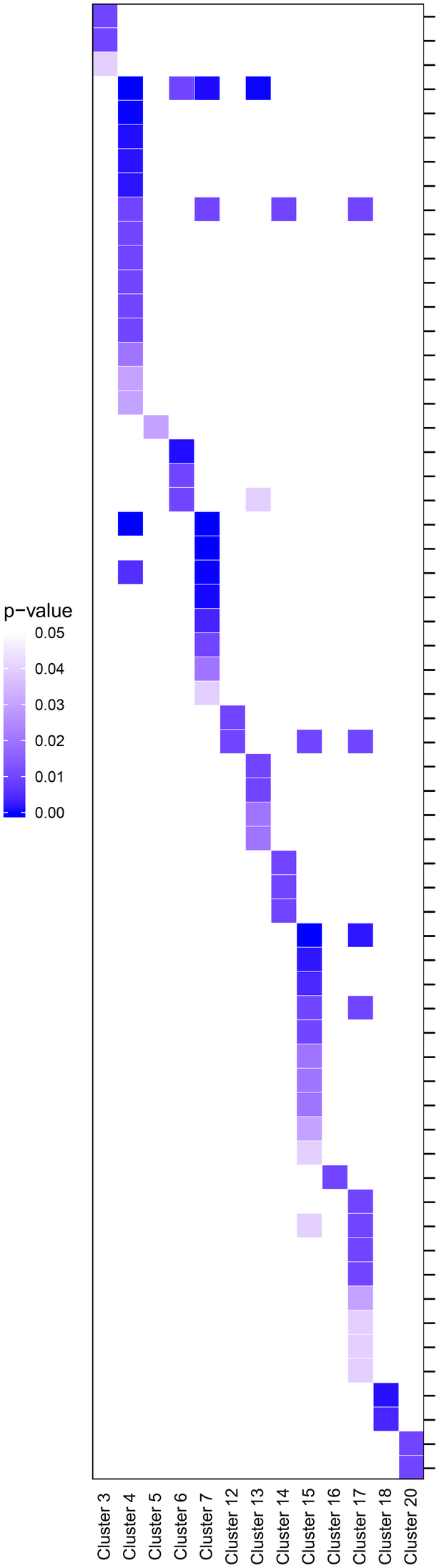

GO:0020037 HEME BINDING
GO:0045297 POST−MATING BEHAVIOR
GO:0004835 TUBULIN−TYROSINE LIGASE ACTIVITY
GO:0005811 LIPID PARTICLE
GO:0003954 NADH DEHYDROGENASE ACTIVITY
GO:0005747 MITOCHONDRIAL RESPIRATORY CHAIN COMPLEX I
GO:0008137 NADH DEHYDROGENASE (UBIQUINONE) ACTIVITY
GO:0006120 MITOCHONDRIAL ELECTRON TRANSPORT, NADH TO UBIQUINONE
GO:0005737 CYTOPLASM
GO:0006458 'DE NOVO' PROTEIN FOLDING
GO:0006890 RETROGRADE VESICLE−MEDIATED TRANSPORT, GOLGI TO ER
GO:0015992 PROTON TRANSPORT
GO:0022627 CYTOSOLIC SMALL RIBOSOMAL SUBUNIT
GO:0030126 COPI VESICLE COAT
GO:0045169 FUSOME
GO:0006886 INTRACELLULAR PROTEIN TRANSPORT
GO:0050660 FLAVIN ADENINE DINUCLEOTIDE BINDING
GO:0005576 EXTRACELLULAR REGION
GO:0055085 TRANSMEMBRANE TRANSPORT
GO:0030170 PYRIDOXAL PHOSPHATE BINDING
GO:0055114 OXIDATION−REDUCTION PROCESS
GO:0003735 STRUCTURAL CONSTITUENT OF RIBOSOME
GO:0000022 MITOTIC SPINDLE ELONGATION
GO:0022625 CYTOSOLIC LARGE RIBOSOMAL SUBUNIT
GO:0007052 MITOTIC SPINDLE ORGANIZATION
GO:0010507 NEGATIVE REGULATION OF AUTOPHAGY
GO:0005832 CHAPERONIN−CONTAINING T−COMPLEX
GO:0042254 RIBOSOME BIOGENESIS
GO:0051082 UNFOLDED PROTEIN BINDING
GO:0004386 HELICASE ACTIVITY
GO:0005524 ATP BINDING
GO:0004129 CYTOCHROME−C OXIDASE ACTIVITY
GO:0005751 MITOCHONDRIAL RESPIRATORY CHAIN COMPLEX IV
GO:0005740 MITOCHONDRIAL ENVELOPE
GO:0007606 SENSORY PERCEPTION OF CHEMICAL STIMULUS
GO:0003676 NUCLEIC ACID BINDING
GO:0004177 AMINOPEPTIDASE ACTIVITY
GO:0008235 METALLOEXOPEPTIDASE ACTIVITY
GO:0005515 PROTEIN BINDING
GO:0006897 ENDOCYTOSIS
GO:0007476 IMAGINAL DISC−DERIVED WING MORPHOGENESIS
GO:0005886 PLASMA MEMBRANE
GO:0005938 CELL CORTEX
GO:0005768 ENDOSOME
GO:0006911 PHAGOCYTOSIS, ENGULFMENT
GO:0035160 MAINTENANCE OF EPITHELIAL INTEGRITY, OPEN TRACHEAL SYSTEM
GO:0004672 PROTEIN KINASE ACTIVITY
GO:0007420 BRAIN DEVELOPMENT
GO:0016491 OXIDOREDUCTASE ACTIVITY
GO:0005634 NUCLEUS
GO:0006468 PROTEIN PHOSPHORYLATION
GO:0007391 DORSAL CLOSURE
GO:0007498 MESODERM DEVELOPMENT
GO:0003702 RNA POLYMERASE II TRANSCRIPTION FACTOR ACTIVITY
GO:0002121 INTER−MALE AGGRESSIVE BEHAVIOR
GO:0007268 SYNAPTIC TRANSMISSION
GO:0008360 REGULATION OF CELL SHAPE
GO:0043169 CATION BINDING
GO:0005975 CARBOHYDRATE METABOLIC PROCESS
GO:0005739 MITOCHONDRION
GO:0006626 PROTEIN TARGETING TO MITOCHONDRION

Figure S10. Between sex gene intersections for <u>mtDNA</u> genes. Those genes listed are consistently differentially expressed and intersected across the sexes.

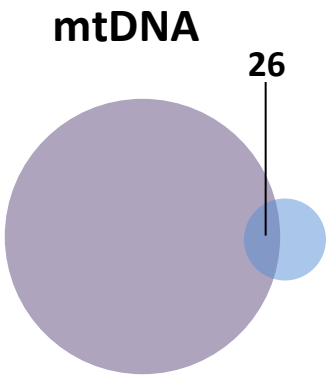

Computed gene ID	Flybase ID	Gene ID
CG10011	FBgn0039590	*CG10011*
CG1165	FBgn0004430	*LysS*
CG11966	FBgn0037645	*CG11966*
CG15505	FBgn0039684	*Obp99d*
CG33256	FBgn0261565	*Lmpt*
CG3350	FBgn0039509	*bigmax*
CG34063	FBgn0013680	*mt:ND2*
CG34067	FBgn0013674	*mt:CoI*
CG34069	FBgn0013675	*mt:CoII*
CG34072	FBgn0013673	*mt:ATPase8*
CG34073	FBgn0013672	*mt:ATPase6*
CG34074	FBgn0013676	*mt:CoIII*
CG34076	FBgn0013681	*mt:ND3*
CG34086	FBgn0013683	*mt:ND4L*
CG34090	FBgn0013678	*mt:Cyt-b*
CG34092	FBgn0013679	*mt:ND1*
CG4099	FBgn0014033	*Sr-CI*
CG42254	FBgn0259112	*CR42254*
CG4950	FBgn0036587	*CG4950*
CG5779	FBgn0283437	*PPO1*
CG7002	FBgn0029167	*Hml*
CG7106	FBgn0040099	*lectin-28C*
CG7171	FBgn0003961	*Uro*
CG8193	FBgn0033367	*PPO2*
CG8942	FBgn0259896	*NimC1*
CG9192	FBgn0035193	*CG9192*

Figure S11. Between sex gene intersections for nuclear genes. Those genes listed are consistently differentially expressed and intersected across the sexes.

nDNA

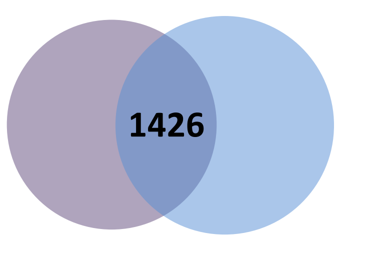

Computed gene ID	Flybase ID	Gene ID
CG10000	FBgn0039596	CG10000
CG10011	FBgn0039590	CG10011
CG10016	FBgn0024244	drm
CG10018	FBgn0037338	Snm1
CG10033	FBgn0000721	for
CG10038	FBgn0038013	CG10038
CG10059	FBgn0037481	MAGE
CG10078	FBgn0041194	Prat2
CG10091	FBgn0038020	GstD9
CG10109	FBgn0267824	PRAS40
CG10119	FBgn0010397	LamC
CG10120	FBgn0002719	Men
CG10146	FBgn0012042	AttA
CG10157	FBgn0039099	GILT2
CG10165	FBgn0032801	CG10165
CG10168	FBgn0039087	CG10168
CG10170	FBgn0039085	CG10170
CG10182	FBgn0039091	CG10182
CG10185	FBgn0038397	CG10185
CG10208	FBgn0039118	CG10208
CG10221	FBgn0028475	Hrd3
CG10242	FBgn0033978	Cyp6a23
CG10245	FBgn0033980	Cyp6a20
CG10248	FBgn0013772	Cyp6a8
CG10283	FBgn0032681	CG10283
CG10320	FBgn0034645	ND-B12
CG10337	FBgn0032805	CG10337
CG10352	FBgn0030348	CG10352
CG10357	FBgn0035453	CG10357
CG10363	FBgn0041180	Tep4
CG10365	FBgn0039109	CG10365
CG10369	FBgn0032706	Irk3
CG10382	FBgn0025878	wrapper
CG10388	FBgn0003944	Ubx
CG10390	FBgn0014342	mia
CG10395	FBgn0033019	CG10395
CG10419	FBgn0036850	Gem2
CG1044	FBgn0016794	dos
CG10440	FBgn0034636	twz
CG10444	FBgn0034494	CG10444
CG10460	FBgn0034443	cer
CG10472	FBgn0035670	CG10472
CG10475	FBgn0035667	Jon65Ai
CG10477	FBgn0035661	CG10477
CG10479	FBgn0035656	CG10479
CG10484	FBgn0261396	Rpn3
CG10497	FBgn0010415	Sdc
CG10508	FBgn0037060	CG10508
CG10512	FBgn0037057	CG10512
CG10513	FBgn0039311	CG10513
CG10531	FBgn0034582	Cht9
CG10550	FBgn0039321	CG10550
CG10553	FBgn0039324	CG10553
CG10559	FBgn0039323	CG10559
CG10560	FBgn0039325	CG10560
CG10562	FBgn0039326	CG10562
CG10572	FBgn0015618	Cdk8
CG10596	FBgn0015766	Msr-110
CG10618	FBgn0045761	CHKov1
CG10630	FBgn0035608	blanks
CG10654	FBgn0036294	CG10654
CG10657	FBgn0036289	CG10657
CG10658	FBgn0014000	Hf
CG10659	FBgn0032839	CG10659
CG10664	FBgn0032833	COX4
CG10681	FBgn0036291	CG10681
CG10703	FBgn0037881	GCC88
CG10800	FBgn0017551	Rca1
CG10806	FBgn0031865	Nha1
CG10810	FBgn0283461	Drs
CG10812	FBgn0035434	Drsl5
CG10824	FBgn0038865	cDIP
CG10844	FBgn0011286	RyR
CG10880	FBgn0031398	CG10880
CG10888	FBgn0003249	Rh3
CG10904	FBgn0034945	CG10904
CG10910	FBgn0034289	CG10910
CG10912	FBgn0034296	CG10912
CG1092	FBgn0037228	CG1092
CG10924	FBgn0003067	Pepck
CG10932	FBgn0029969	CG10932
CG10962	FBgn0030073	CG10962
CG10965	FBgn0030028	Corp
CG10967	FBgn0260945	Atg1
CG10975	FBgn0014007	Ptp69D
CG10988	FBgn0001612	Grip91
CG11012	FBgn0026756	Ugt37a1
CG1102	FBgn0027930	MP1
CG11020	FBgn0016920	nompC
CG11024	FBgn0000318	cl
CG11034	FBgn0031741	CG11034
CG11050	FBgn0031836	CG11050
CG11089	FBgn0039241	CG11089
CG11124	FBgn0033170	sPLA2
CG11129	FBgn0004047	Yp3
CG1113	FBgn0037304	CG1113
CG11137	FBgn0037199	CG11137
CG11142	FBgn0031737	obst-E
CG11143	FBgn0025885	Inos
CG11156	FBgn0002878	mus101
CG11158	FBgn0030511	CG11158
CG11164	FBgn0030507	CG11164
CG11170	FBgn0034705	CG11170
CG11181	FBgn0000392	cup
CG11192	FBgn0034507	CG11192
CG11198	FBgn0033246	ACC
CG11206	FBgn0034720	Liprin-gamma
CG11218	FBgn0034470	Obp56d
CG11237	FBgn0034452	Oseg6
CG1124	FBgn0037290	CG1124
CG11253	FBgn0266709	Zmynd10
CG11267	FBgn0036334	CG11267
CG11274	FBgn0036340	SRm160
CG11275	FBgn0034706	CG11275
CG11282	FBgn0023095	caps
CG11301	FBgn0034726	Mes4
CG1131	FBgn0015569	alpha-Est10
CG11314	FBgn0039800	Npc2g
CG11318	FBgn0039818	CG11318
CG11321	FBgn0031857	CG11321
CG11325	FBgn0025595	AkhR
CG11330	FBgn0000351	cort
CG11334	FBgn0039849	CG11334
CG11342	FBgn0035537	CG11342
CG11378	FBgn0040364	CG11378
CG11390	FBgn0011695	EbpIII
CG11395	FBgn0034200	Gbp2
CG1140	FBgn0035298	SCOT
CG1143	FBgn0035359	CG1143
CG11437	FBgn0037165	CG11437
CG11448	FBgn0024985	CG11448
CG11459	FBgn0037396	CG11459
CG11466	FBgn0038037	Cyp9f2
CG11495	FBgn0024194	rasp
CG11498	FBgn0039749	CG11498
CG11502	FBgn0003651	svp
CG11508	FBgn0260398	Pbp49
CG11527	FBgn0011722	Tig
CG11533	FBgn0039908	Asator
CG11550	FBgn0039864	CG11550
CG11576	FBgn0039882	CG11576
CG11594	FBgn0035484	CG11594
CG11628	FBgn0086779	step
CG11655	FBgn0030638	CG11655
CG11668	FBgn0038113	CG11668
CG11671	FBgn0037562	CG11671
CG1172	FBgn0264712	CG1172
CG11750	FBgn0030294	Pa1
CG11765	FBgn0033518	Prx2540-2
CG11777	FBgn0033527	CG11777
CG11788	FBgn0034495	CG11788
CG1179	FBgn0004425	LysB
CG11793	FBgn0003462	Sod
CG11797	FBgn0034468	Obp56a
CG11798	FBgn0015371	chn
CG11814	FBgn0265988	mv
CG11821	FBgn0038680	Cyp12a5
CG11835	FBgn0031264	CG11835
CG11842	FBgn0039629	CG11842
CG11861	FBgn0261268	Cul3
CG11878	FBgn0039310	CG11878
CG11892	FBgn0039313	CG11892
CG11893	FBgn0039316	CG11893
CG11896	FBgn0038488	m-cup
CG11899	FBgn0014427	CG11899
CG11911	FBgn0031249	CG11911
CG11912	FBgn0031248	CG11912
CG11961	FBgn0034436	CG11961
CG11971	FBgn0260243	E(var)3-9
CG11985	FBgn0040534	CG11985
CG12001	FBgn0037265	spartin
CG12010	FBgn0035443	CG12010
CG12026	FBgn0262624	Tmhs
CG12045	FBgn0039805	Cpr100A
CG12057	FBgn0030098	CG12057
CG1208	FBgn0037386	CG1208
CG12086	FBgn0011204	cue
CG12090	FBgn0035227	Iml1
CG12101	FBgn0015245	Hsp60A
CG12105	FBgn0035241	CG12105
CG12110	FBgn0033075	Pld
CG12112	FBgn0030048	CG12112
CG12116	FBgn0030041	CG12116
CG12117	FBgn0014032	Sptr
CG12120	FBgn0086367	t
CG12129	FBgn0033475	CG12129
CG12131	FBgn0027619	Adam
CG12142	FBgn0033128	Tsp42Eg
CG12149	FBgn0040234	c12.2
CG12175	FBgn0030502	tth
CG12179	FBgn0025388	CG12179
CG12184	FBgn0025387	CG12184
CG12190	FBgn0034763	RYBP
CG1221	FBgn0027111	miple1
CG12242	FBgn0010041	GstD5
CG12284	FBgn0260635	Diap1
CG12287	FBgn0004394	pdm2
CG12290	FBgn0039419	CG12290
CG12298	FBgn0003545	sub
CG12299	FBgn0032295	CG12299
CG12346	FBgn0017414	cag
CG12366	FBgn0033901	O-fut1
CG12367	FBgn0033686	Hen1
CG12372	FBgn0028683	spt4
CG12374	FBgn0033774	CG12374
CG12413	FBgn0039588	CG12413
CG12483	FBgn0040688	CG12483
CG12505	FBgn0033926	Arc1
CG12519	FBgn0036872	CG12519
CG12560	FBgn0031974	CG12560
CG12581	FBgn0037213	CG12581
CG12592	FBgn0037811	CG12592
CG12625	FBgn0265595	CG44422
CG12655	FBgn0031080	CG12655
CG12664	FBgn0030090	fend
CG12665	FBgn0030103	Obp8a
CG12703	FBgn0031069	Pmp70
CG1271	FBgn0035392	CG1271
CG12717	FBgn0030420	CG12717
CG12730	FBgn0029771	CG12730
CG12765	FBgn0033813	fsd
CG12789	FBgn0025697	santa-maria
CG12795	FBgn0031535	CG12795
CG12824	FBgn0033222	CG12824
CG12825	FBgn0033221	CG12825
CG12833	FBgn0263934	esn
CG12837	FBgn0033139	Tsp42Er
CG12844	FBgn0033129	Tsp42Eh
CG12868	FBgn0033945	CG12868
CG12892	FBgn0033526	Caf1-105
CG12908	FBgn0026403	Ndg
CG12910	FBgn0033502	CG12910
CG12926	FBgn0033437	CG12926
CG12934	FBgn0033541	CG12934
CG13003	FBgn0030798	CG13003
CG13024	FBgn0036665	CG13024
CG1303	FBgn0028427	agt
CG1304	FBgn0031141	CG1304
CG13059	FBgn0036607	CG13059
CG13078	FBgn0032809	CG13078
CG13085	FBgn0032780	CG13085
CG13088	FBgn0032047	CG13088
CG13094	FBgn0032048	Dh31
CG13102	FBgn0032088	CG13102
CG1311	FBgn0035523	CG1311
CG13142	FBgn0032251	Nse4
CG1318	FBgn0041630	Hexo1
CG13215	FBgn0033592	CG13215
CG13222	FBgn0033602	Cpr47Ee
CG13229	FBgn0033579	CG13229
CG13281	FBgn0022213	Cas
CG13309	FBgn0035933	CG13309
CG13310	FBgn0035928	CG13310
CG13311	FBgn0035929	CG13311
CG13315	FBgn0040827	CG13315
CG13318	FBgn0037627	CG13318
CG13324	FBgn0033789	CG13324
CG13335	FBgn0261989	CG42807
CG13348	FBgn0275436	PheRS-m
CG13388	FBgn0027932	Akap200
CG13397	FBgn0014417	CG13397
CG13422	FBgn0034511	GNBP-like3
CG13428	FBgn0034515	CG13428
CG13439	FBgn0040726	dpr1
CG1344	FBgn0027507	CG1344
CG13458	FBgn0036479	CG13458
CG13463	FBgn0036470	EAChm
CG13475	FBgn0040318	HGTX
CG13482	FBgn0036419	CG13482
CG13488	FBgn0034670	CG13488
CG13492	FBgn0034662	CG13492
CG13510	FBgn0034758	CG13510
CG13512	FBgn0260767	CG42565
CG13568	FBgn0034965	ppk29
CG13603	FBgn0039135	CG13603
CG13607	FBgn0039151	CG13607
CG13623	FBgn0039205	CG13623
CG13624	FBgn0039209	REPTOR
CG13656	FBgn0039307	CR13656
CG13658	FBgn0039315	CG13658
CG13659	FBgn0039319	CG13659
CG13667	FBgn0035890	CG13667
CG1368	FBgn0030539	CG1368
CG13688	FBgn0031267	Ipk2
CG13704	FBgn0035583	CG13704
CG13705	FBgn0035582	CG13705
CG13739	FBgn0033403	CG13739
CG13741	FBgn0033374	CG13741
CG13780	FBgn0031888	Pvf2
CG13794	FBgn0031936	CG13794
CG13822	FBgn0039098	GILT3
CG13833	FBgn0039040	CG13833
CG13836	FBgn0265042	Irk1
CG13841	FBgn0040588	CG13841
CG13856	FBgn0038959	CG13856
CG1386	FBgn0026268	antdh
CG13880	FBgn0035122	mRpL17
CG13895	FBgn0035158	CG13895
CG13897	FBgn0035160	hng3
CG13901	FBgn0035164	CG13901
CG13905	FBgn0035176	CG13905
CG13912	FBgn0035186	CG13912
CG13934	FBgn0035279	Cpr62Ba
CG13936	FBgn0035282	CNMa
CG13941	FBgn0033928	Arc2
CG13950	FBgn0031289	CG13950
CG13976	FBgn0039520	Gr98a
CG13977	FBgn0039519	Cyp6a18
CG14021	FBgn0031702	fusl
CG14022	FBgn0031700	CG14022
CG14027	FBgn0031701	TotM
CG14031	FBgn0031695	Cyp4ac3
CG14033	FBgn0046776	CR14033
CG14057	FBgn0036696	CG14057
CG14073	FBgn0036814	CG14073
CG14102	FBgn0036906	CG14102
CG14112	FBgn0036349	SNCF
CG14120	FBgn0036321	CG14120
CG14125	FBgn0036232	CG14125
CG14141	FBgn0036146	CG14141
CG14153	FBgn0036094	CG14153
CG14160	FBgn0036066	CG14160
CG14183	FBgn0036931	CG14183
CG14191	FBgn0030981	CG14191
CG14219	FBgn0031033	CG14219
CG14221	FBgn0031042	CG14221
CG14235	FBgn0031066	COX6B
CG14253	FBgn0039467	CG14253
CG14257	FBgn0039479	CG14257
CG14259	FBgn0039483	CG14259
CG14292	FBgn0038658	CG14292
CG14314	FBgn0038581	CG14314
CG1433	FBgn0019637	Atu
CG1435	FBgn0026144	CBP
CG14351	FBgn0261509	haf
CG14356	FBgn0038207	CG14356
CG14375	FBgn0038147	CCHa2
CG1438	FBgn0015032	Cyp4c3
CG14390	FBgn0038084	beat-Vc
CG14400	FBgn0032896	CG14400
CG14401	FBgn0032900	CG14401
CG14406	FBgn0030595	CG14406
CG14430	FBgn0261284	bou
CG14495	FBgn0034293	CG14495
CG14500	FBgn0034318	CG14500
CG14511	FBgn0039641	CG14511
CG14526	FBgn0027578	CG14526
CG14545	FBgn0040602	CG14545
CG1455	FBgn0010015	CanA1
CG14567	FBgn0037126	CG14567
CG1462	FBgn0016123	Alp4
CG14636	FBgn0037217	CG14636
CG14645	FBgn0040687	CG14645
CG14666	FBgn0037307	Tim17a2
CG14683	FBgn0037822	CG14683
CG14696	FBgn0037853	CG14696
CG14746	FBgn0043576	PGRP-SC1a
CG14764	FBgn0033236	CG14764
CG14796	FBgn0025390	Mur2B
CG14805	FBgn0023514	CG14805
CG14817	FBgn0026089	CG14817
CG14823	FBgn0035734	CG14823
CG14855	FBgn0038260	CG14855
CG14872	FBgn0264775	CG44013
CG14880	FBgn0038422	CG14880
CG14945	FBgn0032402	CG14945
CG14959	FBgn0035427	ckd
CG14961	FBgn0035439	CG14961
CG14963	FBgn0035409	CG14963
CG14969	FBgn0035440	CG14969
CG15010	FBgn0041171	ago
CG15012	FBgn0035528	CG15012
CG15044	FBgn0030928	CG15044
CG15066	FBgn0034328	IM23
CG15088	FBgn0034381	List
CG15093	FBgn0034390	CG15093
CG15102	FBgn0034405	Jheh2
CG1512	FBgn0032956	Cul2
CG15120	FBgn0034454	CG15120
CG15124	FBgn0034461	CG15124
CG15154	FBgn0041184	Socs36E
CG1518	FBgn0031149	CG1518
CG15199	FBgn0030270	CG15199
CG15203	FBgn0030261	CG15203
CG15209	FBgn0030237	CG15209
CG15231	FBgn0040653	IM4
CG15254	FBgn0028949	CG15254
CG15261	FBgn0086691	UK114
CG15279	FBgn0028886	CG15279
CG15324	FBgn0029966	Ir7c
CG15347	FBgn0030040	CG15347
CG15350	FBgn0014465	Cp7Fb
CG15358	FBgn0031373	CG15358
CG15390	FBgn0031419	CG15390
CG15408	FBgn0031523	CG15408
CG15414	FBgn0031542	CG15414
CG15431	FBgn0031602	CG15431
CG15437	FBgn0027609	morgue
CG15441	FBgn0019982	Gs1l
CG15456	FBgn0040650	CG15456
CG15505	FBgn0039684	Obp99d
CG15531	FBgn0039755	CG15531
CG15544	FBgn0039804	CG15544
CG15547	FBgn0039809	CG15547
CG1561	FBgn0030317	CG1561
CG15617	FBgn0034151	CG15617
CG15666	FBgn0034622	CG15666
CG15674	FBgn0034642	CG15674
CG15695	FBgn0038832	CG15695
CG15737	FBgn0260780	wisp
CG15760	FBgn0030508	CG15760
CG15773	FBgn0029795	CG15773
CG15784	FBgn0029766	CG15784
CG15818	FBgn0031910	CG15818
CG15822	FBgn0035308	CG15822
CG15865	FBgn0015336	CG15865
CG1587	FBgn0024811	Crk
CG15879	FBgn0035309	CG15879
CG15902	FBgn0040250	Ugt86Dj
CG15918	FBgn0034197	Cda9
CG1600	FBgn0033188	Drat
CG1605	FBgn0025185	az2
CG1615	FBgn0017561	Ork1
CG1629	FBgn0039896	yellow-h
CG1633	FBgn0040309	Jafrac1
CG1637	FBgn0030245	CG1637
CG1648	FBgn0033446	CG1648
CG1652	FBgn0040092	lectin-46Cb
CG1664	FBgn0003321	sbr
CG16710	FBgn0039101	CG16710
CG16718	FBgn0038721	subdued
CG16727	FBgn0038719	CG16727
CG16749	FBgn0037678	CG16749
CG16752	FBgn0029768	SPR
CG16756	FBgn0029765	CG16756
CG16758	FBgn0035348	CG16758
CG16761	FBgn0035344	Cyp4d20
CG16762	FBgn0035343	CG16762
CG16772	FBgn0032835	CG16772
CG16775	FBgn0036767	CG16775
CG16778	FBgn0266129	lov
CG16783	FBgn0034937	fzr2
CG1681	FBgn0030484	GstT4
CG16836	FBgn0040735	CG16836
CG16844	FBgn0040736	IM3
CG16858	FBgn0016075	vkg
CG16885	FBgn0032538	CG16885
CG16888	FBgn0032533	CG16888
CG16896	FBgn0035073	CG16896
CG16898	FBgn0034480	CG16898
CG16904	FBgn0037763	CG16904
CG1691	FBgn0262735	Imp
CG16928	FBgn0020270	mre11
CG16978	FBgn0040972	CG16978
CG1698	FBgn0033443	CG1698
CG16984	FBgn0062517	CG16984
CG16996	FBgn0263234	Phae1
CG17029	FBgn0036551	CG17029
CG17065	FBgn0031099	CG17065
CG17100	FBgn0259938	cwo
CG17108	FBgn0032285	CG17108
CG17124	FBgn0032297	CG17124
CG17127	FBgn0032299	CG17127
CG17129	FBgn0035151	CG17129
CG17131	FBgn0029128	tyn
CG17145	FBgn0036953	CG17145
CG17150	FBgn0035581	Dnah3
CG17189	FBgn0039485	CG17189
CG17190	FBgn0038761	CG17190
CG17192	FBgn0039472	CG17192
CG17219	FBgn0031494	CG17219
CG17230	FBgn0046225	CG17230
CG17244	FBgn0039031	Gbp3
CG17256	FBgn0029970	Nek2
CG17264	FBgn0031490	CG17264
CG17267	FBgn0038821	CG17267
CG17286	FBgn0027500	spd-2
CG17322	FBgn0027070	CG17322
CG17323	FBgn0032713	CG17323
CG17342	FBgn0017581	Lk6
CG1740	FBgn0031145	Ntf-2
CG1742	FBgn0025814	Mgstl
CG1744	FBgn0267435	chp
CG17453	FBgn0033982	Cyp317a1
CG17461	FBgn0039925	Kif3C
CG17477	FBgn0038479	CG17477
CG17490	FBgn0040009	CG17490
CG17493	FBgn0040010	CG17493
CG17523	FBgn0063498	GstE2
CG17527	FBgn0063495	GstE5
CG17530	FBgn0063494	GstE6
CG17531	FBgn0063493	GstE7
CG17533	FBgn0063492	GstE8
CG17544	FBgn0032775	CG17544
CG17556	FBgn0038462	CG17556
CG17560	FBgn0038450	CG17560
CG17562	FBgn0038449	CG17562
CG17565	FBgn0038424	CG17565
CG17574	FBgn0038153	CG17574
CG17577	FBgn0033775	Cyp9h1
CG17600	FBgn0031195	CG17600
CG17636	FBgn0025837	CG17636
CG17646	FBgn0264494	CG17646
CG17725	FBgn0003067	Pepck
CG17751	FBgn0038717	CG17751
CG17752	FBgn0038718	CG17752
CG17814	FBgn0040959	Peritrophin-15a
CG17820	FBgn0038914	fit
CG17876	FBgn0000078	Amy-d
CG17914	FBgn0032601	yellow-b
CG17928	FBgn0032603	CG17928
CG18009	FBgn0261793	Trf2
CG1801	FBgn0031171	CG1801
CG18013	FBgn0261976	Psf2
CG18031	FBgn0023550	CG18031
CG18039	FBgn0028422	GluRIID
CG1809	FBgn0033423	CG1809
CG18095	FBgn0028872	CG18095
CG18104	FBgn0023535	arg
CG18107	FBgn0034330	CG18107
CG18111	FBgn0039678	Obp99a
CG18131	FBgn0031343	CG18131
CG18136	FBgn0036839	SmydA-2
CG1814	FBgn0033426	CG1814
CG18155	FBgn0029945	CG18155
CG18156	FBgn0035725	Mis12
CG18171	FBgn0035262	CG18171
CG18188	FBgn0033659	Damm
CG18211	FBgn0010357	betaTry
CG1827	FBgn0037263	six1
CG18296	FBgn0262870	axo
CG18314	FBgn0035538	DopEcR
CG18327	FBgn0033904	CG18327
CG18343	FBgn0033683	CG18343
CG18345	FBgn0005614	trpl
CG18372	FBgn0041581	AttB
CG18377	FBgn0033524	Cyp49a1
CG18404	FBgn0039761	CG18404
CG1842	FBgn0013813	Dhc98D
CG18444	FBgn0003863	alphaTry
CG18473	FBgn0037683	CG18473
CG1851	FBgn0026602	Ady43A
CG18547	FBgn0037973	CG18547
CG18548	FBgn0042206	GstD10
CG18559	FBgn0041337	Cyp309a2
CG18578	FBgn0040259	Ugt86Da
CG18594	FBgn0038973	Pebp1
CG18596	FBgn0038953	CG18596
CG18609	FBgn0034382	CG18609
CG18617	FBgn0028670	Vha100-2
CG18622	FBgn0038460	CG18622
CG18649	FBgn0036469	CG18649
CG1865	FBgn0042293	Spn43Ab
CG18661	FBgn0040964	CG18661
CG18681	FBgn0010425	epsilonTry
CG18744	FBgn0042101	CG18744
CG18765	FBgn0042110	CG18765
CG18783	FBgn0266450	Kr-h1
CG18809	FBgn0042132	CG18809
CG18854	FBgn0042174	CR18854
CG18858	FBgn0042175	CG18858
CG1900	FBgn0030391	Rab40
CG1901	FBgn0039914	mav
CG1944	FBgn0033395	Cyp4p2
CG1946	FBgn0033216	CG1946
CG1963	FBgn0024841	Pcd
CG1982	FBgn0024289	Sodh-1
CG2022	FBgn0037292	plh
CG2023	FBgn0037383	CG2023
CG2034	FBgn0015359	CG2034
CG2047	FBgn0001077	ftz
CG2056	FBgn0030051	spirit
CG2064	FBgn0033205	CG2064
CG2071	FBgn0011834	Ser6
CG2083	FBgn0263392	Tet
CG2092	FBgn0261385	scra
CG2101	FBgn0035374	mRpS35
CG2105	FBgn0033192	Corin
CG2107	FBgn0035383	CPT2
CG2155	FBgn0003965	v
CG2187	FBgn0017448	CG2187
CG2191	FBgn0039873	Smvt
CG2201	FBgn0032955	CG2201
CG2211	FBgn0035211	CG2211
CG2229	FBgn0039777	Jon99Fii
CG2233	FBgn0029990	CG2233
CG2248	FBgn0010333	Rac1
CG2341	FBgn0004780	Ccp84Ad
CG2469	FBgn0035205	CG2469
CG2505	FBgn0015570	alpha-Est2
CG2507	FBgn0002306	sas
CG2530	FBgn0010313	corto
CG2555	FBgn0030398	Cpr11B
CG2679	FBgn0004919	gol
CG2680	FBgn0024995	CG2680
CG2759	FBgn0003996	w
CG2772	FBgn0031533	CG2772
CG2827	FBgn0023477	Taldo
CG2837	FBgn0031646	CG2837
CG2849	FBgn0015286	Rala
CG2947	FBgn0029676	HIP-R
CG2956	FBgn0003900	twi
CG2958	FBgn0040102	lectin-24Db
CG2961	FBgn0030187	Ipod
CG2979	FBgn0005391	Yp2
CG2985	FBgn0004045	Yp1
CG30000	FBgn0050000	GstT1
CG30008	FBgn0050008	CG30008
CG30011	FBgn0050011	gem
CG30022	FBgn0050022	CG30022
CG30028	FBgn0010359	gammaTry
CG30033	FBgn0050033	CG30033
CG30047	FBgn0050047	CG30047
CG3008	FBgn0031643	CG3008
CG30080	FBgn0050080	CG30080
CG30083	FBgn0050083	CG30083
CG30104	FBgn0050104	NT5E-2
CG30108	FBgn0050108	CG30108
CG30127	FBgn0264753	Rgk1
CG3014	FBgn0037519	CG3014
CG30148	FBgn0050148	CG30148
CG3022	FBgn0031275	GABA-B-R3
CG30263	FBgn0050263	stum
CG30281	FBgn0050281	CG30281
CG30285	FBgn0050285	CG30285
CG30344	FBgn0050344	CG30344
CG3036	FBgn0031645	CG3036
CG30377	FBgn0050377	CG30377
CG30383	FBgn0050383	CG30383
CG30403	FBgn0050403	CG30403
CG30427	FBgn0043792	CG30427
CG30456	FBgn0050456	CG30456
CG30466	FBgn0050466	CG30466
CG30470	FBgn0263980	CG43729
CG30489	FBgn0050489	Cyp12d1-p
CG3056	FBgn0024987	ssx
CG3060	FBgn0002791	mr
CG3097	FBgn0029804	CG3097
CG31000	FBgn0011224	heph
CG31006	FBgn0086704	stops
CG31022	FBgn0039776	PH4alphaEFB
CG31028	FBgn0051028	CG31028
CG31029	FBgn0051029	CG31029
CG31034	FBgn0003356	Jon99Cii
CG31039	FBgn0003358	Jon99Ci
CG31041	FBgn0051041	CG31041
CG31052	FBgn0263390	Nha2
CG31075	FBgn0051075	CG31075
CG31086	FBgn0051086	CG31086
CG31089	FBgn0051089	CG31089
CG31091	FBgn0051091	CG31091
CG31097	FBgn0051097	CG31097
CG31098	FBgn0051098	CG31098
CG31100	FBgn0051100	CG31100
CG31102	FBgn0051102	CG31102
CG31108	FBgn0051108	CG31108
CG31142	FBgn0047114	CG31142
CG31150	FBgn0265048	cv-d
CG31157	FBgn0051157	CG31157
CG31163	FBgn0051163	SKIP
CG31169	FBgn0263047	CG43342
CG31217	FBgn0051217	modSP
CG31233	FBgn0051233	CG31233
CG31259	FBgn0051259	CG31259
CG31266	FBgn0051266	CG31266
CG31293	FBgn0003227	rec
CG31304	FBgn0261859	CG42788
CG31313	FBgn0051313	CG31313
CG31344	FBgn0051344	CG31344
CG31345	FBgn0051345	CG31345
CG31362	FBgn0003357	Jon99Ciii
CG31363	FBgn0051363	Jupiter
CG31368	FBgn0051368	CG31368
CG31370	FBgn0051370	CG31370
CG31386	FBgn0051386	CR31386
CG31392	FBgn0261679	CG42726
CG31414	FBgn0051414	Gba1b
CG31421	FBgn0046689	Takl1
CG31436	FBgn0051436	CG31436
CG31445	FBgn0051445	CG31445
CG31463	FBgn0051463	CG31463
CG31465	FBgn0051465	CG31465
CG31509	FBgn0028396	TotA
CG3153	FBgn0038198	Npc2b
CG31547	FBgn0051547	CG31547
CG31555	FBgn0263353	CG11000
CG31557	FBgn0046876	Obp83ef
CG31562	FBgn0051562	CR31562
CG31672	FBgn0028952	Kebab
CG31673	FBgn0051673	CG31673
CG3168	FBgn0029896	CG3168
CG31683	FBgn0051683	CG31683
CG31692	FBgn0032820	fbp
CG31705	FBgn0028490	CG31705
CG31716	FBgn0051716	Cnot4
CG3173	FBgn0034964	IntS1
CG31753	FBgn0045852	ham
CG31761	FBgn0262475	bru2
CG31777	FBgn0051777	CG31777
CG31778	FBgn0051778	CG31778
CG3178	FBgn0004584	Rrp1
CG31781	FBgn0051781	CR31781
CG31792	FBgn0051792	CG31792
CG3181	FBgn0024920	Ts
CG31811	FBgn0028509	CenG1A
CG31812	FBgn0051812	CG31812
CG3182	FBgn0003353	sei
CG31826	FBgn0051826	CG31826
CG31871	FBgn0051871	CG31871
CG31886	FBgn0032079	CG31886
CG31901	FBgn0051901	Mur29B
CG3192	FBgn0029888	ND-ASHI
CG31956	FBgn0051956	pgant4
CG31957	FBgn0051957	CG31957
CG31973	FBgn0051973	Cda5
CG31999	FBgn0051999	CG31999
CG32021	FBgn0052021	CG32021
CG32023	FBgn0052023	CG32023
CG32025	FBgn0266084	Fhos
CG32030	FBgn0266084	Fhos
CG32037	FBgn0052037	CG32037
CG32040	FBgn0052040	CG32040
CG32050	FBgn0264489	CG43897
CG32096	FBgn0041096	rols
CG32107	FBgn0052107	CG32107
CG3212	FBgn0031547	Sr-CIV
CG32152	FBgn0052152	CG32152
CG32165	FBgn0042178	CG32165
CG3217	FBgn0025676	CkIIalpha-i3
CG32187	FBgn0052187	CG32187
CG32230	FBgn0052230	ND-MLRQ
CG32243	FBgn0052243	CG32243
CG32266	FBgn0052266	CG32266
CG32280	FBgn0052280	CG32280
CG32282	FBgn0052282	Drsl4
CG32296	FBgn0052296	Mrtf
CG32302	FBgn0052302	CG32302
CG3234	FBgn0014396	tim
CG32364	FBgn0052364	tut
CG32373	FBgn0261788	Ank2
CG32379	FBgn0052379	CG32379
CG3239	FBgn0029769	frma
CG32397	FBgn0263973	jv
CG32412	FBgn0052412	QC
CG32428	FBgn0052428	CG32428
CG32435	FBgn0021760	chb
CG32436	FBgn0052436	CG32436
CG32438	FBgn0052438	SMC5
CG3244	FBgn0031629	Clect27
CG32444	FBgn0043783	CG32444
CG3246	FBgn0031538	CG3246
CG32476	FBgn0052476	mthl14
CG3248	FBgn0031536	Cog3
CG32485	FBgn0052485	CG32485
CG32500	FBgn0052500	CG32500
CG32521	FBgn0052521	CG32521
CG32523	FBgn0052523	CG32523
CG32549	FBgn0052549	CG32549
CG32557	FBgn0052557	CG32557
CG32564	FBgn0052564	CG32564
CG32581	FBgn0052581	CG32581
CG32592	FBgn0030600	hiw
CG32597	FBgn0040153	l(1)G0469
CG32604	FBgn0026713	l(1)G0007
CG32633	FBgn0052633	CG32633
CG32656	FBgn0052656	Muc11A
CG32663	FBgn0266019	rudhira
CG32669	FBgn0052669	CG32669
CG32675	FBgn0052675	Tango5
CG32683	FBgn0052683	CG32683
CG32687	FBgn0052687	CG32687
CG32695	FBgn0052695	CG32695
CG32698	FBgn0052698	CG32698
CG32732	FBgn0052732	CG32732
CG32744	FBgn0086558	Ubi-p5E
CG32751	FBgn0052751	CG32751
CG32754	FBgn0040069	vanin-like
CG32756	FBgn0052756	CG32756
CG32763	FBgn0026702	l(1)G0045
CG32774	FBgn0052774	Muc4B
CG32778	FBgn0263772	CG43689
CG32789	FBgn0260484	HIP
CG3280	FBgn0267796	CG46121
CG32816	FBgn0052816	CG32816
CG32823	FBgn0052823	Sdic3
CG3290	FBgn0283480	Alp2
CG3298	FBgn0028426	Jhl-1
CG33012	FBgn0053012	CG33012
CG3308	FBgn0038877	CG3308
CG3309	FBgn0029756	CG3309
CG33109	FBgn0053109	CG33109
CG33116	FBgn0053116	CG33116
CG33122	FBgn0015376	cutlet
CG33138	FBgn0053138	AGBE
CG33156	FBgn0053156	CG33156
CG33173	FBgn0263747	CG43672
CG33213	FBgn0053213	CG33213
CG3323	FBgn0029750	CG3323
CG33250	FBgn0065035	AlkB
CG33255	FBgn0053255	CR33255
CG33256	FBgn0261565	Lmpt
CG33258	FBgn0053258	CG33258
CG33265	FBgn0053265	Muc68E
CG33282	FBgn0053282	CG33282
CG33301	FBgn0053301	CG33301
CG33302	FBgn0053302	Cpr31A
CG33306	FBgn0053306	CG33306
CG3331	FBgn0000527	e
CG3332	FBgn0031514	CG3332
CG33338	FBgn0267339	p38c
CG33346	FBgn0053346	CG33346
CG33493	FBgn0053493	CG33493
CG33494	FBgn0053494	CG33494
CG33503	FBgn0053503	Cyp12d1-d
CG33532	FBgn0053532	lectin-37Da
CG33533	FBgn0053533	lectin-37Db
CG33546	FBgn0250732	gfzf
CG33547	FBgn0053547	Rim
CG33653	FBgn0053653	Cadps
CG3376	FBgn0034997	CG3376
CG3394	FBgn0034999	CG3394
CG33969	FBgn0053969	CG33969
CG3397	FBgn0037975	CG3397
CG33977	FBgn0053977	CG33977
CG34005	FBgn0054005	CG34005
CG34017	FBgn0260965	CG42588
CG34026	FBgn0054026	CG34026
CG34035	FBgn0262003	CG42821
CG34043	FBgn0054043	CG34043
CG34057	FBgn0054057	CG34057
CG34067	FBgn0013674	mt:CoI
CG34069	FBgn0013675	mt:CoII
CG34072	FBgn0013673	mt:ATPase8
CG34073	FBgn0013672	mt:ATPase6
CG34076	FBgn0013681	mt:ND3
CG34083	FBgn0013684	mt:ND5
CG34085	FBgn0262952	mt:ND4
CG34090	FBgn0013678	mt:Cyt-b
CG34092	FBgn0013679	mt:ND1
CG34109	FBgn0083945	CG34109
CG34149	FBgn0083985	CG34149
CG3415	FBgn0030731	Mfe2
CG34165	FBgn0085194	CG34165
CG34166	FBgn0085195	CG34166
CG34172	FBgn0085201	CG34172
CG34176	FBgn0085205	CG34176
CG34208	FBgn0085237	CG34208
CG34213	FBgn0085242	CG34213
CG34232	FBgn0085261	CG34232
CG34236	FBgn0085265	CG34236
CG34255	FBgn0085284	Blos3
CG34261	FBgn0085290	CG34261
CG34291	FBgn0085320	CG34291
CG3430	FBgn0031875	CG3430
CG34329	FBgn0085358	Diedel3
CG34330	FBgn0085359	CG34330
CG34331	FBgn0085360	CG34331
CG34334	FBgn0085363	CG34334
CG34343	FBgn0263873	sick
CG34379	FBgn0085408	Shroom
CG34386	FBgn0085415	CG34386
CG34396	FBgn0085425	CG34396
CG34411	FBgn0085440	Lgr4
CG34426	FBgn0085455	CG34426
CG34452	FBgn0085481	CG34452
CG34454	FBgn0085483	CG34454
CG34456	FBgn0085485	CG34456
CG34462	FBgn0085491	CG34462
CG3454	FBgn0005619	Hdc
CG3488	FBgn0014906	Hydr2
CG3504	FBgn0001263	inaD
CG3523	FBgn0283427	FASN1
CG3533	FBgn0004055	uzip
CG3564	FBgn0029709	CHOp24
CG3568	FBgn0029710	CG3568
CG3584	FBgn0022984	qkr58E-3
CG3585	FBgn0023458	Rbcn-3A
CG3597	FBgn0031417	CG3597
CG3609	FBgn0031418	CG3609
CG3625	FBgn0031245	CG3625
CG3653	FBgn0028369	kirre
CG3656	FBgn0005670	Cyp4d1
CG3688	FBgn0001974	l(2)35Bd
CG3690	FBgn0034050	CG3690
CG3706	FBgn0040342	CG3706
CG3709	FBgn0031227	CG3709
CG3734	FBgn0038700	CG3734
CG3740	FBgn0023530	CG3740
CG3758	FBgn0001981	esg
CG3775	FBgn0030425	CG3775
CG3819	FBgn0036833	CG3819
CG3825	FBgn0034948	Gadd34
CG3829	FBgn0035091	CG3829
CG3842	FBgn0029866	CG3842
CG3850	FBgn0033782	sug
CG3857	FBgn0032520	CG3857
CG3868	FBgn0036422	CG3868
CG3869	FBgn0029870	Marf
CG3902	FBgn0036824	CG3902
CG3918	FBgn0029873	CG3918
CG3920	FBgn0021800	Reph
CG3926	FBgn0014031	Spat
CG3938	FBgn0010382	CycE
CG3941	FBgn0034878	pita
CG3943	FBgn0020545	kraken
CG3953	FBgn0086359	Invadolysin
CG3954	FBgn0000382	csw
CG3955	FBgn0033793	CG3955
CG3969	FBgn0263998	Ack-like
CG3980	FBgn0031575	Cep97
CG3984	FBgn0038291	CG3984
CG3986	FBgn0022700	Cht4
CG3989	FBgn0020513	ade5
CG3999	FBgn0037801	CG3999
CG40045	FBgn0058045	CG40045
CG4016	FBgn0086532	Spt-I
CG40160	FBgn0058160	CG40160
CG4019	FBgn0034885	CG4019
CG40198	FBgn0058198	CG40198
CG40376	FBgn0058376	CG40376
CG40485	FBgn0069973	CG40485
CG40486	FBgn0263830	CG40486
CG4068	FBgn0266000	CG44774
CG4078	FBgn0029798	CG4078
CG40793	FBgn0085517	CG40793
CG40844	FBgn0085524	CG40844
CG40973	FBgn0085549	CG40973
CG4099	FBgn0014033	Sr-CI
CG4104	FBgn0027560	Tps1
CG4105	FBgn0015035	Cyp4e3
CG4118	FBgn0036640	nxf2
CG4122	FBgn0004648	svr
CG4123	FBgn0026061	Mipp1
CG4145	FBgn0000299	Col4a1
CG4147	FBgn0001218	Hsc70-3
CG4154	FBgn0038295	Gyc88E
CG4157	FBgn0028693	Rpn12
CG4214	FBgn0011708	Syx5
CG4220	FBgn0004858	elB
CG42237	FBgn0250862	CG42237
CG42240	FBgn0250869	CG42240
CG42251	FBgn0264542	CG43921
CG4226	FBgn0046113	GluRIIC
CG42269	FBgn0259164	CG42269
CG42270	FBgn0261570	CG42684
CG42275	FBgn0259170	alpha-Man-Ia
CG42285	FBgn0266801	CG45263
CG42309	FBgn0259209	Mlp60A
CG42326	FBgn0259226	CG42326
CG42344	FBgn0259246	brp
CG42351	FBgn0263979	Jabba
CG42365	FBgn0259711	CG42365
CG42369	FBgn0259715	CG42369
CG42370	FBgn0259716	CG42370
CG42450	FBgn0259927	CG42450
CG4250	FBgn0034761	CG4250
CG4259	FBgn0031389	CG4259
CG4267	FBgn0264979	CG4267
CG4274	FBgn0001086	fzy
CG4300	FBgn0036272	CG4300
CG4302	FBgn0027073	CG4302
CG4319	FBgn0011706	rpr
CG4335	FBgn0038795	CG4335
CG4370	FBgn0039081	Irk2
CG4373	FBgn0034756	Cyp6d2
CG4389	FBgn0028479	Mtpalpha
CG4393	FBgn0039075	CG4393
CG4415	FBgn0031296	CG4415
CG4428	FBgn0031298	Atg4a
CG4429	FBgn0262734	Rbp2
CG4452	FBgn0035981	CG4452
CG4454	FBgn0032105	borr
CG4459	FBgn0038753	CG4459
CG4461	FBgn0035982	CG4461
CG4466	FBgn0001226	Hsp27
CG4468	FBgn0038749	Xport-A
CG4475	FBgn0020415	Idgf2
CG4500	FBgn0028519	hll
CG4511	FBgn0037843	CG4511
CG4559	FBgn0020414	Idgf3
CG4563	FBgn0035006	CG4563
CG4577	FBgn0031306	CG4577
CG4594	FBgn0032161	CG4594
CG4598	FBgn0032160	CG4598
CG4600	FBgn0040064	yip2
CG4608	FBgn0014135	bnl
CG4610	FBgn0034735	CG4610
CG4617	FBgn0029936	CG4617
CG4649	FBgn0022359	Sodh-2
CG4653	FBgn0030776	CG4653
CG4666	FBgn0029838	CG4666
CG4710	FBgn0016926	Pino
CG4715	FBgn0031305	Iris
CG4716	FBgn0033820	CG4716
CG4717	FBgn0001320	kni
CG4721	FBgn0039024	CG4721
CG4723	FBgn0039023	CG4723
CG4725	FBgn0039022	CG4725
CG4734	FBgn0033826	CG4734
CG4739	FBgn0040257	Ugt86Dc
CG4740	FBgn0041579	AttC
CG4757	FBgn0027584	CG4757
CG4760	FBgn0011206	bol
CG4766	FBgn0027546	CG4766
CG4772	FBgn0040252	Ugt86Dh
CG4775	FBgn0031312	Tango14
CG4779	FBgn0040211	hgo
CG4783	FBgn0038756	CG4783
CG4784	FBgn0036619	Cpr72Ec
CG4802	FBgn0034215	Mtap
CG4805	FBgn0030795	ppk28
CG4816	FBgn0022987	qkr54B
CG4821	FBgn0023479	teq
CG4838	FBgn0028644	beat-Ic
CG4857	FBgn0026083	tyf
CG4866	FBgn0034232	CG4866
CG4881	FBgn0000287	salr
CG4962	FBgn0036597	CG4962
CG4968	FBgn0032214	CG4968
CG4999	FBgn0035936	Tsp66E
CG5008	FBgn0040321	GNBP3
CG5025	FBgn0032224	Sps2
CG5036	FBgn0028743	Dhit
CG5055	FBgn0000163	baz
CG5080	FBgn0031313	CG5080
CG5083	FBgn0038390	Rbf2
CG5096	FBgn0032235	CG5096
CG5097	FBgn0038790	MtnC
CG5098	FBgn0034300	CG5098
CG5099	FBgn0011666	msi
CG5104	FBgn0037009	CG5104
CG5106	FBgn0037879	scpr-C
CG5118	FBgn0031317	CG5118
CG5126	FBgn0031320	CG5126
CG5160	FBgn0031906	CG5160
CG5164	FBgn0034335	GstE1
CG5165	FBgn0003076	Pgm
CG5174	FBgn0034345	CG5174
CG5178	FBgn0000047	Act88F
CG5179	FBgn0019949	Cdk9
CG5207	FBgn0037889	scpr-A
CG5224	FBgn0034354	GstE11
CG5246	FBgn0038484	CG5246
CG5279	FBgn0014019	Rh5
CG5288	FBgn0263199	Galk
CG5315	FBgn0038984	AdipoR
CG5322	FBgn0032253	LManI
CG5341	FBgn0266671	Sec6
CG5360	FBgn0261786	mi
CG5371	FBgn0011703	RnrL
CG5377	FBgn0038974	CG5377
CG5399	FBgn0038353	CG5399
CG5404	FBgn0038354	CG5404
CG5413	FBgn0025456	CREG
CG5431	FBgn0265052	St3
CG5455	FBgn0039430	CG5455
CG5492	FBgn0036769	Tsp74F
CG5498	FBgn0027565	CG5498
CG5524	FBgn0266282	jnj
CG5527	FBgn0039564	CG5527
CG5532	FBgn0034902	CG5532
CG5535	FBgn0036764	CG5535
CG5543	FBgn0034908	CG5543
CG5546	FBgn0036761	MED19
CG5550	FBgn0034160	CG5550
CG5553	FBgn0259676	DNApol-alpha60
CG5580	FBgn0010575	sbb
CG5590	FBgn0039537	CG5590
CG5594	FBgn0261794	kcc
CG5621	FBgn0038840	CG5621
CG5639	FBgn0039527	CG5639
CG5644	FBgn0035948	CG5644
CG5685	FBgn0013995	Calx
CG5691	FBgn0265988	mv
CG5697	FBgn0038846	CG5697
CG5705	FBgn0032486	CG5705
CG5707	FBgn0026593	CG5707
CG5711	FBgn0000120	Arr1
CG5712	FBgn0040507	ACXD
CG5724	FBgn0038082	CG5724
CG5773	FBgn0034290	CG5773
CG5779	FBgn0283437	PPO1
CG5783	FBgn0032670	CG5783
CG5791	FBgn0040582	CG5791
CG5804	FBgn0035926	CG5804
CG5830	FBgn0036556	CG5830
CG5848	FBgn0000250	cact
CG5864	FBgn0039132	AP-1sigma
CG5867	FBgn0027586	CG5867
CG5872	FBgn0036991	CG5872
CG5887	FBgn0086687	Desat1
CG5897	FBgn0036220	CG5897
CG5904	FBgn0036557	mRpS31
CG5910	FBgn0036993	CG5910
CG5921	FBgn0029835	CG5921
CG5923	FBgn0005696	DNApol-alpha73
CG5932	FBgn0036996	mag
CG5953	FBgn0032587	CG5953
CG5991	FBgn0026576	CG5991
CG6004	FBgn0036203	Muc68D
CG6019	FBgn0002905	mus308
CG6043	FBgn0264894	CG44085
CG6048	FBgn0029827	CG6048
CG6055	FBgn0031918	CG6055
CG6064	FBgn0036746	Crtc
CG6067	FBgn0029828	CG6067
CG6074	FBgn0039486	caix
CG6106	FBgn0030914	CG6106
CG6108	FBgn0264894	CG44085
CG6137	FBgn0000146	aub
CG6145	FBgn0033853	CG6145
CG6163	FBgn0036155	CG6163
CG6172	FBgn0261930	vnd
CG6186	FBgn0022355	Tsf1
CG6191	FBgn0027581	CG6191
CG6201	FBgn0032343	CG6201
CG6202	FBgn0019925	Surf4
CG6217	FBgn0001321	knk
CG6241	FBgn0037792	TAF1B
CG6254	FBgn0037794	CG6254
CG6277	FBgn0039475	CG6277
CG6283	FBgn0039474	CG6283
CG6293	FBgn0037807	CG6293
CG6295	FBgn0039471	CG6295
CG6298	FBgn0023197	Jon74E
CG6300	FBgn0038730	CG6300
CG6312	FBgn0020379	Rfx
CG6321	FBgn0036117	CG6321
CG6349	FBgn0259113	DNApol-alpha180
CG6367	FBgn0030926	psh
CG6385	FBgn0034276	Sardh
CG6403	FBgn0039453	CG6403
CG6405	FBgn0032428	CG6405
CG6414	FBgn0029690	CG6414
CG6421	FBgn0025827	CG6421
CG6425	FBgn0039449	CG6425
CG6426	FBgn0034162	CG6426
CG6433	FBgn0003187	qua
CG6488	FBgn0032361	CG6488
CG6495	FBgn0027550	CG6495
CG6503	FBgn0040606	CG6503
CG6511	FBgn0035923	CG6511
CG6519	FBgn0000355	Cp15
CG6530	FBgn0028956	mthl3
CG6535	FBgn0045035	tefu
CG6539	FBgn0011802	Gem3
CG6553	FBgn0033880	CG6553
CG6580	FBgn0035666	Jon65Aii
CG6583	FBgn0032420	CG6583
CG6593	FBgn0003134	Pp1alpha-96A
CG6613	FBgn0034694	CG6613
CG6621	FBgn0037855	CG6621
CG6633	FBgn0040256	Ugt86Dd
CG6640	FBgn0262007	CG42825
CG6660	FBgn0039030	CG6660
CG6698	FBgn0029147	NtR
CG6704	FBgn0033887	St4
CG6707	FBgn0036058	CG6707
CG6733	FBgn0039052	CG6733
CG6738	FBgn0039053	CG6738
CG6749	FBgn0036040	CG6749
CG6754	FBgn0261530	nbs
CG6755	FBgn0039066	EloA
CG6781	FBgn0086348	se
CG6783	FBgn0037913	fabp
CG6798	FBgn0004118	nAChRbeta2
CG6827	FBgn0013997	Nrx-IV
CG6839	FBgn0036831	CG6839
CG6863	FBgn0004885	tok
CG6891	FBgn0030955	CG6891
CG6904	FBgn0266064	GlyS
CG6906	FBgn0027843	CAH2
CG6908	FBgn0037936	CG6908
CG6912	FBgn0038290	CG6912
CG6917	FBgn0000592	Est-6
CG6934	FBgn0261859	CG42788
CG6953	FBgn0026721	fat-spondin
CG6958	FBgn0039004	Nup133
CG6966	FBgn0038286	CG6966
CG6972	FBgn0039008	CG6972
CG6999	FBgn0030085	CG6999
CG7000	FBgn0260004	Snmp1
CG7002	FBgn0029167	Hml
CG7021	FBgn0013949	Elal
CG7029	FBgn0039026	CG7029
CG7047	FBgn0035103	Vdup1
CG7066	FBgn0087039	Sbp2
CG7068	FBgn0041181	Tep3
CG7106	FBgn0040099	lectin-28C
CG7123	FBgn0261800	LanB1
CG7125	FBgn0038603	PKD
CG7134	FBgn0031952	cdc14
CG7169	FBgn0037105	S1P
CG7171	FBgn0003961	Uro
CG7183	FBgn0038583	CG7183
CG7194	FBgn0035868	CG7194
CG7219	FBgn0031973	Spn28Dc
CG7225	FBgn0004003	wbl
CG7266	FBgn0000565	Eip71CD
CG7296	FBgn0032283	CG7296
CG7298	FBgn0036948	CG7298
CG7300	FBgn0032286	CG7300
CG7313	FBgn0036783	CheA75a
CG7322	FBgn0030968	CG7322
CG7352	FBgn0037581	CG7352
CG7372	FBgn0036522	CG7372
CG7375	FBgn0035853	UbcE2M
CG7381	FBgn0038098	CG7381
CG7384	FBgn0030262	CG7384
CG7390	FBgn0038257	smp-30
CG7399	FBgn0001208	Hn
CG7402	FBgn0036768	CG7402
CG7422	FBgn0035815	Snmp2
CG7447	FBgn0035539	slow
CG7449	FBgn0029082	hbs
CG7458	FBgn0037144	CG7458
CG7461	FBgn0034432	CG7461
CG7464	FBgn0029091	CS-2
CG7497	FBgn0036742	CG7497
CG7512	FBgn0036168	CG7512
CG7526	FBgn0035798	frac
CG7529	FBgn0037090	Est-Q
CG7538	FBgn0014861	Mcm2
CG7560	FBgn0036157	CG7560
CG7567	FBgn0039670	CG7567
CG7571	FBgn0036732	Oatp74D
CG7583	FBgn0020496	CtBP
CG7584	FBgn0039682	Obp99c
CG7586	FBgn0267488	Mcr
CG7601	FBgn0027583	CG7601
CG7607	FBgn0036145	CG7607
CG7616	FBgn0036142	CG7616
CG7629	FBgn0038530	AttD
CG7635	FBgn0030993	Mec2
CG7639	FBgn0033989	CG7639
CG7643	FBgn0000063	Mps1
CG7665	FBgn0016650	Lgr1
CG7675	FBgn0038610	CG7675
CG7676	FBgn0038612	cona
CG7678	FBgn0038613	Vha100-4
CG7725	FBgn0036697	rogdi
CG7754	FBgn0015001	iotaTry
CG7758	FBgn0027945	ppl
CG7762	FBgn0028695	Rpn1
CG7768	FBgn0036415	CG7768
CG7780	FBgn0000477	DNaseII
CG7789	FBgn0039698	CG7789
CG7802	FBgn0039704	neo
CG7825	FBgn0025808	Rad17
CG7828	FBgn0261112	APP-BP1
CG7838	FBgn0263855	BubR1
CG7840	FBgn0032014	CG7840
CG7848	FBgn0034127	CG7848
CG7851	FBgn0032013	Scgalpha
CG7882	FBgn0033047	CG7882
CG7900	FBgn0037548	CG7900
CG7912	FBgn0039736	CG7912
CG7916	FBgn0028534	CG7916
CG7930	FBgn0010424	TpnC73F
CG7952	FBgn0001150	gt
CG7953	FBgn0028533	CG7953
CG7966	FBgn0038115	CG7966
CG7972	FBgn0002899	mus301
CG8024	FBgn0002567	Rab32
CG8032	FBgn0037606	CG8032
CG8063	FBgn0038105	yellow-f2
CG8066	FBgn0038243	CG8066
CG8067	FBgn0033891	CG8067
CG8094	FBgn0001187	Hex-C
CG8121	FBgn0037680	pasi2
CG8129	FBgn0037684	CG8129
CG8147	FBgn0043791	phu
CG8175	FBgn0014865	Mtk
CG8180	FBgn0026066	MagR
CG8210	FBgn0262512	Vha14-1
CG8226	FBgn0033357	Tom7
CG8234	FBgn0033644	Tret1-2
CG8243	FBgn0033349	CG8243
CG8292	FBgn0032004	CG8292
CG8299	FBgn0034052	CG8299
CG8303	FBgn0034143	CG8303
CG8315	FBgn0034058	Pex11
CG8345	FBgn0033065	Cyp6w1
CG8353	FBgn0032002	CG8353
CG8357	FBgn0024732	Drep1
CG8358	FBgn0037727	CG8358
CG8359	FBgn0037634	hng2
CG8360	FBgn0032001	CG8360
CG8367	FBgn0000289	cg
CG8376	FBgn0267978	ap
CG8380	FBgn0034136	DAT
CG8396	FBgn0015299	Ssb-c31a
CG8404	FBgn0005613	Sox15
CG8420	FBgn0037664	CG8420
CG8422	FBgn0033932	Dh44-R1
CG8425	FBgn0010052	Jhe
CG8426	FBgn0033029	Not3
CG8428	FBgn0086676	spin
CG8431	FBgn0027091	CysRS
CG8448	FBgn0034091	mrj
CG8453	FBgn0025454	Cyp6g1
CG8457	FBgn0033697	Cyp6t3
CG8458	FBgn0038134	wntD
CG8486	FBgn0264953	Piezo
CG8533	FBgn0260874	Ir76a
CG8560	FBgn0035781	CG8560
CG8562	FBgn0035779	CG8562
CG8579	FBgn0001285	Jon44E
CG8587	FBgn0033753	Cyp301a1
CG8627	FBgn0010387	Dbi
CG8639	FBgn0033313	Cirl
CG8661	FBgn0030837	CG8661
CG8665	FBgn0032945	CG8665
CG8668	FBgn0031988	CG8668
CG8687	FBgn0033302	Cyp6a14
CG8693	FBgn0033294	Mal-A4
CG8721	FBgn0013307	Odc1
CG8740	FBgn0027585	CG8740
CG8757	FBgn0036380	CG8757
CG8770	FBgn0004623	Gbeta76C
CG8785	FBgn0033760	CG8785
CG8788	FBgn0028955	CG8788
CG8791	FBgn0033234	MFS12
CG8801	FBgn0028473	Non1
CG8804	FBgn0016078	wun
CG8806	FBgn0033413	prel
CG8819	FBgn0033749	achi
CG8821	FBgn0033748	vis
CG8825	FBgn0260817	gkt
CG8827	FBgn0012037	Ance
CG8859	FBgn0033696	Cyp6g2
CG8864	FBgn0028940	Cyp28a5
CG8867	FBgn0020906	Jon25Bi
CG8871	FBgn0031653	Jon25Biii
CG8891	FBgn0031663	CG8891
CG8892	FBgn0031664	CG8892
CG8928	FBgn0030711	Rrp47
CG8936	FBgn0065032	Arpc3B
CG8947	FBgn0250848	26-29-p
CG8950	FBgn0034186	CG8950
CG8952	FBgn0030688	CG8952
CG8960	FBgn0035315	CG8960
CG8991	FBgn0033654	Sobp
CG8997	FBgn0028920	CG8997
CG9001	FBgn0034175	ste24b
CG9042	FBgn0001128	Gpdh
CG9057	FBgn0030608	Lsd-2
CG9111	FBgn0004426	LysC
CG9118	FBgn0004427	LysD
CG9120	FBgn0004431	LysX
CG9128	FBgn0283500	Sac1
CG9149	FBgn0035203	CG9149
CG9150	FBgn0031775	CG9150
CG9181	FBgn0267487	Ptp61F
CG9186	FBgn0035206	CG9186
CG9187	FBgn0035194	Psf1
CG9188	FBgn0031878	sip2
CG9198	FBgn0004391	shtd
CG9232	FBgn0263200	Galt
CG9240	FBgn0030669	CG9240
CG9245	FBgn0030670	Pis
CG9259	FBgn0032913	CG9259
CG9265	FBgn0032910	CG9265
CG9270	FBgn0032908	CG9270
CG9273	FBgn0032906	RPA2
CG9280	FBgn0001114	Glt
CG9324	FBgn0032884	Pomp
CG9377	FBgn0032507	CG9377
CG9380	FBgn0035094	CG9380
CG9400	FBgn0030562	CG9400
CG9413	FBgn0030574	CG9413
CG9414	FBgn0028406	Drep4
CG9416	FBgn0034438	CG9416
CG9427	FBgn0037721	CG9427
CG9431	FBgn0032484	kek4
CG9434	FBgn0037724	Fst
CG9436	FBgn0033101	CG9436
CG9444	FBgn0037730	CG9444
CG9451	FBgn0036876	CG9451
CG9452	FBgn0036877	CG9452
CG9463	FBgn0032066	LManIII
CG9468	FBgn0032069	LManVI
CG9470	FBgn0002868	MtnA
CG9505	FBgn0031805	CG9505
CG9506	FBgn0043854	slam
CG9527	FBgn0031813	CG9527
CG9528	FBgn0031814	retm
CG9538	FBgn0015010	Ag5r
CG9540	FBgn0020508	Ag5r2
CG9577	FBgn0031092	CG9577
CG9609	FBgn0030787	CG9609
CG9617	FBgn0265101	Sgt1
CG9621	FBgn0038172	Adgf-D
CG9629	FBgn0036857	CG9629
CG9633	FBgn0010173	RpA-70
CG9649	FBgn0038211	CG9649
CG9650	FBgn0029939	CG9650
CG9668	FBgn0003250	Rh4
CG9672	FBgn0030777	CG9672
CG9675	FBgn0030774	spheroide
CG9676	FBgn0030773	CG9676
CG9682	FBgn0039760	CG9682
CG9707	FBgn0034628	Acox57D-p
CG9753	FBgn0039747	AdoR
CG9771	FBgn0040466	Dlip2
CG9772	FBgn0037236	Skp2
CG9792	FBgn0041711	yellow-e
CG9811	FBgn0264753	Rgk1
CG9812	FBgn0034860	CG9812
CG9819	FBgn0267912	CanA-14F
CG9842	FBgn0011826	Pp2B-14D
CG9852	FBgn0010340	140up
CG9889	FBgn0041712	yellow-d
CG9893	FBgn0010622	DCTN3-p24
CG9914	FBgn0030737	CG9914
CG9925	FBgn0038191	CG9925
CG9930	FBgn0008646	E5
CG9932	FBgn0262160	CG9932
CG9943	FBgn0029117	Surf1
CG9964	FBgn0031432	Cyp309a1
CG9976	FBgn0016675	Lectin-galC1
CG9977	FBgn0035371	CG9977
CG9981	FBgn0030746	CG9981
CG9993	FBgn0034553	CG9993
CG9994	FBgn0032782	Rab9
CG9999	FBgn0003346	RanGAP

Figure S12. Between sex gene intersections for <u>mitonuclear</u> genes. Those genes listed are consistently differentially expressed and intersected across the sexes.

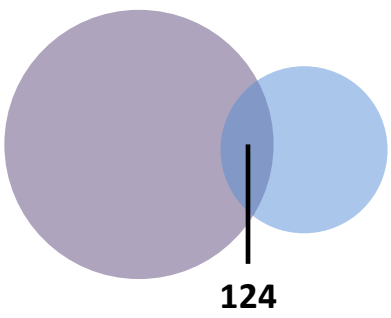

Computed gene ID	Flybase ID	Gene ID
CG10011	FBgn0039590	*CG10011*
CG10182	FBgn0039091	*CG10182*
CG10248	FBgn0013772	*Cyp6a8*
CG10275	FBgn0032683	*kon*
CG10623	FBgn0032727	*CG10623*
CG10799	FBgn0033821	*CG10799*
CG10816	FBgn0010388	*Dro*
CG10842	FBgn0015037	*Cyp4p1*
CG11263	FBgn0036330	*CG11263*
CG1131	FBgn0015569	*alpha-Est10*
CG1143	FBgn0035359	*CG1143*
CG11586	FBgn0035520	*CG11586*
CG1165	FBgn0004430	*LysS*
CG11752	FBgn0030292	*CG11752*
CG1179	FBgn0004425	*LysB*
CG1180	FBgn0004428	*LysE*
CG11966	FBgn0037645	*CG11966*
CG11985	FBgn0040534	*CG11985*
CG12400	FBgn0031505	*ND-B14.5B*
CG12763	FBgn0004240	*DptA*
CG12883	FBgn0039538	*CG12883*
CG12934	FBgn0033541	*CG12934*
CG13177	FBgn0040759	*CG13177*
CG13306	FBgn0040828	*CG13306*
CG13321	FBgn0033787	*CG13321*
CG13482	FBgn0036419	*CG13482*
CG13551	FBgn0040660	*CG13551*
CG13751	FBgn0033340	*CG13751*
CG14120	FBgn0036321	*CG14120*
CG14125	FBgn0036232	*CG14125*
CG14688	FBgn0037819	*CG14688*
CG14715	FBgn0037930	*CG14715*
CG14745	FBgn0043575	*PGRP-SC2*
CG14746	FBgn0043576	*PGRP-SC1a*
CG15065	FBgn0040734	*CG15065*
CG15066	FBgn0034328	*IM23*
CG15083	FBgn0034399	*CG15083*
CG15168	FBgn0032732	*CG15168*
CG15231	FBgn0040653	*IM4*
CG15534	FBgn0039769	*CG15534*
CG15707	FBgn0034098	*krimp*
CG15918	FBgn0034197	*Cda9*
CG1623	FBgn0033448	*hebe*
CG1648	FBgn0033446	*CG1648*
CG16725	FBgn0036641	*Smn*
CG16727	FBgn0038719	*CG16727*
CG17003	FBgn0031082	*CG17003*
CG17327	FBgn0038107	*CG17327*
CG17776	FBgn0040899	*CG17776*
CG1836	FBgn0026777	*Rad23*
CG18585	FBgn0031929	*CG18585*
CG18600	FBgn0038601	*CG18600*
CG18624	FBgn0029971	*ND-MNLL*
CG1981	FBgn0026869	*Thd1*
CG2065	FBgn0033204	*CG2065*
CG2083	FBgn0263392	*Tet*
CG2210	FBgn0000150	*awd*
CG2222	FBgn0030196	*Psf3*
CG30273	FBgn0050273	*CG30273*
CG30494	FBgn0263077	*CG43340*
CG3085	FBgn0034816	*CG3085*
CG31034	FBgn0003356	*Jon99Cii*
CG31089	FBgn0051089	*CG31089*
CG31148	FBgn0051148	*Gba1a*
CG31205	FBgn0051205	*CG31205*
CG31362	FBgn0003357	*Jon99Ciii*
CG31463	FBgn0051463	*CG31463*
CG32019	FBgn0005666	*bt*
CG32025	FBgn0266084	*Fhos*
CG32030	FBgn0266084	*Fhos*
CG32038	FBgn0266124	*ghi*
CG32557	FBgn0052557	*CG32557*
CG32599	FBgn0260482	*CG32599*
CG3264	FBgn0034712	*CG3264*
CG33002	FBgn0053002	*mRpL27*
CG33196	FBgn0053196	*dpy*
CG33256	FBgn0261565	*Lmpt*
CG33346	FBgn0053346	*CG33346*
CG3350	FBgn0039509	*bigmax*
CG33533	FBgn0053533	*lectin-37Db*
CG34073	FBgn0013672	*mt:ATPase6*
CG34083	FBgn0013684	*mt:ND5*
CG34089	FBgn0013685	*mt:ND6*
CG34212	FBgn0085241	*CG34212*
CG34227	FBgn0085256	*CG34227*
CG3683	FBgn0035046	*ND-19*
CG3759	FBgn0032116	*Mco1*
CG3939	FBgn0040396	*CG3939*
CG3986	FBgn0022700	*Cht4*
CG4000	FBgn0038820	*CG4000*
CG41421	FBgn0085643	*CG41421*
CG41536	FBgn0085675	*CG41536*
CG4178	FBgn0002563	*Lsp1beta*
CG42254	FBgn0259112	*CR42254*
CG4847	FBgn0034229	*CG4847*
CG4869	FBgn0003890	*betaTub97EF*
CG5242	FBgn0037892	*mRpL40*
CG5381	FBgn0032218	*CG5381*
CG5646	FBgn0039525	*CG5646*
CG5767	FBgn0034292	*CG5767*
CG5830	FBgn0036556	*CG5830*
CG6004	FBgn0036203	*Muc68D*
CG6272	FBgn0036126	*CG6272*
CG6503	FBgn0040606	*CG6503*
CG6602	FBgn0035673	*CG6602*
CG6620	FBgn0024227	*aurB*
CG6972	FBgn0039008	*CG6972*
CG7014	FBgn0038277	*RpS5b*
CG7068	FBgn0041181	*Tep3*
CG7291	FBgn0031381	*Npc2a*
CG7407	FBgn0037134	*CG7407*
CG7542	FBgn0036738	*CG7542*
CG7601	FBgn0027583	*CG7601*
CG7622	FBgn0002579	*RpL36*
CG8147	FBgn0043791	*phu*
CG8577	FBgn0033327	*PGRP-SC1b*
CG8958	FBgn0030725	*CG8958*
CG9025	FBgn0034542	*Fem-1*
CG9034	FBgn0040931	*CG9034*
CG9044	FBgn0031752	*CG9044*
CG9111	FBgn0004426	*LysC*
CG9116	FBgn0004429	*LysP*
CG9118	FBgn0004427	*LysD*
CG9450	FBgn0003891	*tud*

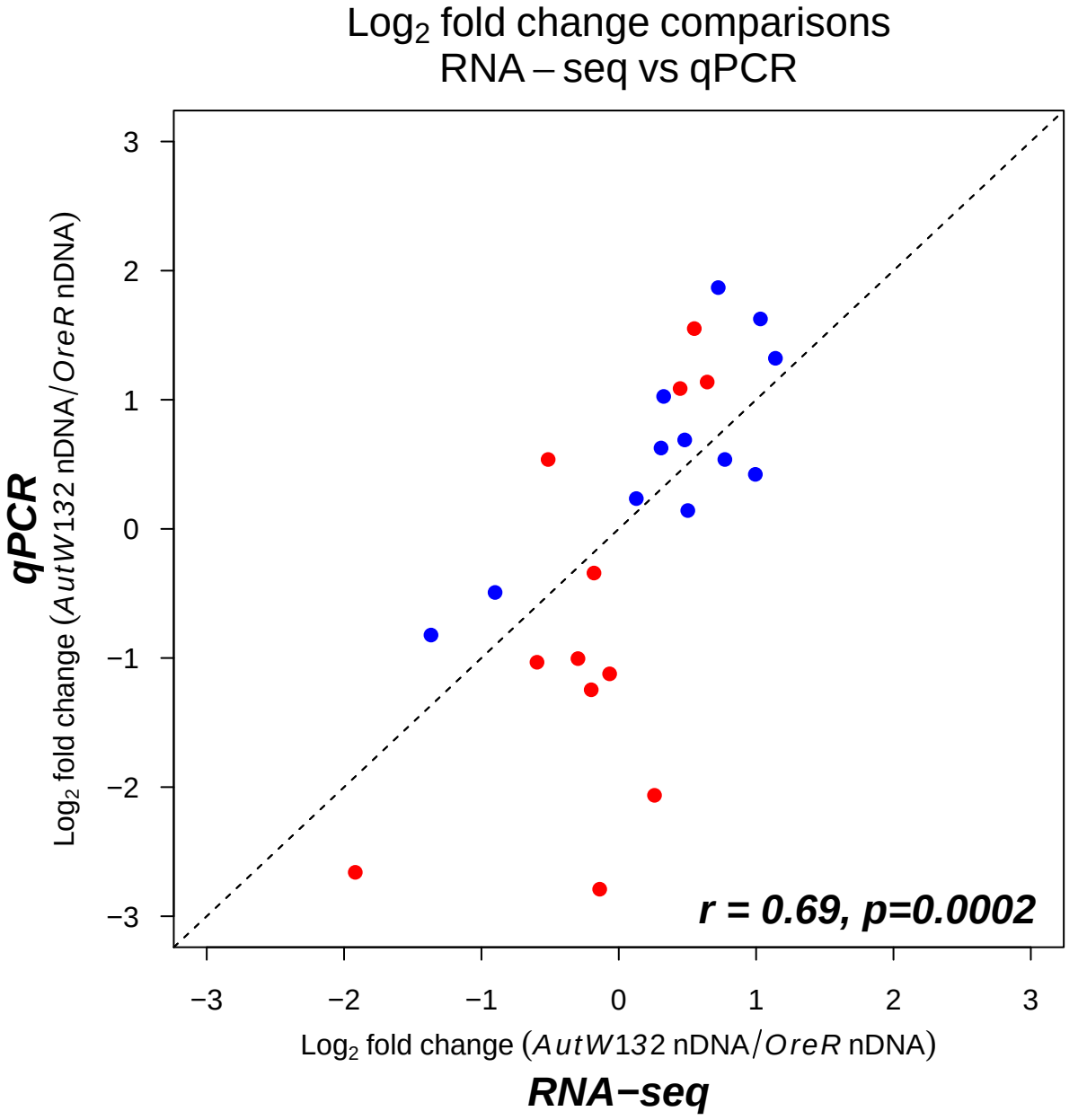
Log2 fold change comparisons
RNA – seq vs qPCR
qPCR
Log2 fold change (AutW132 nDNA/OreR nDNA)
RNA−seq
Log2 fold change (AutW132 nDNA/OreR nDNA)
r = 0.69, p=0.0002
3
2
1
0
−1
−2
−3
−3
−2
−1
0
1
2
3

A

Females

B

Males

Offspring per vial

200
150
100
50
0

OreR; AutW132
sil; AutW132
OreR; OreR
sil; OreR

Genotype

Table S1. qPCR primers and sequences used in the RNA-seq validation. Gene names, CG IDs and primer sequences are shown (5'->3' direction).

Gene name	Computed gene ID	Forward primer (5'->3')	Reverse primer (5'->3')
RpL32 (*rp49*)	CG7939	GATATGCTAAGCTGTCGCACAAA	TAACCGATGTTGGGCATCAGA
Cox4A	CG10664	CCAGCTTCTGCCAGACTATCG	GGCAGCTCATCGTACACGAA
Cox5B	CG11015	TGCATCTGCGAAGAGGATCA	TCTCCACCAGCTTGAACCAA
Cox6B	CG14235	TCGACCCACGGTTCCCTAA	GCACATCGACTTGTAGACCTTCTG
Cox7AL	CG18193	CCGAAGACACGTCCTGGAA	TGTTATCCATACTGCCGCCTTT
Cox8	CG7181	CATCTCCACCGCCGAGAA	TTGTAGTCCCGGATGTGGTAGA
Hsp68	CG5436	AACTGGAGACCTATTTGTTTGG	CCTTCAGTTTGTACTCGTACTC

Table S2. Generalized linear models of offspring production in females (analysis of deviance). Terms in the model were nDNA type, mtDNA type, and block. All first order effects and interaction terms were fitted. We report the degrees-of-freedom (df), deviance, residual degrees-of-freedom, residual deviance and p-values based on a Chi-squared distribution. P-values in bold are significant at α=0.05.

Model term	df	Deviance	Residual df	Residual deviance	P (>Chi)
	-	-	92	148.51	-
nDNA	1	0.84	91	147.67	0.36
mtDNA	1	0.23	90	147.45	0.63
Block	1	44.96	89	102.49	**2.014E-11**
nDNA x mtDNA	1	0.54	88	101.95	0.46
nDNA x block	1	0.31	87	101.64	0.58
mtDNA x block	1	0.17	86	101.47	0.68
nDNA x mtDNA x block	1	2.01	85	99.46	0.16

Table S3. Generalized linear models of offspring production in males (analysis of deviance). Terms in the model were nDNA type, mtDNA type, and block. All first order effects and interaction terms were fitted. We report the degrees-of-freedom (df), deviance, residual degrees-of-freedom, residual deviance and p-values based on a Chi-squared distribution. P-values in bold are significant at α=0.05.

Model term	df			Residual deviance	P (>Chi)
	-	-	92	130.25	-
nDNA	1	0.65	91	129.60	0.42
mtDNA	1	0.03	90	129.58	0.87
Block	1	26.71	89	102.87	**2.368E-07**
nDNA x mtDNA	1	1.18	88	101.68	0.28
nDNA x block	1	0.68	87	101.00	0.41
mtDNA x block	1	0.22	86	100.78	0.64
nDNA x mtDNA x block	1	0.96	85	99.82	0.33

Supporting Information

Mitochondrial-nuclear interactions mediate sex-specific transcriptional profiles in *Drosophila*

Mossman JA, Tross JG, Li N, Wu Z, Rand DM

qPCR validation of RNA-seq data obtained on an Illumina Hiseq 2000 platform

To validate transcription expression measurements, we conducted qPCR on seven primer pairs to determine if the RNA-seq data showed qualitatively and quantitatively similar results to those obtained by qPCR. We aimed to test whether the $\log_2$-fold changes obtained on the RNA-seq platform (Illumina Hiseq 2000, Illumina, Inc, CA, USA) were similar to those from qPCR (Applied Biosystems™ 7300 Real Time PCR System, Applied Biosystems, ThermoFisher Scientific, MA, USA).

The accuracy of qPCR depends on the magnitude of log fold change between the contrasting treatments and small fold changes can be difficult to interpret (MOREY *et al.* 2006). Since the mtDNA effects we observed for nuclear genes were small in magnitude, we used the contrast between nuclear backgrounds within a mitochondrial haplotype to validate the expression results. This was done for both mtDNA haplotypes and the contrast was the effect of *AutW132* nuclear background relative to the *Oregon R* nuclear background.

MtDNA primers for qPCR for the two mtDNA haplotypes we studied are problematic to design because of the high A+T content of Drosophila mtDNA and the haplotype variation between *D. melanogaster* and *D. simulans* mtDNA introduces SNPs into useful primer sequences and differential expression cannot be easily teased apart from differential annealing efficiency. To circumvent this problem, we focused on nuclear genes that encode mitochondrial protein products in cytochrome c oxidase (complex IV of the electron transport chain), along with heat shock protein 68 (*hsp68*). These genes showed differences in expression between nuclear backgrounds, as judged by read counts from RNA-seq. We also measured a

reference housekeeping gene: Ribosomal protein L32 (*rp49*), which was used as an internal control for RNA concentration. A list of primers and primer sequences are shown in Table S1. Two biological replicates of each genotype were measured, with triplicate technical replicates, totaling 96 PCRs for each gene of interest (48x 'focal' gene and 48x 'internal *rp49* controls'). Conducting the qPCRs in this way prevented comparison across plates for a focal gene. Negative samples were run on a separate plate. All negative samples showed no detectable values of fluorescence.

Table S1. qPCR primers and sequences used in the RNA-seq validation. Gene names, CG IDs and primer sequences are shown (5'->3' direction).

Gene name	Computed gene ID	Forward primer (5'->3')	Reverse primer (5'->3')
RpL32 (*rp49*)	CG7939	GATATGCTAAGCTGTCGCACAAA	TAACCGATGTTGGGCATCAGA
Cox4A	CG10664	CCAGCTTCTGCCAGACTATCG	GGCAGCTCATCGTACACGAA
Cox5B	CG11015	TGCATCTGCGAAGAGGATCA	TCTCCACCAGCTTGAACCAA
Cox6B	CG14235	TCGACCCACGGTTCCCTAA	GCACATCGACTTGTAGACCTTCTG
Cox7AL	CG18193	CCGAAGACACGTCCTGGAA	TGTTATCCATACTGCCGCCTTT
Cox8	CG7181	CATCTCCACCGCCGAGAA	TTGTAGTCCCGGATGTGGTAGA
Hsp68	CG5436	AACTGGAGACCTATTTGTTTGG	CCTTCAGTTTGTACTCGTACTC

To obtain relevant RNA-seq values, we conducted separate DESeq (ANDERS and HUBER 2010) analyses using the same two biological replicates as used in the qPCR with the contrast between nuclear backgrounds. The $\log_2$-fold changes for the focal genes were used as comparison in the qPCR-RNA-seq correlation.

qPCRs were conducted using Power SYBR® Green system (Applied Biosystems, CA, USA) using a two-step protocol. We used the same mRNA template that was used in the main Illumina RNA-seq study.

DNase treatment

Briefly, 44µl mRNA + H_20 were mixed with 5µl 10x Turbo DNase buffer (Invitrogen, ThermoFisher Scientific, MA, USA) and 1µl Turbo DNase (Invitrogen, ThermoFisher Scientific, MA, USA) to remove any contaminating DNA. After 30 minutes of incubation at 37°C, an additional 1µl of DNase was added and

this mixture was further incubated for 30 minutes at 37°C. Following, we added 10µl of DNase inactivation buffer (Invitrogen, ThermoFisher Scientific, MA, USA), which was mixed then centrifuged. The supernatant was aspirated, then re-centrifuged. The supernatant from the second centrifugation was the template for cDNA synthesis.

cDNA synthesis

We quantified the RNA concentration using a Nanodrop (ThermoFisher Scientific, MA, USA) and standardized to 5ng/µl. 15µl of 5ng/µl RNA solution was added to 4µl iScript cDNA synthesis reaction mixture (Bio-Rad Laboratories, Inc, CA, USA) and 1µl reverse transcriptase (Bio-Rad Laboratories, Inc, CA, USA). cDNA synthesis was carried out using the following thermocycling protocol: 5 minutes at 25^{o}C, 30 minutes at 42^{o}C, then 5 minutes at 85^{o}C. cDNA concentration was measured using a Nanodrop and diluted to a standard concentration (120ng/µl). qPCR was conducted on the cDNAs using the following reaction mixture: 10µl SYBR Green reaction mixture, 0.5µl of each primer (at 50 pmol/µl concentration), 6µl H_20, and 3µl cDNA.

qPCR

qPCR was conducted using an Applied Biosystems 7300 Real Time PCR System (Applied Biosystems, ThermoFisher Scientific, MA, USA). The thermocycling protocol was as follows: an initial incubation at 50^{o}C (2 minutes), followed by 95^{o}C (10 minutes), then 40 cycles of 95^{o}C (15 seconds) -> 60^{o}C (60 seconds). A dissociation step was added: (95^{o}C, 15 seconds), followed by 60^{o}C (1 minute), 95^{o}C (15 seconds), then 60^{o}C (15 seconds). Melting curves were checked for primer dimers and none were detected. Amplification curves were analyzed using Applied Biosystems Sequence Detection Software v1.4.0.27, with the auto C_T function.

Log_2-fold changes

For each focal gene, we assessed $\log_2$-fold changes of *AutW132* nuclear background against the *Oregon R* reference using the comparative threshold cycle, C_T, method ($2^{-\Delta\Delta CT}$) (SCHMITTGEN and LIVAK 2008), with samples standardized to the *rp49* gene reference (internal control). We estimated the $\log_2$-fold difference against each biological replicate 'calibrator', and used the mean value of these two measures in the correlation analysis.

In total, we correlated 24 samples (4x genotypes, 6x genes) and found a significant positive correlation between $\log_2$-fold change estimated by RNA-seq and qPCR (r=0.69, t = 4.52, df=22, p=0.00016: Figure S13). When the data were parsed into female and male datasets- the red and blue data in Figure S13, respectively- both subsets demonstrated significtant positive correlations between measurement estimates; female correlation: r= 0.60, t= 2.40, df= 10, p= 0.037; male correlation: r= 0.81, t=4.375, df=10, p= 0.001.

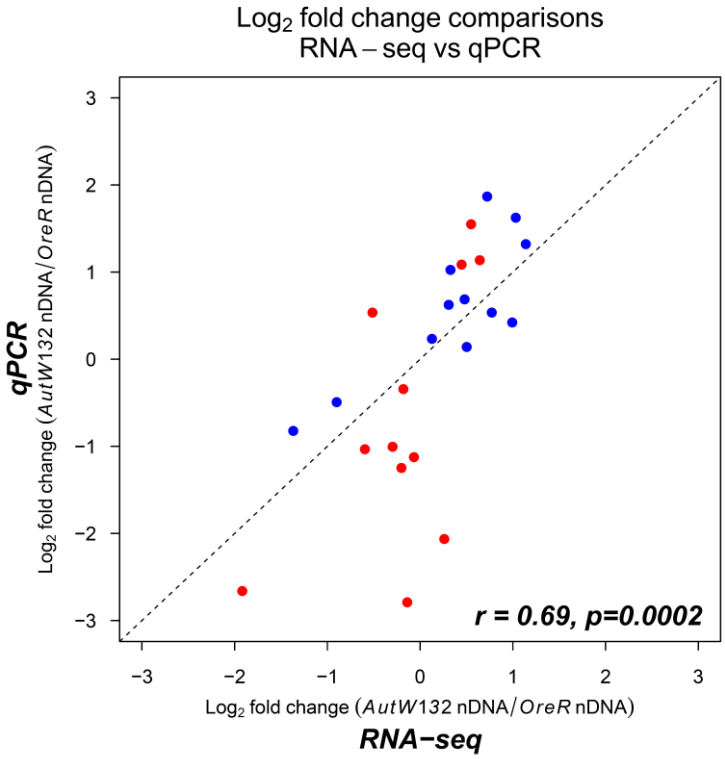

Figure S13. Correlation between RNA-seq and qPCR estimates of log2-fold change. Data from all 4 mitonuclear genotypes across 6 nuclear loci are shown. Samples in blue are male genotypes, samples in red are female genotypes. Log_2-fold change estimates were judged using the ΔΔCT method (qPCR) and

DESeq (RNA-seq). The genotype contrasts are between *AutW132* and *Oregon R* (*OreR*) in both mtDNA backgrounds (*sil* and *Oregon R*). The dashed line shows $\log_2$-fold change equality between the expression measurement platforms.

Offspring production in the mitonuclear genotype panel

We used results from a previous study (MONTOOTH *et al.* 2010) to investigate whether there were differences in fecundity between the genotypes for females and males. Full details on the materials and methods for this assay can be found in (MONTOOTH *et al.* 2010). Briefly, we summed the total number of offspring that were produced in a fitness assay. The assay consisted of six replicate vials of five females and five males that were allowed to continually mate and lay eggs for two days. Each set of parents were flipped onto fresh food after two days, for a total of 12 days, giving six two-day broods. Each genotype x sex combination (individual boxes in Figure S14) represents 11-12 vials. Figure S14 describes these data.

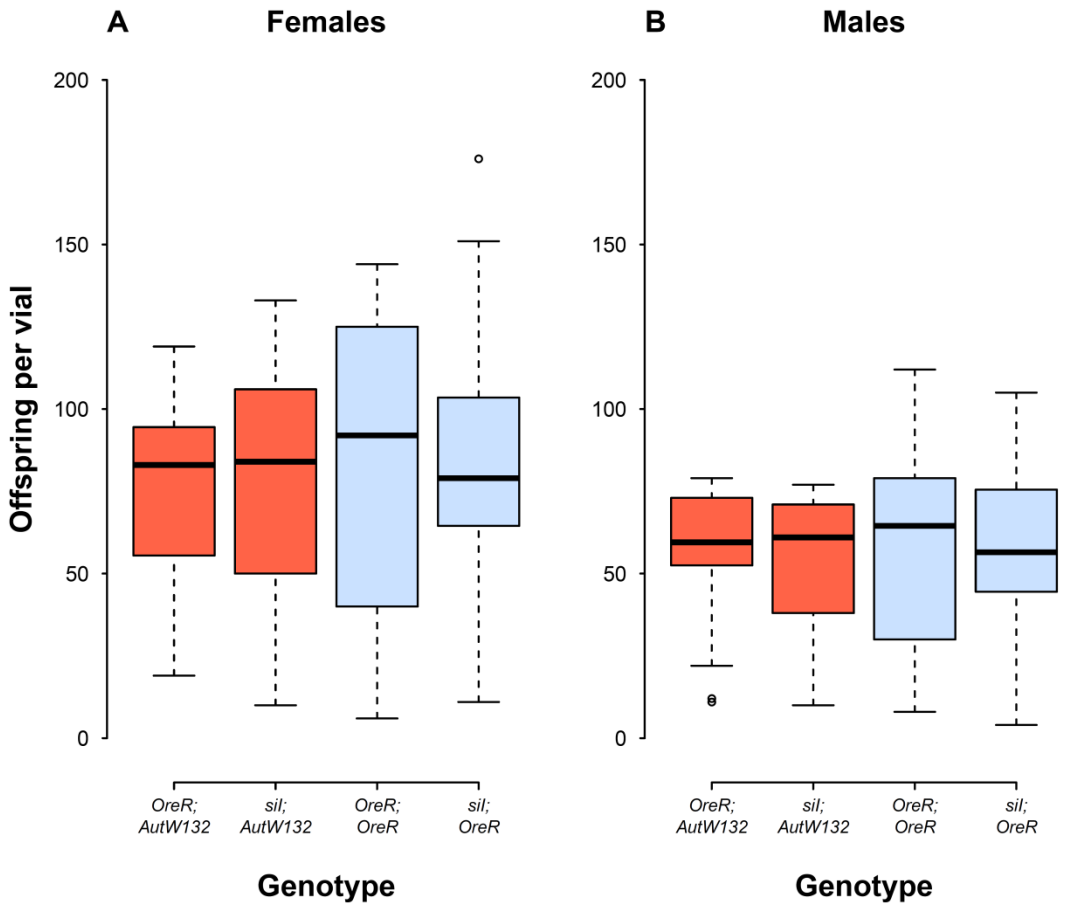

Figure S14. Offspring production within the four genotypes used in this study. Female (A) and male (B) results are shown. The two nuclear backgrounds are distinguished by color; *AutW132* (orange) and *OreR* (blue). Data are from (MONTOOTH *et al.* 2010). Within each sex there were no significant main effects of nuclear background or mtDNA haplotype on offspring numbers, and their interaction was not significant (see Tables S2 and S3 for the female and male results, respectively). The *mito;nuclear* genotypes are labeled on the abscissa.

We tested whether nuclear background, mtDNA haplotype, or their interaction were significantly associated with the number of offspring. The offspring numbers per vial were (overdispersed) count data and we therefore used a negative binomial error structure with log-link function in generalized linear models. We confirmed the analyses results using a quasipoisson error and the results were qualitatively identical. Here, we report only the results of the negative binomial models. The offspring number estimates were conducted in two separate blocks and we therefore fit 'block' as a term in our models.

Across all model terms, block as a first order effect was the only significant association with offspring numbers in females (Table S2) and males (Table S3). nDNA, mtDNA, and their nDNA x mtDNA interaction were non-significant terms. Interactions between mtDNA and nDNA with block, along with the 3-way interaction (mtDNA x nDNA x block) were non-significant in both sexes. These results demonstrate that mtDNA and nDNA, along with their interaction are not associated with offspring numbers – our measure of fecundity- in this genotype panel. It also confirms that first and second order effects were not different between the blocks.

Table S2. Generalized linear models of offspring production in females (analysis of deviance). Terms in the model were nDNA type, mtDNA type, and block. All first order effects and interaction terms were fitted. We report the degrees-of-freedom (df), deviance, residual degrees-of-freedom, residual deviance and p-values based on a Chi-squared distribution. P-values in bold are significant at α=0.05.

Model term	df	Deviance	Residual df	Residual deviance	P (>Chi)
	-	-	92	148.51	-
nDNA	1	0.84	91	147.67	0.36
mtDNA	1	0.23	90	147.45	0.63
Block	1	44.96	89	102.49	**2.014E-11**
nDNA x mtDNA	1	0.54	88	101.95	0.46
nDNA x block	1	0.31	87	101.64	0.58
mtDNA x block	1	0.17	86	101.47	0.68
nDNA x mtDNA x block	1	2.01	85	99.46	0.16

Table S3. Generalized linear models of offspring production in males (analysis of deviance). Terms in the model were nDNA type, mtDNA type, and block. All first order effects and interaction terms were fitted. We report the degrees-of-freedom (df), deviance, residual degrees-of-freedom, residual deviance and p-values based on a Chi-squared distribution. P-values in bold are significant at α=0.05.

Model term	df	Deviance	Residual df	Residual deviance	P (>Chi)
	-	-	92	130.25	-
nDNA	1	0.65	91	129.60	0.42
mtDNA	1	0.03	90	129.58	0.87
Block	1	26.71	89	102.87	**2.368E-07**
nDNA x mtDNA	1	1.18	88	101.68	0.28
nDNA x block	1	0.68	87	101.00	0.41
mtDNA x block	1	0.22	86	100.78	0.64
nDNA x mtDNA x block	1	0.96	85	99.82	0.33

Supporting References

ANDERS, S., and W. HUBER, 2010 Differential expression analysis for sequence count data. Genome Biology **11:** 1-12.

MONTOOTH, K. L., C. D. MEIKLEJOHN, D. N. ABT and D. M. RAND, 2010 Mitochondrial-nuclear epistasis affects fitness within species but does not contribute to fixed incompatibilities between species of Drosophila. Evolution **64:** 3364-3379.

MOREY, J. S., J. C. RYAN and F. M. VAN DOLAH, 2006 Microarray validation: factors influencing correlation between oligonucleotide microarrays and real-time PCR. Biological Procedures Online **8:** 175-193.

SCHMITTGEN, T. D., and K. J. LIVAK, 2008 Analyzing real-time PCR data by the comparative CT method. Nat. Protocols **3:** 1101-1108.